Wrist

Stefano Bianchi and Carlo Martinoli

CONTENTS

10.1
Introduction

In recent years, substantial improvement in transducer technology has led to a growing interest in the US evaluation of the hand and wrist (Bianchi et al. 1999, 2001; Chiou et al. 2001; Creteur and Peetrons 2000; Ferrara and Marcelis 1997; Fornage and Rifkin 1988; Lee 1998; Milbrat et al. 1990; Read et al. 1996; Teefey et al. 2000; Lee and Healy 2005). US transducers with frequencies ranging from 10 to 15 MHz allow accurate assessment of tendons, joints, nerves and vessels of the extremities without requiring stand-off pads. The association of standard radiographs with high-resolution US works well in the

S. Bianchi, MD
Privat-docent, Université de Genève, Consultant Radiologist, Fondation et Clinique des Grangettes, 7, ch. des Grangettes, 1224 Genève, Switzerland
C. Martinoli, MD
Associate Professor of Radiology, Cattedra "R" di Radiologia – DICMI – Università di Genova, Largo Rosanna Benzi 8, 16132 Genova, Italy

evaluation of wrist and hand disorders. Radiographs can recognize most bone and joint disorders and US can be used to assess a wide spectrum of pathologic conditions affecting soft-tissue structures.

10.2
Clinical Anatomy

From the anatomic point of view, the wrist is complex. For this reason, we will take a little time here to review the basic anatomy of the wrist with emphasis on the structures that can be assessed with US.

10.2.1
Osseous and Articular Anatomy

The wrist is composed of eight carpal bones arranged in two rows: proximal and distal. From lateral to medial, the proximal row includes the scaphoid, lunate, triquetrum and pisiform, whereas the distal row is formed by the trapezium, trapezoid, capitate and hamate. The arrangement of the carpal bones forms a ventral concavity which is transformed in an osteofibrous tunnel, the carpal tunnel, by the transverse carpal ligament. There are three joints in the wrist which, in normal conditions, do not communicate with one another: the distal radio-ulnar, radiocarpal and midcarpal joints (Fig. 10.1). Wrist movements are obtained by the concurrent action of the radiocarpal joint and midcarpal joint: wrist flexion and extension is produced half at the radiocarpal joint and half at the midcarpal joint, whereas radial and ulnar deviation of the wrist involves, at a higher extent (60%), the midcarpal joint.

10.2.1.1
Distal Radio-ulnar Joint

The distal radio-ulnar joint articulates the rounded head of the ulna with the ulnar notch of the distal
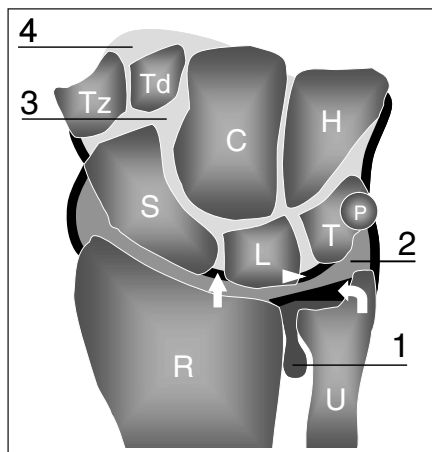
Fig. 10.1. Schematic drawing of a coronal view through the wrist outlines the relation among carpal bones and wrist joint spaces. Distal to the radius *(R)* and ulna *(U)*, the proximal row of carpal bones includes the scaphoid *(S)*, lunate *(L)*, triquetrum *(T)* and pisiform *(P)*, whereas the distal row is formed by the trapezium *(Tz)*, trapezoid *(Td)*, capitate *(C)* and hamate *(H)*. The distal radio-ulnar joint *(1)* is separated from the radiocarpal joint *(2)* by the triangular fibrocartilage (*curved arrow*). The scapholunate (*straight arrow*) and lunotriquetral (*arrowhead*) ligaments separate the radiocarpal from the midcarpal *(3)* joint. The carpometacarpal joint spaces *(4)* lie ahead of the distal carpal row

epiphysis of the radius and the triangular fibrocartilage. The distal radio-ulnar joint cavity is L-shaped and is separated from the radiocarpal joint by the triangular fibrocartilage. The capsule is formed by ventral and dorsal bands which extend from the surface of the radius to the ulna and includes a proximal pouch. The distal radio-ulnar joint is a pivotal type of articulation which allows pronation and supination movements of the hand.

10.2.1.2
Radiocarpal Joint

The radiocarpal joint, which is also referred to as the proper "wrist joint", is a condyloid type of synovial joint located between the distal end of the radius and the carpus. In the radiocarpal joint, the proximal concave articular surface is formed by the articular facet of the radius and the distal surface of the triangular fibrocartilage, a fibrocartilaginous structure filling the space between the ulnar head and the ulnar side of the carpus; the distal surface is composed of the convex surfaces of the scaphoid, lunate and triquetrum. On its ulnar side, the radiocarpal joint space may be in communication with the pisotriqu-

etral joint, formed by the pisiform, a sesamoid bone found inside the flexor carpi ulnaris tendon, and the anterior facet of the triquetrum. The capsule of the radiocarpal joint is attached to the distal margins of the radius and ulna and to the proximal row of the carpal bones and is reinforced by extrinsic carpal ligaments.

10.2.1.3
Midcarpal Joint

The midcarpal (intercarpal) joint is located between the proximal and distal rows of carpal bones. Its capsule connects the proximal and distal rows and is reinforced by a high number of intrinsic ligaments. The midcarpal joint improves the range of movements of the radiocarpal joint and especially the grasp of the hand. More distally, the carpometacarpal joints articulate the bases of the metacarpals with the distal row of the carpal bones. These latter spaces normally communicate with the midcarpal joint.

10.2.1.4
Wrist Ligaments and
Triangular Fibrocartilage Complex

The wrist ligaments can be classified as extrinsic and intrinsic. The extrinsic ligaments stabilize the wrist connecting the radius, the ulna and the bases of metacarpals with the carpal bones. Extrinsic ligaments are thicker and stronger on the volar side of the wrist. They are intracapsular and extrasynovial in location, being located between the capsule and the synovial layer of the joint. Overall, they have little clinical significance. Intrinsic (interosseous) ligaments connect and stabilize the carpal bones to one another, thus retaining the carpal bones (and especially those of the proximal carpal row) in the proper position during the complex movements of the hand. From a biomechanical point of view, the most relevant intrinsic ligaments of the wrist are the scapholunate ligament and the lunotriquetral ligament (Fig. 10.1). The scapholunate ligament has thick volar and dorsal components with a thinner portion in between them. Relative to the scapholunate ligament, the lunotriquetral ligament is smaller but has a similar shape. Intrinsic ligament tears may lead to instability of the adjacent joints and to irreversible degenerative changes resulting in limitation of range of movements, impaired function and pain.

The triangular fibrocartilage complex is formed by several soft-tissue structures located in the ulno-

carpal space which increase stability to the ulnar side of the wrist and the distal radio-ulnar joint and absorb mechanical forces across the ulnar side of the wrist during axial loading. The complex includes the triangular fibrocartilage itself and other supporting structures which blend with it, such as the meniscus homologus, the ulnar collateral ligament, the volar and dorsal radio-ulnar ligament and the sheath of the extensor carpi ulnaris tendon. The triangular fibrocartilage is a biconcave disk positioned between the ulnar styloid and the radius. Its thickness is inversely proportional to the degree of ulnar variance.

Even using high-resolution transducers, most wrist ligaments are not visible with US and their proper evaluation requires MR imaging, MR arthrography or thin collimation spiral CT arthrography. Clinically relevant structures that are amenable to US examination are the scapholunate ligament and the triangular fibrocartilage complex.

10.2.2
Tendons and Retinacula

The wrist is crossed by flexor and extensor tendons which course along its ventral and dorsal aspects respectively. Among them, nine flexor tendons and nine extensor tendons move toward the fingers without any attachment to the carpal bones; two primary wrist flexors and three wrist extensors insert onto the distal carpal row and the metacarpals; and one tendon, the palmaris longus tendon, attaches to the transverse carpal ligament and to the palmar aponeurosis.

10.2.2.1
Extensor Tendons

The extensor tendons course over the dorsal aspect of the wrist. They run within series of adjacent osteofibrous tunnels delimited by depressions of the surface of radius and ulna and by the extensor retinaculum, a 2 cm wide thickening of the dorsal fascia attached to the radial styloid laterally and to the pisiform and triquetrum medially. From the deep surface of the retinaculum, vertical fibrous bands insert into the cortical bones, at both sides of the tendons, dividing the extensor tunnel into six compartments numbered from radial (I) to ulnar (VI). In each compartment, a single synovial sheath formed by visceral and parietal layers surrounds one or more tendons (Fig. 10.2). A variable amount of fatty tissue fills the space between the synovial sheath and the bone surface. From the biomechanical point of view, these tunnels give lateral stabilization and avoid bowstringing of the extensor tendons during wrist and finger movements. A bony protuberance, the Lister tubercle, is found between the second and third tunnels, acting as a useful landmark in the US identification of these compartments (Fig. 10.2).

The first compartment, the most radial, contains the abductor pollicis longus and extensor pollicis brevis tendons (Fig. 10.3). Medial to this, the second compartment houses the extensor carpi radialis longus and brevis which insert on the dorsal aspect of the base of the second and third metacarpals respectively. The third compartment contains the extensor pollicis longus. As already stated, this compartment is separated from the second one by the Lister tubercle of the radius (Fig. 10.3a). The fourth compartment is wide and encloses the tendons of the extensor digitorum for the second through the fifth fingers, and the tendon of the extensor indicis proprius, which is absent or rudimentary in approximately 40% of individuals (Fig. 10.4). The fifth compartment encloses the extensor digiti quinti proprius, whereas the sixth compartment, the most ulnar, includes the extensor carpi ulnaris tendon which courses along the dorsomedial aspect of the distal ulna to insert onto the base of the fifth metacarpal (Fig. 10.4). The tendons of the first compartment and the tendon of the extensor pollicis longus form the volar and dorsal boundaries of the anatomic snuff-box, a skin depression on the radial aspect of wrist crossed by the radial artery (Fig. 10.3a,b). To recall the exact name of the extensor tendons seems difficult but it is even harder to remember the exact position of them in each individual compartment, and especially in the first, second and fourth compartments. For an easier comprehension, one should keep in mind that: in the first compartment the extensor pollicis brevis tendon is more dorsal than the abductor pollicis longus; in the second compartment, the extensor carpi radialis brevis tendon is closer to the Lister tubercle than the extensor carpi radialis longus; in the fourth compartment, the extensor indicis proprius tendon is positioned on the ulnar side of the tendon for the index finger of the extensor digitorum; the tendon of the extensor pollicis longus crosses the tendons of the second compartment to reach the thumb (Fig. 10.3a,b). As a memo, the tendons from the first to the third compartment alternate as to longus and brevis as they proceed in an ulnar direction: abductor pollicis longus, extensor pollicis brevis, extensor carpi radialis longus, extensor carpi radialis brevis, extensor pollicis longus.
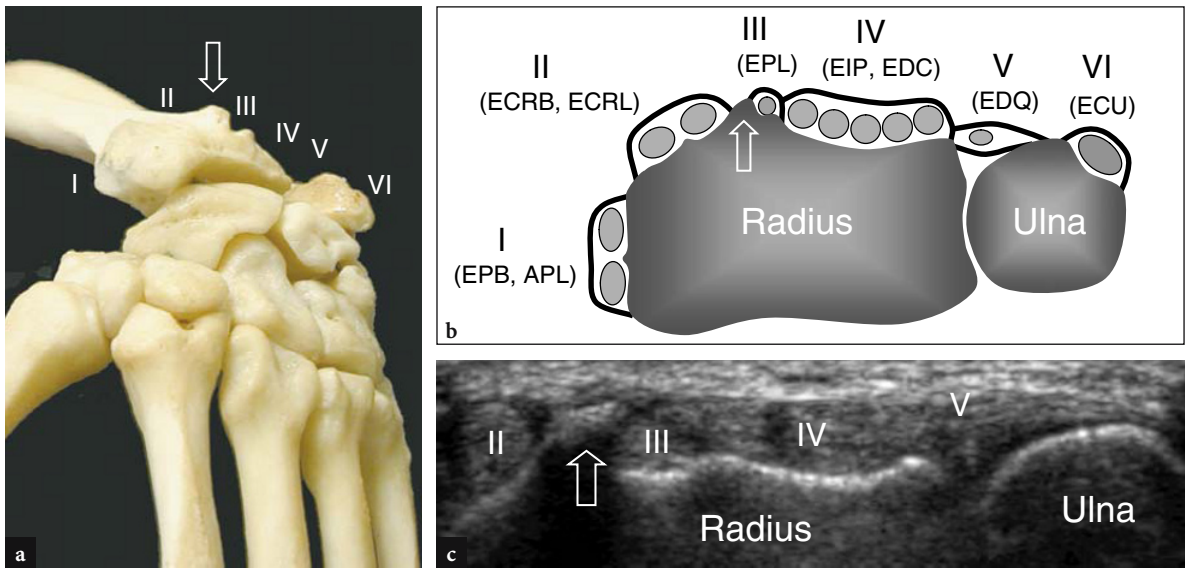
Fig. 10.2 a–c. Position of the extensor tendons relative to the bony surfaces of the dorsal radius and ulna. **a** Dorsal aspect of the wrist bones illustrates the relationships of the six compartments of the extensor tendons *(I–VI)* with the Lister tubercle *(arrow)*. **b** Schematic drawing of a transverse view at the level of the distal radio-ulnar joint outlines the extensor tendons and their synovial sheath. The tendons are labeled with numbers that correlate with the dorsal compartments *(I–VI)*. The first compartment contains the abductor pollicis longus *(APL)* and extensor pollicis brevis *(EPB)*, the second the extensor carpi radialis longus *(ECRL)* and extensor carpi radialis brevis *(ECRB)*, the third the extensor pollicis longus *(EPL)*, the fourth the extensor indicis proprius *(EIP)* and extensor digitorum (EDC), the fifth the extensor digiti quinti *(EDQ)*, the sixth the extensor carpi ulnaris *(ECU)*. Observe the prominence of the Lister tubercle *(arrow)* which separates the second from the third compartment. **c** Transverse 15–8 MHz US image over the dorsal wrist illustrates the typical dorsal shape of the distal radius and ulna shown in the diagram in **b**. The depiction of the Lister tubercle *(arrow)* makes the identification of the overlying extensor tendons easier
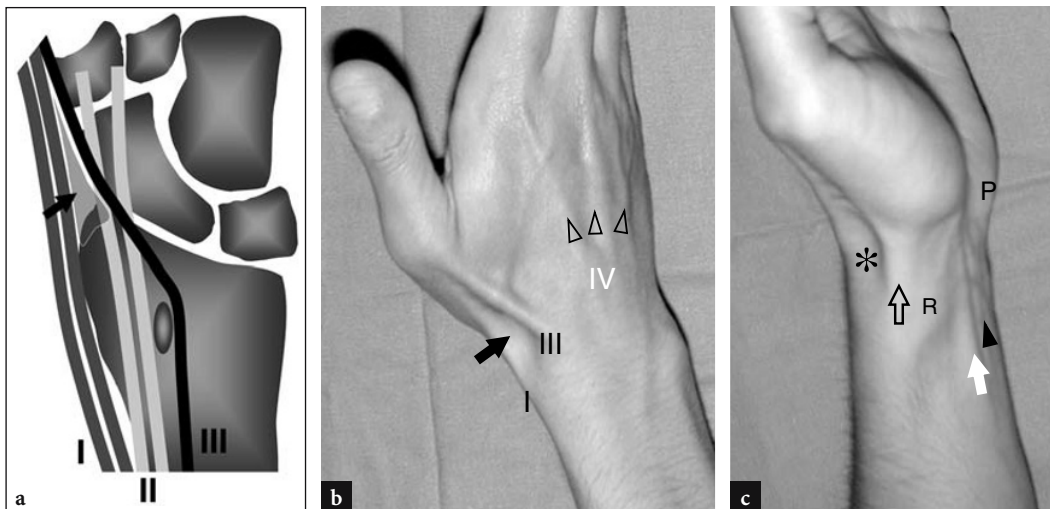
Fig. 10.3 a–c. Anatomic snuff-box. **a** Schematic drawing of a coronal view of the wrist bones illustrates the relationship among the tendons of the first *(I)*, second *(II)* and third *(III)* compartments. Note the course of the extensor pollicis longus tendon *(III)* which crosses the tendons of the second compartment to reach the thumb. The anatomic snuff-box *(arrow)* is a triangular space delimited by the tendons of the first and third compartments. **b** Photograph of the dorsolateral aspect of the wrist in a young woman showing the main surface features visible during contraction of the radial extensors. The abductor pollicis longus and extensor pollicis brevis *(I)* bound the hollow of the anatomic snuff-box *(arrow)* anteriorly, and the extensor pollicis longus *(III)* bounds it posteriorly. Observe the tendons of the fourth compartment *(arrowheads)* which diverge as they proceed distally over the dorsal hand. **c** Photograph of the ventral lateral aspect of the wrist shows the position of the abductor pollicis longus and extensor pollicis brevis tendons *(open arrow)* relative to the anatomic snuff-box *(asterisk)* and the radial styloid *(R)*. The flexor carpi radialis *(white arrow)* and palmaris longus *(arrowhead)* tendons are also delineated on a more ventral location. Note the pisiform bone *(P)*
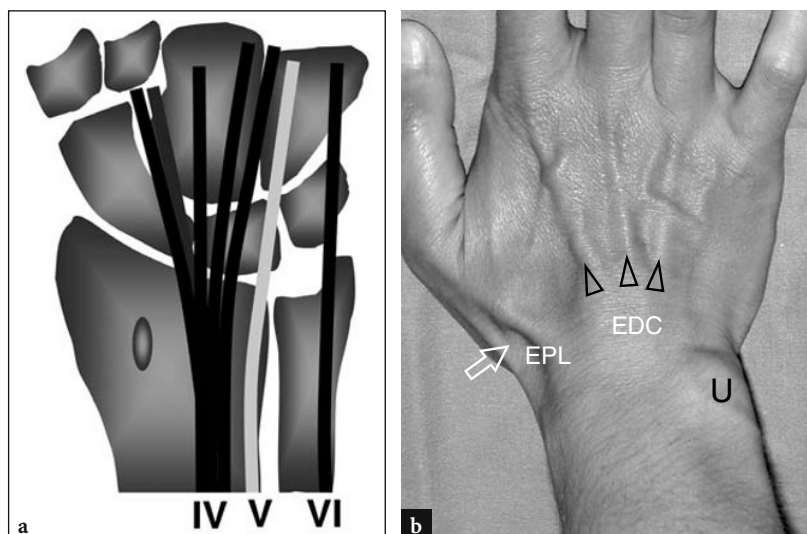
Fig. 10.4 a,b. Anatomy of the extensor tendons. **a** Schematic drawing of a coronal view of the dorsal wrist showing the relation among tendons of the fourth, fifth and sixth compartments. In the fourth compartment, the extensor indicis proprius *(intermediate gray)* runs together with the extensor digitorum *(black)*. **b** Photograph of the dorsal wrist in a young woman during forced wrist dorsiflexion demonstrates the diverging tendons of the extensor digitorum *(EDC)* over the skin. Other surface landmarks include the skin depression of the anatomic snuff-box *(arrow)*, the extensor pollicis longus tendon *(EPL)* and the head of the ulna *(U)*

10.2.2.2
Flexor Tendons

At the volar aspect of the wrist, nine flexor tendons enter the carpal tunnel to reach the fingers. There are four tendons from the flexor digitorum superficialis for the second through fifth fingers, four from the flexor digitorum profundus for the same fingers and the flexor pollicis longus tendon.

The flexor digitorum superficialis muscle gives rise to four tendons at the distal radius, just cranial to the proximal edge of the transverse carpal ligament. Then, these tendons pass within the carpal tunnel to diverge toward the fingers. During active finger movements, tendons of the flexor digitorum superficialis can be palpated at the wrist between the prominences of the flexor carpi radialis and ulnaris tendons. The four tendons of the flexor digitorum profundus traverse the wrist just deep to the respective tendons of the flexor digitorum superficialis. In the carpal tunnel, the tendon of the index finger is separate whereas the remaining tendons to the third through fifth fingers may become completely independent only in the palm. The lumbrical muscles arise in the palm from the tendons of the flexor digitorum profundus. The tendon of the flexor pollicis longus lies deep to the flexor carpi radialis in the distal forearm and passes on the radial side of the flexor digitorum tendons of the index finger in the carpal tunnel. On approaching the wrist, the tendons of the flexor digitorum superficialis and profundus become enveloped by a common synovial sheath. On transverse views, this sheath is "ε" shaped with a superficial extension which lies in front of the flexor digitorum superficialis, a middle extension lying between the flexor digitorum superfi-

cialis and profundus and a deep extension behind the flexor profundus. Just radial to the common flexor tendon sheath, the flexor pollicis longus tendon is enveloped by a separate sheath.

The primary flexors of the wrist, the flexor carpi radialis and the flexor carpi ulnaris, course outside the carpal tunnel and are readily palpable because they lie in a more superficial position than the flexor digitorum tendons (Fig. 10.5). The flexor carpi radialis tendon is a long flattened tendon which becomes oval in shape as it approaches the wrist. This tendon originates nearly midway between the elbow and wrist, is invested by an own synovial sheath and inserts on the palmar aspect of the base of the second metacarpal after coursing in a separate fibrous tunnel (vertical groove) made by an extension of the transverse carpal ligament. Its action allows flexion and concurrent radial deviation of the wrist. The flexor carpi ulnaris, the only tendon of the wrist not invested by a synovial sheath together with the palmaris longus tendon, is smaller in size and shorter relative to the flexor carpi radialis. This tendon courses on the ulnar side of the wrist housing the pisiform, which is considered a sesamoid bone in it, and inserts on the hook of the hamate (piso-hamate ligament) and on the fifth metacarpal (piso-metacarpal ligament). The flexor carpi ulnaris tendon is a landmark for the adjacent ulnar artery and nerve, both located just radial to them. Its action allows flexion and concurrent ulnar deviation of the wrist, an essential action in some tasks such as using a screwdriver or a mallet.

The palmaris longus tendon is a long thin tendon which passes in the midline and superficial to the transverse carpal ligament (Fig. 10.5). Distally, it splits into diverging bundles which intermingle with
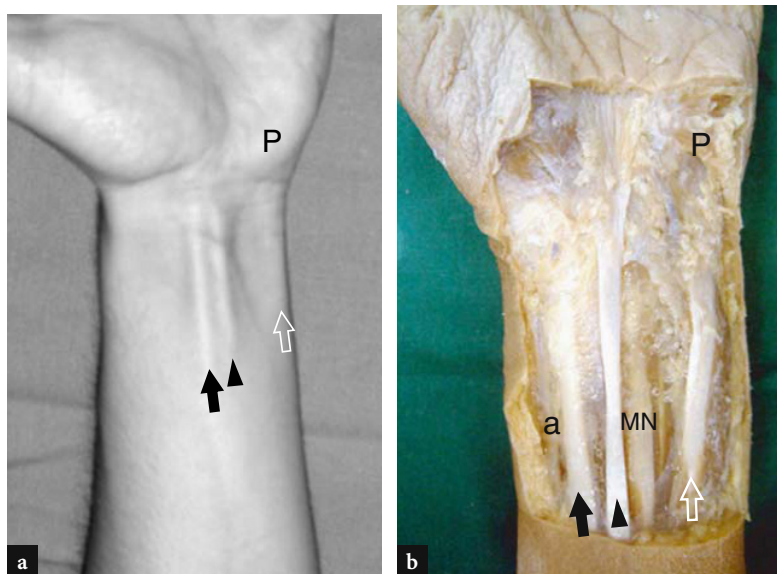
Fig. 10.5 a,b. a Photograph of the anterior aspect of the wrist with **b** cadaveric correlation shows the flexor carpi radialis tendon (*black arrow*) which serves as a guide to the radial artery (a) which lies just lateral to it. The long lean tendon of the palmaris longus (*arrowhead*) is a landmark for the median nerve *(MN)* which is deep and frequently lateral to it. More medially, the flexor carpi ulnaris tendon (*open arrow*) is seen moving down to the pisiform *(P)*. This tendon may be used as a key reference for the ulnar artery and nerve which lie lateral to it

the transverse carpal ligament and the palmar aponeurosis. It is absent in approximately 20% of individuals.

10.2.3
Neurovascular Structures

The wrist is crossed by the median nerve, the ulnar nerve and the superficial cutaneous branch of the radial nerve. In the wrist area, the ulnar nerve is accompanied by the ulnar artery and the median nerve gives off a sensory branch, the palmar cutaneous branch.

10.2.3.1
Median Nerve

At the distal forearm, the median nerve courses in the fascial plane intervening between the flexor digitorum profundus and the flexor digitorum superficialis muscles. As the nerve approaches the wrist, it shifts radially and then moves superficially along the lateral margin of the flexor digitorum superficialis to align itself with the midline before entering the carpal tunnel (Fig. 10.6). Inside the tunnel, the median nerve runs superficial to the tendons of the flexor pollicis longus and the flexor digitorum superficialis for the second finger although its position may vary somewhat depending on wrist position. The nerve has an oval cross-section at the proximal tunnel and tends to become more flattened as it progresses distally through the tunnel (level of the hamate hook).

Throughout the carpal tunnel, the median nerve is covered by a strong fibrous band commonly referred to as the transverse carpal ligament or the flexor retinaculum (Fig. 10.6a,b). This is a localized thickening of the fascia that inserts on the tubercle of the scaphoid and trapezium (radial side) and on the pisiform and hook of the hamate (ulnar side) (Fig. 10.7). The median nerve provides sensory supply to the palmar aspect of the first three fingers and the radial half of the fourth, and motor supply for the muscles of the thenar eminence. Just proximal to the transverse carpal ligament, the median nerve sends a palmar cutaneous branch, which is a sensory nerve that supplies the radial half of the palm. This latter branch is very small and typically vulnerable to injury during carpal tunnel release.

10.2.3.2
Ulnar Nerve

In the distal forearm, the ulnar nerve lies on the radial side of the flexor carpi ulnaris and on the ulnar side of the ulnar artery. Here, it gives off two small branches: the palmar and dorsal cutaneous branches. More distally, the ulnar nerve pierces the deep fascia to continue in the wrist superficial to the transverse carpal ligament throughout the Guyon tunnel (Fig. 10.8). This small tunnel lies in a more superficial and medial location relative to the carpal tunnel. It is bounded by the pisiform medially (proximal tunnel), the hook of the hamate laterally (distal tunnel), the transverse carpal ligament (floor) and the palmar carpal ligament (roof). The Guyon tunnel contains
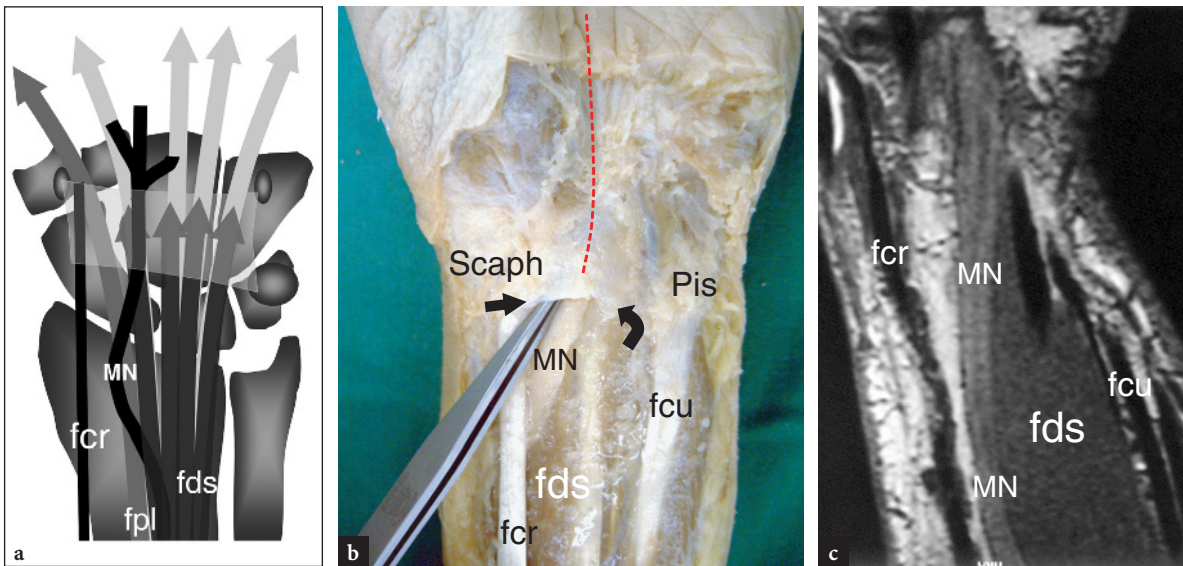
Fig. 10.6 a–c. Anatomy of the ventral wrist proximal to the carpal tunnel. **a** Schematic drawing of a coronal view through the ventral wrist shows the relationships of the median nerve *(MN)* with the flexor digitorum superficialis *(fds)*, flexor pollicis longus *(fpl)* and flexor carpi radialis *(fcr)* tendons. Note the transverse carpal ligament *(light gray)*. Compare this drawing with **b** the view of a gross dissection and **c** a coronal T1-weighted SE MR image of the ventral wrist. In **b**, the median nerve is seen as it enters the carpal tunnel passing deep to the proximal edge *(arrows)* of the transverse carpal ligament, joined between the scaphoid *(Scaph)* and the pisiform *(Pis)*. The dashed line in red indicates the course of the nerve through the carpal tunnel. In **c** observe the curvilinear course of the median nerve at the distal radius. The nerve approaches the midline and becomes superficial to the flexor digitorum superficialis before entering the carpal tunnel
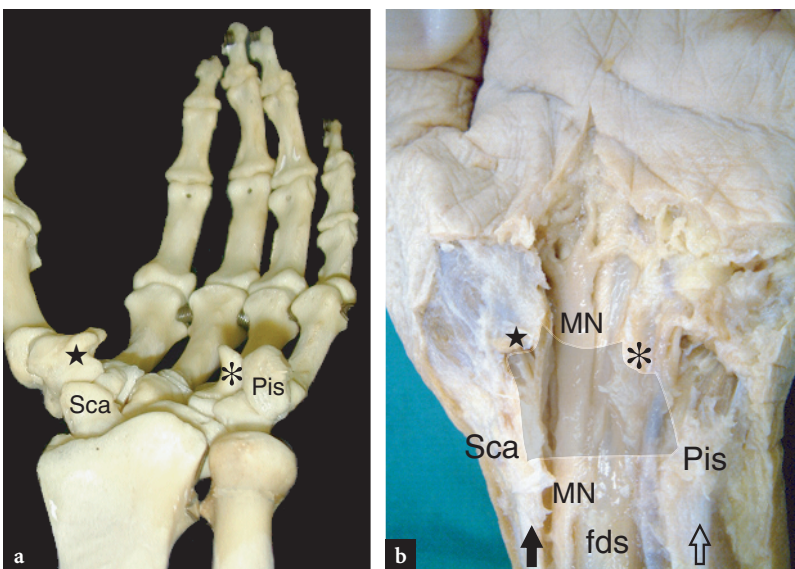
Fig. 10.7 a,b. Carpal tunnel anatomy. **a** Axial view of the wrist bones shows the main bony landmarks of the carpal tunnel. The proximal carpal tunnel is delimited by the pisiform *(Pis)* at its ulnar side and the scaphoid *(Sca)* at its radial side, whereas the distal carpal tunnel is bounded by the hook of the hamate *(asterisk)* at its ulnar side and the tubercle of trapezium *(star)* at its radial side. These bones gives insertion to the transverse carpal ligament. **b** Gross dissection of the ventral wrist demonstrates the position of the median nerve *(MN)* relative to the bony landmarks shown in **a**. The transverse carpal ligament is drawn in light gray. Note the flexor carpi radialis tendon *(black arrow)* straight on the scaphoid and the flexor carpi ulnaris *(open arrow)* inserting on the pisiform. The median nerve and the flexor digitorum superficialis course in between these tendons
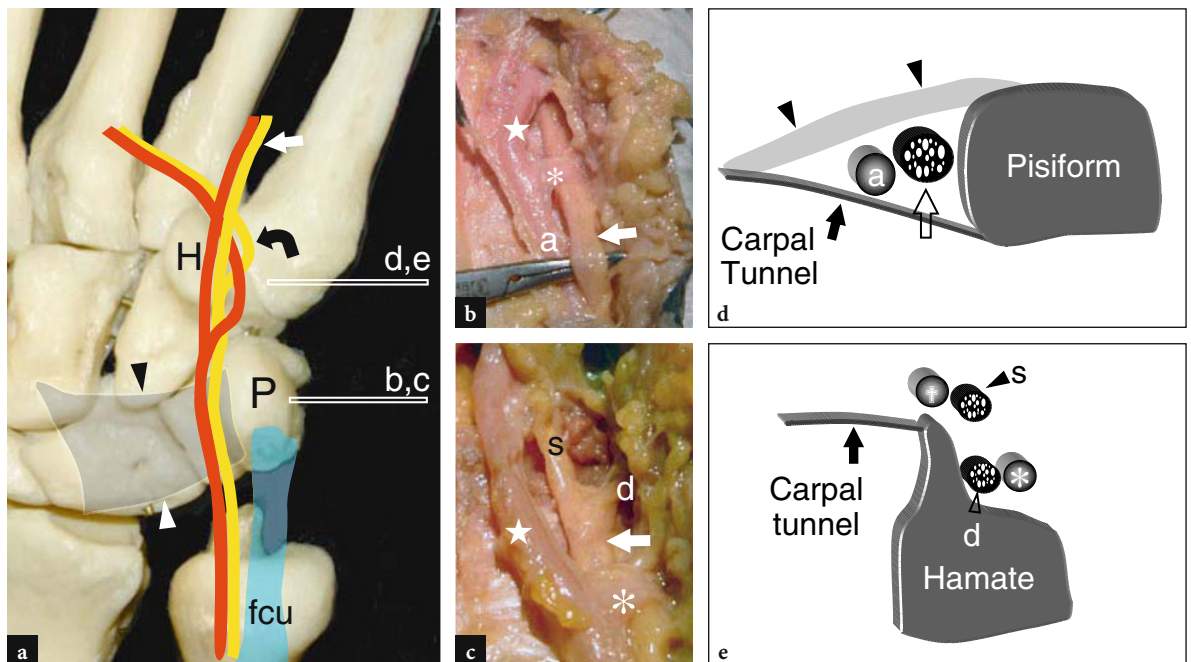
Fig. 10.8 a–e. Guyon tunnel anatomy. **a** Ventral view of the wrist bones illustrates the course of the ulnar artery and the ulnar nerve in the Guyon tunnel relative to the flexor carpi ulnaris tendon *(fcu)*, the pisiform *(P)* and the hook of the hamate *(H)*. The transverse carpal ligament *(arrowheads)* forms the floor of the Guyon tunnel. In the distal portion of the tunnel, the ulnar nerve divides into a superficial sensory branch *(straight arrow)* and a deep motor branch *(curved arrow)*. **b,c** Gross anatomic views with **d,e** corresponding diagrams of the proximal **(b,d)** and distal **(c,e)** Guyon tunnel obtained at the levels *(horizontal white bars)* indicated in a show the main trunk of the ulnar nerve *(void arrow)* and its divisions, deep *(d)* and superficial *(s)*. Close to the nerve, the ulnar artery *(a)* bifurcates in the respective deep *(asterisk)* and superficial *(star)* branches. In **d**, observe the position of the ulnar nerve relative to the pisiform, the transverse carpal ligament *(black arrow)* and the palmar carpal ligament *(arrowheads)*

the ulnar nerve (medial) and the ulnar artery (lateral) and veins embedded in fatty tissue. The ulnar nerve bifurcates within this tunnel into two terminal divisions – the superficial sensory branch and the deep motor branch – the latter supplying most of the intrinsic muscles of the hand, including the hypothenar muscles, the two medial lumbrical muscles, the adductor pollicis and the interosseous muscles. The ulnar nerve gives sensory supply to the medial aspect of the palm, the little finger and the medial half of the ring finger. Distal to the Guyon tunnel, the superficial branch has a straight course while the deep motor branch reflects across the palm to end at the first interosseous space (Fig. 10.8a).

10.2.3.3
Radial Nerve (Cutaneous Terminal Branch)

At the distal radial aspect of the forearm, the superficial cutaneous branch of the radial nerve emerges between the tendons of the extensor carpi radialis longus and the brachioradialis to reach the subcutaneous tissue. At this point, the nerve is covered by a fascial band which connects the tendon and myotendinous junction of the brachioradialis muscle with the tendon of the extensor carpi radialis longus. More distally, the radial nerve pierces the fascia and overlies the anatomic snuff-box traversing the extensor tendons of the first compartment to provide sensory supply to the dorsum of the wrist, hand, thumb and proximal portion of the radial fingers.

10.2.3.4
Radial and Ulnar Arteries

The brachial artery has two terminal branches: the radial artery and the ulnar artery. At the distal forearm, the radial artery courses superficially over the ventral aspect of the distal radius where its pulse can readily be felt. Then, it curves dorsally over the radial aspect of the wrist, passes deep to the extensor tendons of the first compartment and crosses the floor of the anatomic

snuff-box. The ulnar artery enters the wrist on the lateral side of the ulnar nerve and runs together with the nerve throughout the Guyon tunnel, superficial to the transverse carpal ligament (Fig. 10.8). Somewhat similar to the nerve, the ulnar artery splits into a superficial palmar branch and a deep palmar branch.

10.3
Essentials of Clinical History and Physical Examination

Before US examination, the patient's history should be carefully investigated to rule out any possible systemic articular disorder (rheumatoid arthritis and similar conditions), sporting or occupational activities possibly related to tendinitis and overuse syndromes, as well as local trauma (occult fractures, tendon ruptures, ligament sprains). At physical examination, the range of wrist movements (flexion-extension, ulnar-radial deviation, pronation-supination) can readily be assessed. An accurate location of the site of pain may be helpful in the case of tendinitis. In addition, movements that cause pain should also be tested. Recent standard radiographs, if any, should be reviewed for signs of joint and bones disease (i.e., osteoporosis, marginal erosions, focal bone lesions), abnormal position of bones (reflecting ligaments tears) and soft-tissue thickening and calcifications. When a space-occupying mass is encountered over the dorsal or palmar aspects of the wrist, intermittent variations in its size with time can suggest the diagnosis of a ganglion cyst. When the mass is linked to an adjacent tendon and follows it during movements, an intratendinous ganglion should be suspected.

10.3.1
De Quervain Disease

In de Quervain disease, an inflammatory disorder affecting the first compartment of the extensor tendons, patients report tenderness and pain over the radial styloid. Typically, the wrist pain increases during grasping heavy objects. A useful diagnostic test is the Finkelstein test (Fig. 10.9). During this maneuver, the patient holds his or her thumb inside the clenched fist while the examiner tilts the patient's hand in an ulnar direction to stretch the tendons of the first compartment. The Finkelstein test indicates de Quervain disease when it causes pain over the radial styloid that resemble the one described by the patient. Care should be taken, however, not to rely on this finding alone, because the Finkelstein test can be positive in normal subjects if the examiner applies excessive tension and in cases of rizarthrosis and radial styloiditis. As an alternative test, the examiner can maximally abduct the patient's thumb while keeping the wrist in radial deviation. This latter maneuver is more specific because it pushes the tendons against the retinaculum and not toward the bone, thus recalling the same stress forces that generate symptoms in de Quervain disease. Both tests should be performed by the examiner because they help to direct the US examination to the first compartment.

10.3.2
Carpal Tunnel Syndrome

Patients with carpal tunnel syndrome typically complain of night tingling and burning pain over the radial aspect of the hand and the first three fingers.
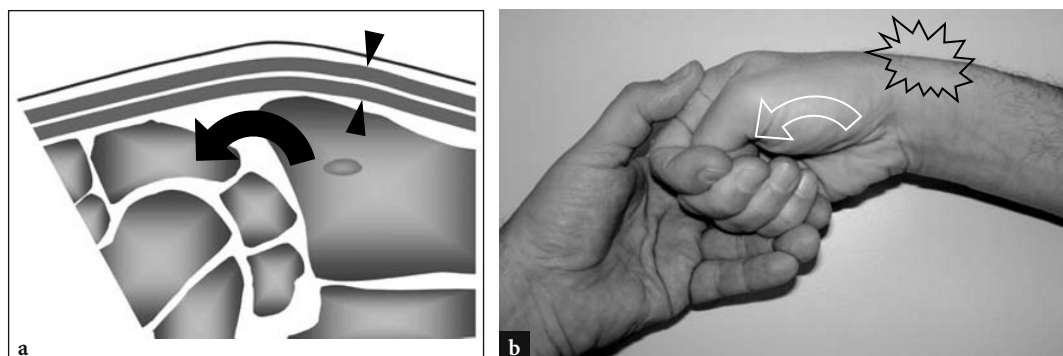
Fig. 10.9 a,b. Finkelstein test for evaluation of de Quervain disease. **a** Schematic drawing of a sagittal view through the wrist during ulnar deviation outlines tension of the first compartment tendons resulting from stretching over the radial styloid. **b** The Finkelstein sign is performed as follows: while the patient adducts the thumb into the palm making a fist, the examiner tilts the wrist in ulnar deviation (*curved arrow*) to stretch the tendons of the first compartment (*arrowheads*). A positive test causes localized excruciating pain over the radial styloid

The same symptoms can be felt during the day when a fixed position of the hand grasping an object is required, such as holding a heavy book or the telephone receiver. Because of the tingling, it is not unusual for patients to refer findings of carpal tunnel syndrome to a vascular disorder. Two clinical tests can be helpful to establish the diagnosis: the Tinel test and the Phalen test. The Tinel test is performed by tapping the volar aspect of the carpal tunnel with a reflex hammer (Fig. 10.10a), while, in the Phalen test, a full flexed wrist position is maintained for 1 min (Fig. 10.10b).Both tests are positive if they reproduce the patient's symptoms. The examiner should be aware, however, that false negatives may occur in cases of chronic entrapment disease.

10.4
US Scanning Technique and Normal US Anatomy

The patient is asked to sit comfortably in front of the examiner with both wrists and elbows resting on the examination table. Aged or traumatized patients may lie supine with the arm resting at the side of the body, although examination of the opposite side may become problematic in this position. For dynamic scanning of the extensor tendons, the hand is best placed on a gel tube with the fingers hanging over its edge to make fingers movements easier.

The routine US examination of the wrist begins with evaluation of its dorsal aspect, followed by the palmar one. Depending on the specific clinical presentation, US images can be obtained in different positions of the wrist (flexion and extension, radial and ulnar deviation, pronation and supination). Evaluation of gliding of the flexor and extensor tendons must always be performed during passive and active movements of the fingers.

10.4.1
Dorsal Wrist

Transverse US images are the best for detection and a proper identification of the extensor tendons. Assessment of the individual tendons is based on their anatomic position and behavior at dynamic examination (Lee anh Healy 2005). Detection of the extensor tendon for the third finger, for instance, is straightforward when transverse US scans are obtained during active flexion and extension of this finger while the others are maintained fixed by the examiner. On the other side, the extensor carpi radialis and the extensor carpi ulnaris are not affected by fingers movements and can be distinguished only on the basis of their anatomic position. US images are first obtained at the level of the distal epiphysis of the radius. The most useful landmark at this level is the Lister tubercle. This appears as a hyperechoic bony prominence over the dorsal surface of the radius. The tubercle separates the medial third compartment from the lateral second compartment (Fig. 10.2c). The extensor tendons appear as oval or rounded hyperechoic structures of different size. The extensor carpi radialis brevis and longus are the largest while the extensor pollicis longus and the extensor digiti quinti are the smallest. With high-resolution transducers, the extensor retinaculum appears as a thin transversely oriented
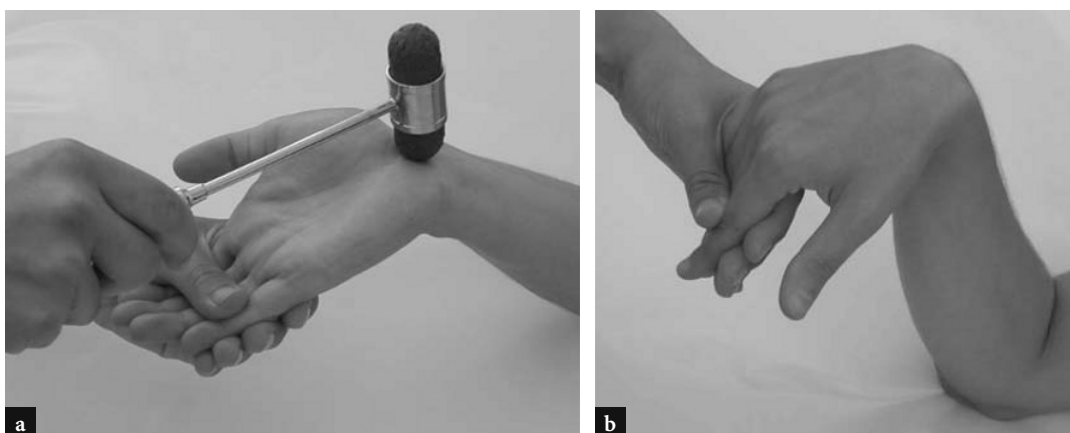
Fig. 10.10 a,b. Clinical tests for evaluation of carpal tunnel syndrome. **a** The Tinel sign elicits paresthesias by tapping the median nerve at the palmar crease. **b** The Phalen sign provokes paresthesias at the end of the range of flexion of the wrist

fibrillar band which overlies each compartment. The septa of the retinaculum appear as thin hypoechoic bands at both sides of the tendons as a result of anisotropy. In most cases, the retinaculum of the fourth compartment is the thickest and more visible compared with the other compartments. In normal conditions, the synovial membrane enveloping the tendons and the sheath fluid cannot be depicted. We believe the best way to explore hand and wrist tendons is to assess each tendon or tendon group separately and to evaluate the different compartments in a sequential way. In clinical practice, one should first recognize the tendon and then follow it on short-axis planes its full length down to the distal insertion. Longitudinal US images may be useful to evaluate the fibrillar pattern of tendons and their dynamic motion in detail.

10.4.1.1
First Compartment

In the tunnel compartment, the abductor pollicis longus and extensor pollicis brevis tendons lie side by side over the lateral aspect of the radial styloid (Fig. 10.11). The floor of the tunnel is formed by a shallow groove of the radius. A small central crest within this groove may occasionally be seen. Two main anatomic variants may be encountered in the first compartment: (1) a vertical septum which splits the compartment into two distinct spaces; (2) accessory tendons that can be found in as many as 75% of cadaver dissections. The role of these anatomic variants in the pathogenesis of local tendinitis is discussed afterwards (see Sect. 10.5.1.1). The central septum can be appreciated with high-resolution US: it appears as a linear, vertically oriented hypoechoic band that divides the tunnel into a larger ventral and a smaller dorsal space (Fig. 10.12b-d). The anterior (ventral) tunnel houses the abductor pollicis longus whereas the posterior (dorsal) tunnel contains the extensor pollicis brevis. Accessory tendons are usually associated with the abductor pollicis longus (Fig. 10.12c,d). Their detection inside the first compartment may be difficult because of crowding of several tendons within a small tunnel. For this purpose, scanning in a more distal position, over the scaphoid, may be helpful to show the accessory slips that diverge to reach their different insertions. Although fluid within the tendon sheath is never seen in normal states, synovial sheath effusions may facilitate the detection of accessory tendons by increasing the contrast among them. More distally, the tendons of the first compartment pass lat-

eral to the scaphoid and form the anterior edge of the anatomic snuff-box. The space between the scaphoid and these tendons is filled by loose connective tissue and houses the radial artery and veins (Figs. 10.3, 10.13). Longitudinal US images over the radial styloid demonstrate these tendons resting on the radial cortex, whereas distal US images depict them at a certain distance from the scaphoid, somewhat forming a bridge between the radius and the base of the first metacarpal. The retinaculum is appreciated at the level of the radial styloid and its thickness can be measured on transverse scans (Fig. 10.11). Just superficial to the lateral aspect of the scaphoid, the radial artery can be assessed with gray-scale and Doppler imaging. In the subcutaneous tissue, the radial nerve is appreciated as a small fascicular structure encroaching the extensor tendons of the first compartment (Fig. 10.14). With high-resolution transducers, dynamic scanning can demonstrate the nerve snapping dorsally and ventrally over these tendons during pronation and supination movements.
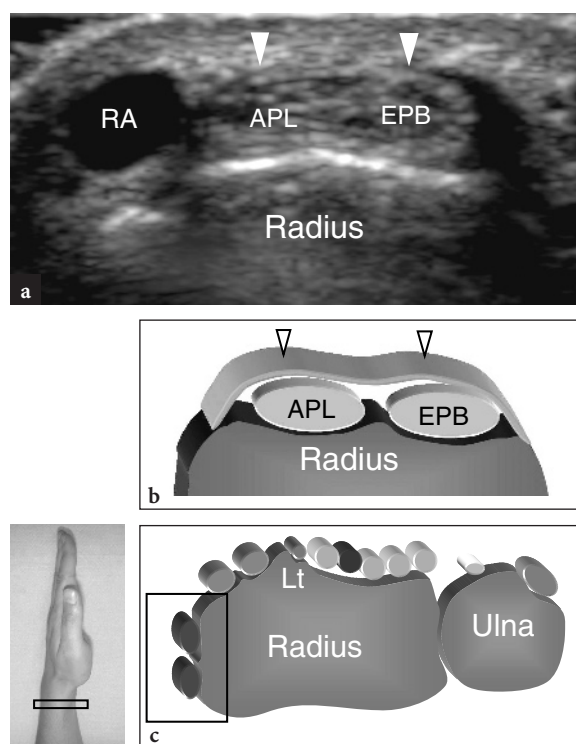
Fig. 10.11 a–c. Extensor tendons: first compartment. **a** Short-axis 15–7 MHz US image obtained over the first compartment of the extensor tendons with **b** diagram correlation demonstrates the abductor pollicis longus *(APL)* and extensor pollicis brevis *(EPB)* tendons which appear closely apposed and retained over the radial styloid by the retinaculum *(arrowheads)*. The radial artery *(RA)* is seen on the lateral aspect of the abductor pollicis longus. **c** Probe positioning and field-of-view of the US image relative to the dorsal wrist structures
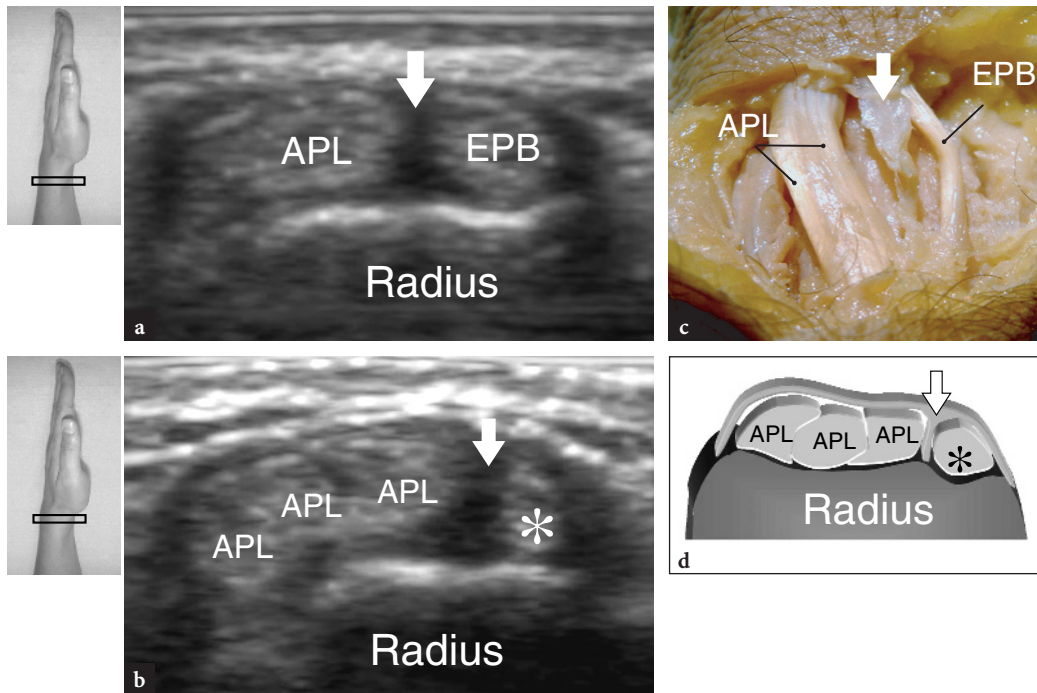
Fig. 10.12 a–d. Extensor tendons: anatomic variants in the first compartment. **a,b** Central septum. **a** Transverse 15–7 MHz US image obtained over the first compartment in an asymptomatic subject with **b** correlative gross anatomic view shows a vertical hypoechoic band *(arrow)* which spits the compartment into two spaces separating the abductor pollicis longus *(APL)* from the extensor pollicis brevis *(EPB)*. **c,d** Accessory tendons. **c** Transverse 15–7 MHz US image obtained over the first compartment of the extensor tendons with **d** diagram correlation demonstrates three tendons of the abductor pollicis longus *(APL)* instead of one. The occurrence of a vertical septum allows the extensor pollicis brevis *(asterisk)* to be distinguished from the supernumerary tendons of the abductor pollicis longus. The inserts at the upper left side of the figure indicate probe positioning
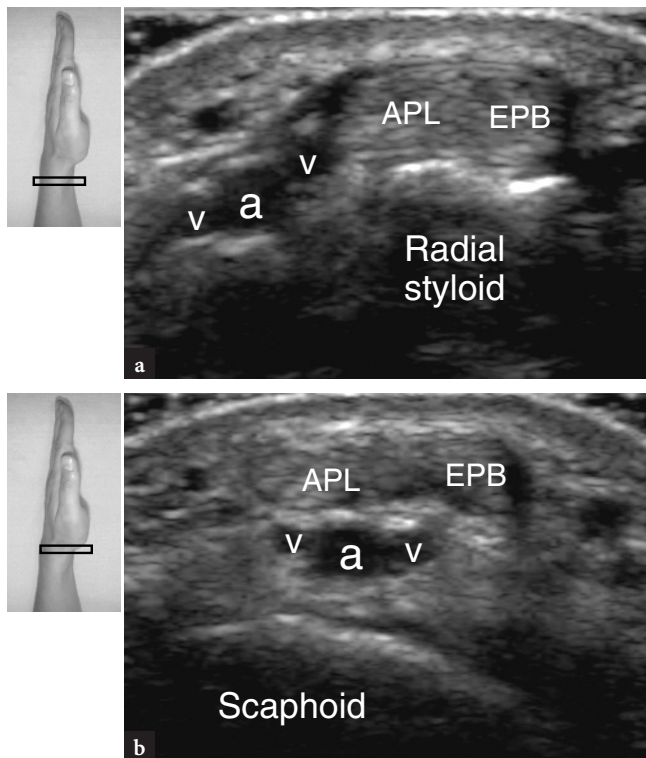
Fig. 10.13 a,b. Radial artery. Transverse 15–7 MHz US images obtained **a** at the radial styloid and, more distally, **b** at the scaphoid bone level demonstrate the relationship of the radial artery *(a)* and veins *(v)* with the abductor pollicis longus *(APL)* and the extensor pollicis brevis *(EPB)* tendons. As the radial vessels proceed distally, they pass deep to the extensor tendons crossing the floor of the anatomic snuff-box to reach the dorsal aspect of the hand. The inserts at the upper sides of the figure indicate probe positioning

Fig. 10.14 a−d. Radial nerve. **a** Photograph of the lateral aspect of the wrist showing the relationship of the superficial cutaneous branch of the radial nerve (*white dashed line*) with the extensor tendons of the first (I) and third (III) compartment. **b−d** Transverse 15−7 MHz US images over the first compartment of the extensor tendons obtained at the levels (*horizontal black bars*) indicated in **a** show the radial nerve (*arrow*) as it crosses the abductor pollicis longus (APL) and extensor pollicis brevis tendons (EPB) to reach the dorsal aspect of the hand. At the wrist, the radial nerve is very small and can be depicted as a tiny hypoechoic image only when very high-frequency transducers are used
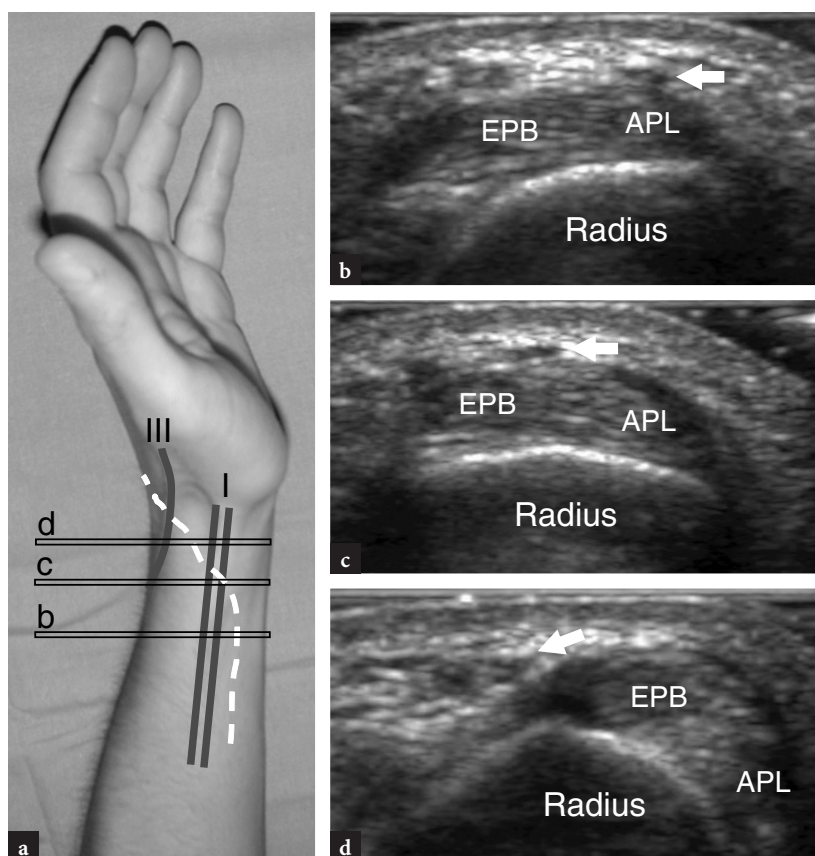
10.4.1.2
Second Compartment

At the distal radius, the extensor carpi radialis longus and the extensor carpi radialis brevis are seen coursing side by side to proceed toward the second compartment, while the muscles of the abductor pollicis longus and extensor pollicis brevis encroach superficial to them to reach the first compartment, the so-called "intersection" (Fig. 10.15). More distally, the extensor carpi radialis longus and brevis tendons diverge to reach the bases of the second and third metacarpals. Because of their greater size, these tendons can be easily evaluated and followed down to their distal insertions by means of short-axis planes. Longitudinal planes may be helpful to depict the internal echotexture of these tendons and are particularly useful to evaluate their distal insertion.

10.4.1.3
Third Compartment

The extensor pollicis longus tendon is a thin tendon that has to be carefully evaluated because it is commonly involved by trauma or arthritis. Once detected at the medial side of the Lister tubercle, it must be followed on short-axis planes (Fig. 10.16). Because this tendon has an oblique course from medial (proximal) to lateral (distal), one should be aware that transverse scans must be oriented obliquely to maintain the scanning plane perpendicular to the long axis of the tendon. In fact, if the tendon is incorrectly imaged, it may exhibit a more pronounced oval shape and a larger cross-sectional profile. As the tendon progresses distally, it crosses the extensor carpi radialis brevis and the extensor carpi radialis longus. A careful scanning technique is required to depict the tendon intersection (Fig. 10.17). More distal images show the extensor pollicis brevis as it progressively joins the ulnar aspect of the extensor pollicis brevis which reaches its distal insertion at the base of the proximal phalanx. Long-axis US images on this small curvilinear tendon are difficult to obtain and, on the whole, not so useful.
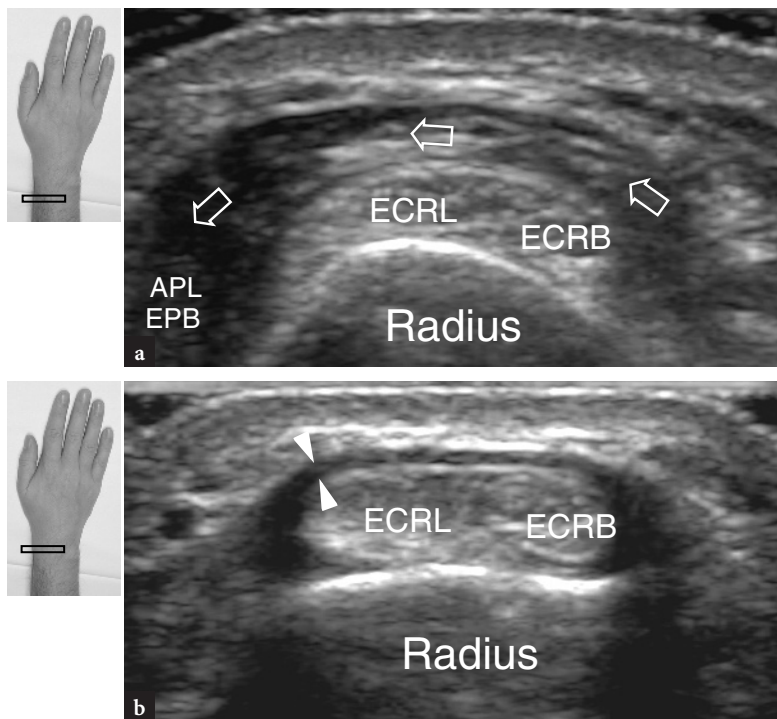
Fig. 10.15a,b. Extensor tendons: second compartment. Transverse 15−7 MHz US images obtained **a** at the distal forearm and **b** at the distal radius over the second compartment of extensor tendons. In **a**, US demonstrates the muscle bellies of the abductor pollicis longus and extensor pollicis brevis (*arrows*) as they cross the tendons of the extensor carpi radialis longus *(ECRL)* and brevis *(ECRB)* to reach the first compartment. More distally, in **b**, the extensor carpi radialis brevis and longus appear as paired tendons resting on the distal radius. The retinaculum (*arrowheads*) appears as a hypoechoic band inserting into the bony cortex. The inserts at the upper sides of the figure indicate probe positioning
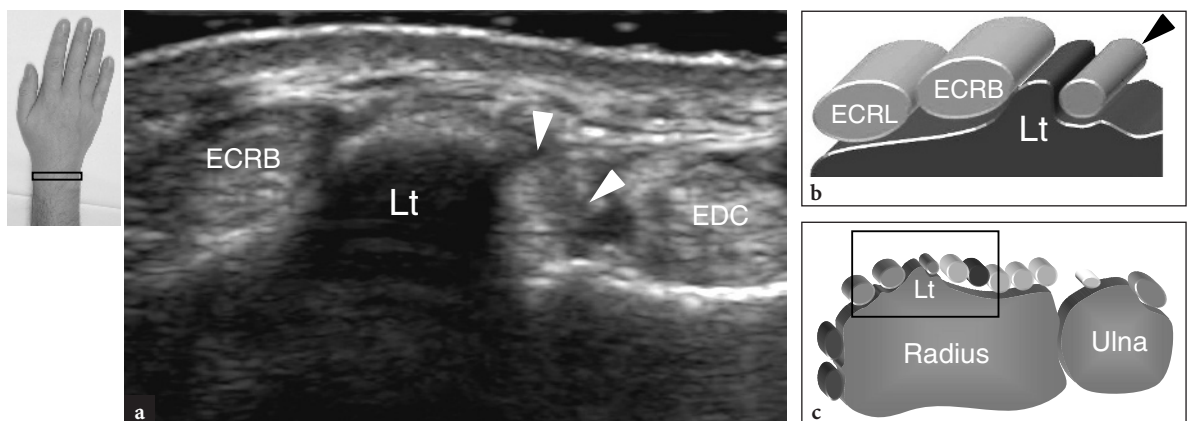
Fig. 10.16a−c. Lister tubercle. **a** Transverse 15−7 MHz US image obtained over the dorsal radius with **b** diagram correlation demonstrates the Lister tubercle *(Lt)* as a discrete hyperechoic bony prominence which separates the extensor pollicis longus (*arrowheads*) on its medial side from the extensor carpi radialis brevis *(ECRB)* on its lateral side. *EDC*, extensor digitorum tendon; *ECRL*, extensor carpi radialis longus tendon. **c** Probe positioning and field-of-view of the US image relative to the dorsal wrist structures
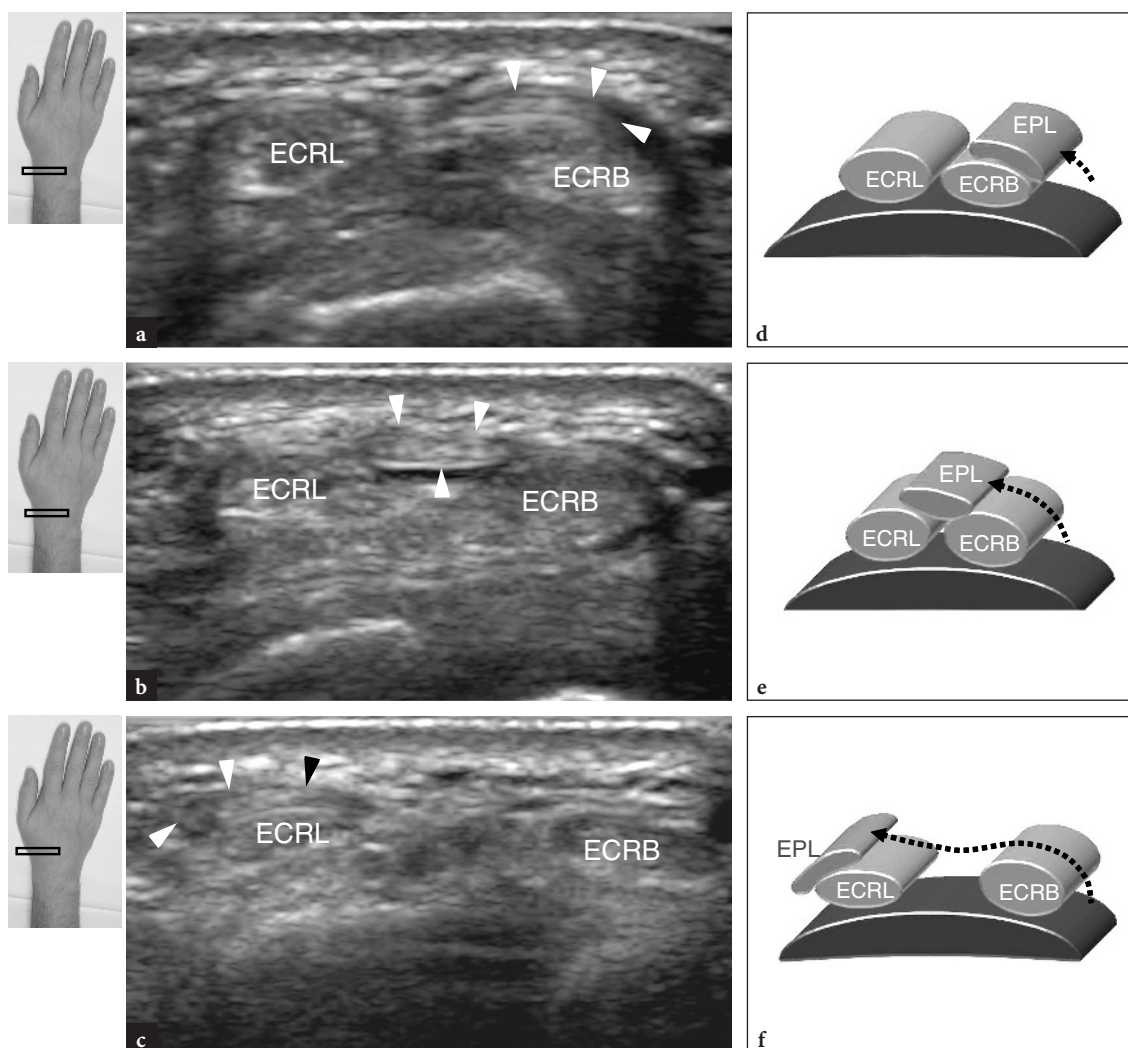
Fig. 10.17 a–f. Extensor tendons: second and third compartments. **a–c** Transverse 15–7 MHz US images obtained distal to the Lister tubercle with **d–f** diagram correlation. From cranial (**a**) to caudal (**c**), US shows the extensor pollicis longus tendon as a thin fibrillar band (*arrowheads*) crossing the extensor carpi radialis brevis *(ECRB)* and longus *(ECRL)*

10.4.1.4
Fourth and Fifth Compartments

The fourth and fifth compartments are routinely assessed together because of the close relation of the extensor digiti quinti with the extensor digitorum and the extensor indicis proprius. Transverse US images over the distal epiphysis of the radius show multiple slips of the extensor digitorum packed together inside the fourth compartment (Fig. 10.18). Because of their close apposition, static examination can hardly differentiate among these tendons. In order to identify them properly, selective dynamic scanning should be obtained while asking the patient to alternately flex and extend the respective finger while the examiner maintains the others fixed. On the ulnar side of the fourth compartment, careful US scanning shows the extensor digiti quinti coursing far from the bone, in a purely fibrous tunnel (Fig. 10.19). This tendon passes just superficial to the distal radio-ulnar joint. Flexion and extension movements of the little finger can enhance the detection of this small tendon. Dynamic US examination can also be useful to evaluate tendon gliding.

10.4.1.5
Sixth Compartment

The sixth compartment is the easiest to be assessed with US as it contains only a large tendon, the exten-
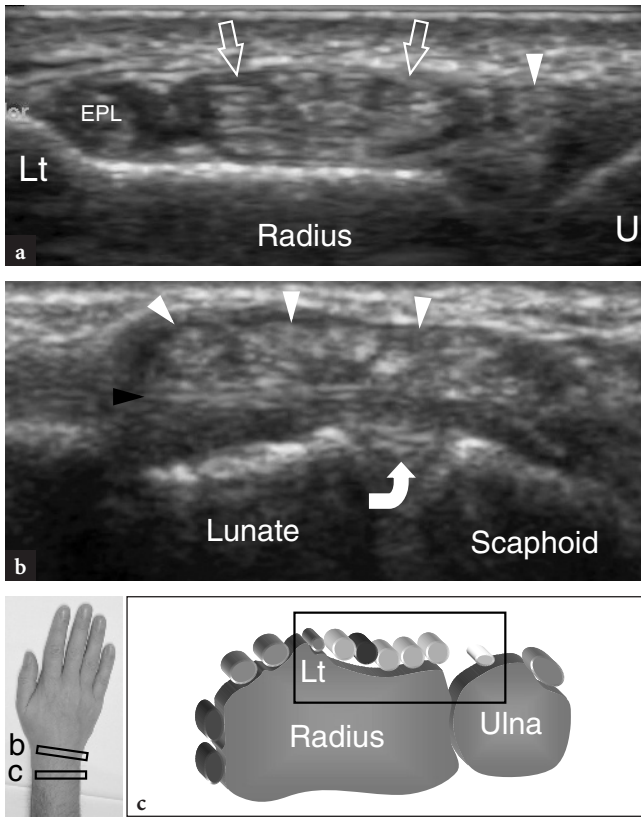
Fig. 10.18 a–c. Extensor tendons: fourth compartment. **a** Transverse 15−7 MHz US image obtained at the distal radius demonstrates the tendons of the fourth compartment (*arrows*) lying over the radial cortex between the extensor pollicis longus (*EPL*) and the extensor digiti quinti (*arrowhead*) tendons. At this level, the tendons of the fourth compartment are tightly packed below the retinaculum and cannot be differentiated from one another except using dynamic scanning with passive flexion and extension movements of the respective fingers. Note the position of these tendons relative to the Lister tubercle (*Lt*) and the ulnar head (*U*). **b** Transverse 15−7 MHz US image obtained at the proximal carpal row level shows the extensor indicis proprius and the extensor digitorum (*white arrowheads*) tendons, which are better individualized than at the level shown in **a** due to a divergent course. These tendons lie just superficial to the dorsal intercarpal ligament (*black arrowhead*) and to the dorsal aspect of the scapholunate ligament (*curved arrow*). **c** Probe positioning and field-of-view of the US images relative to the dorsal wrist structures
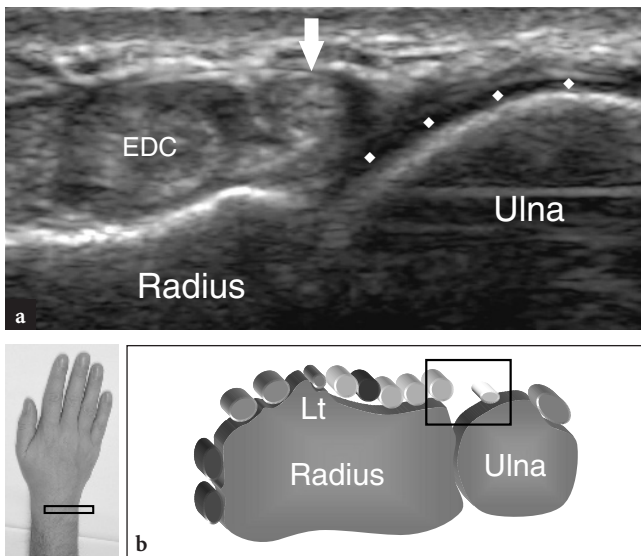
Fig. 10.19 a,b. Extensor tendons: fifth compartment. **a** Transverse 15−7 MHz US image obtained at the distal radio-ulnar joint level reveals the extensor digiti quinti (*arrow*) tendon located medial to the extensor digitorum (*EDC*). Observe the lack of an osseous support for the tunnel of the fifth compartment, which is elevated from the bony surface of the radius and ulna. At the distal radio-ulnar joint level, the ulnar head is covered by articular cartilage (*rhombi*). **b** Probe positioning and field-of-view of the US image relative to the dorsal wrist structures

sor carpi ulnaris. Proximal US images demonstrate a shallow groove in the posteromedial aspect of the distal epiphysis of the ulnar, the extensor retinaculum appearing as a curvilinear anisotropic structure and the extensor carpi ulnaris tendon, located inseide an osteofibrous tunnel (Fig. 10.20). More distally, the tendon can be seen overlying the ulnar styloid,

which appears as a small rounded hyperechoic structure. After leaving the ulna, the extensor carpi ulnaris tendon rests on the dorsal surface of the hamate and then on the base of the fifth metacarpal (Fig. 10.20). Radial deviation of the wrist allows an optimal US depiction of the extensor carpi ulnaris in the longitudinal plane.
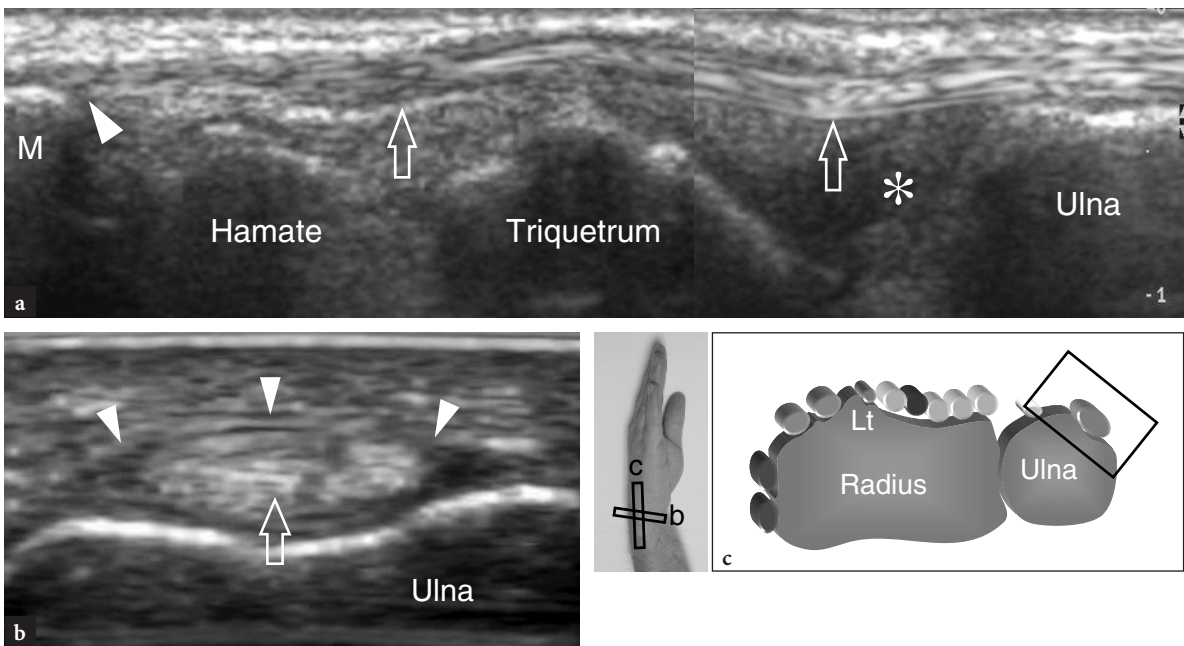
Fig. 10.20 a−c. Extensor tendons: sixth compartment. **a** Long-axis 15−7 MHz US image shows the extensor carpi ulnaris tendon (*arrows*) coursing over the triangular fibrocartilage (*asterisk*), the triquetrum and the hamate to insert into the base of the fifth metacarpal *(M)*. **b** Short-axis 15−7 MHz US image obtained at the level of the ulnar head shows the extensor carpi ulnaris tendon (*arrow*) retained by the retinaculum (*arrowheads*) against the bone. **c** Probe positioning and field-of-view of the US images relative to the dorsal wrist structures
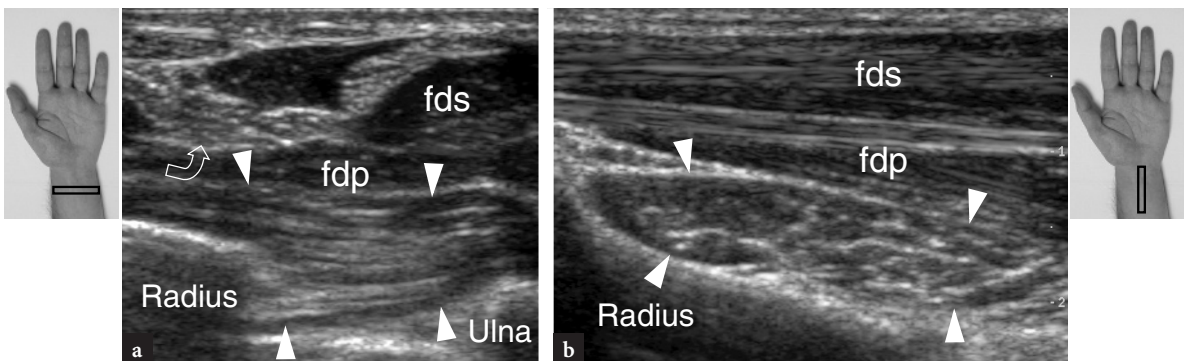
Fig. 10.21a,b. Pronator quadratus muscle. **a** Transverse and **b** longitudinal 15−7 MHz US images obtained at the distal forearm demonstrate the pronator quadratus muscle (*arrowheads*) lying deeply to the flexor digitorum superficialis *(fds)* and profundus *(fdp)*. In **a**, the radial and ulnar insertions of this muscle are depicted. Note that the fibers of the pronator quadratus are oriented perpendicular to those of the overlying flexor digitorum muscles. In addition, this muscle has a squared shape, quite different from the elongated flexors. *Curved arrow*, median nerve. The inserts at the upper sides of the figure indicate probe positioning

10.4.2
Volar Wrist

To evaluate the volar aspect of the wrist, the patient keeps his or her dorsal wrist facing the examination table. A standard US examination usually begins with transverse images obtained from proximal to distal.

10.4.2.1
Scanning the Wrist Outside the Tunnels

The first anatomic level to be examined is over the pronator quadratus muscle. This muscle can be easily detected with US as a hypoechoic muscular belly lying over the volar aspect of the distal metaphyses of

radius and ulna, deep to the flexor muscles and superficial to the distal radio-ulnar joint. As this muscle arises from the volar aspect of the radius to insert into the ulnar head, its fascicles are oriented transversely in contrast to the overlying flexor muscles which are oriented longitudinally (Fig. 10.21). This difference can be clearly appreciated with US by sweeping the probe from longitudinal to transverse planes and vice versa over the distal forearm. More distally, US demonstrates the styloid process of the ulna as a small hyperechoic rounded structure with posterior acoustic shadowing. The gap between the styloid and the radius is filled with the triangular fibrocartilage. This structure can be depicted by means of transverse and oblique coronal images (Fig. 10.22). On both scan planes, the triangular fibrocartilaginous complex appears as a triangular homogeneously hyperechoic area thicker than 2.5 mm (Chiou et al. 1998). At the pronator quadratus level, different tendons can be imaged with US: the flexor digitorum superficialis and flexor digitorum profundus, the flexor pollicis longus, the flexor carpi radialis and flexor carpi ulnaris (Figs. 10.21, 10.23, 10.24). At the radial side of the carpal tunnel, the flexor carpi radialis tendon appears as a hyperechoic oval structure overlying the hyperechoic cortex of the scaphoid. Longitudinal US images demonstrate this tendon as a straight fibrillar structure over the "S"-shaped ventral surface of

the scaphoid (Fig. 10.24b). At the ulnar side of the tunnel, the superficial flexor carpi ulnaris tendon can also be seen (Fig. 10.24d). The location of the distal myotendinous junction of this tendon is variable (Grechenig et al. 2000). The flexor carpi ulnaris has a straight course and can be seen inserting at the proximal pole of the pisiform. In addition, its most superficial fibers may be disclosed as they overlie the pisiform and continue down to reach the pisohamate ligament. Compared with the flexor carpi radialis, the tendon of the flexor carpi ulnaris has a smaller cross-sectional profile.

On gray-scale US images, the ulnar and radial arteries are readily visible because of their pulsatility. The main landmark for the radial artery is the lateral aspect of the flexor carpi radialis while the ulnar artery passes medial to the flexor carpi ulnaris (Fig. 10.23). More distally, the radial artery moves in a lateral position within the subcutaneous tissue, between the skin and the superficial aspect of the pronator quadratus (Fig. 10.24a). As it approaches the distal radius, this artery deepens to pass on the dorsal aspect of the wrist, within the anatomic snuff-box. Its palmar branch can be imaged in the subcutaneous tissue as a small hypoechoic pulsatile structure. Variations in size of the palmar branch are common and this vessel may also appear as large as the radial artery. The ulnar artery can be found in
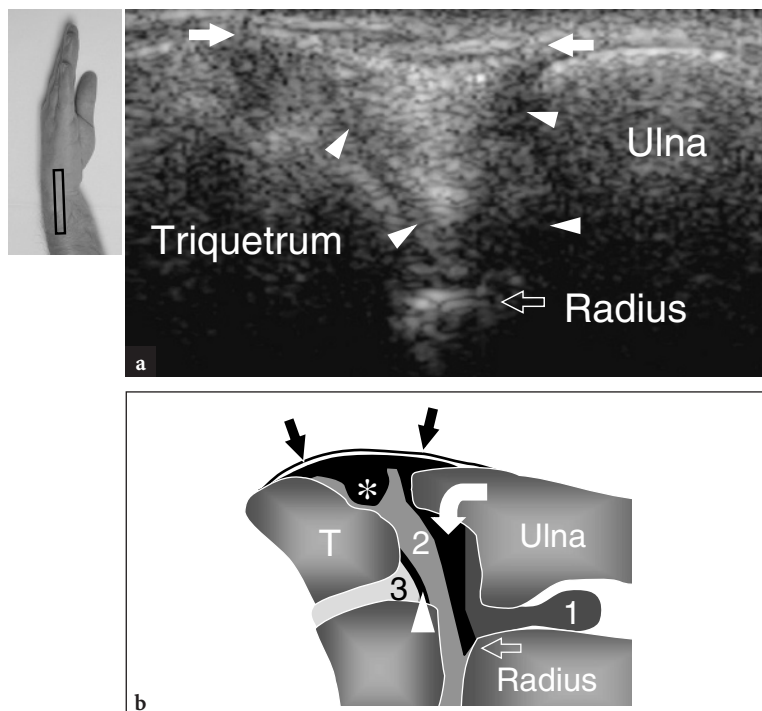
Fig. 10.22a,b. Triangular fibrocartilage complex. **a** Coronal 12–5MHz US image over the ulnar aspect of the wrist with **b** diagram correlation demonstrates a triangular homogeneously hyperechoic space (*arrowheads*) intervening between the triquetrum, the styloid process of the ulna and the radius. On its superficial aspect, this space is delimited by the fibrillar ulnar collateral ligament (*arrows*). US is not able to distinguish the triangular fibrocartilage from the meniscus homologus on the basis of echotextural criteria. In addition, the more proximal portion of the cartilage is partially masked by the acoustic shadowing of the ulnar styloid. In **b**, the relationship between the triangular fibrocartilage (*curved arrow*), meniscus homologus (*asterisk*) and ulnar collateral ligament (*straight arrows*) are shown. Observe the position of these structures relative to the distal radio-ulnar *(1)*, radiocarpal *(2)* and midcarpal *(3)* joints and to the bony landmarks. Arrowhead, lunotriquetral ligament. The insert at the upper left side of the figure indicates probe positioning
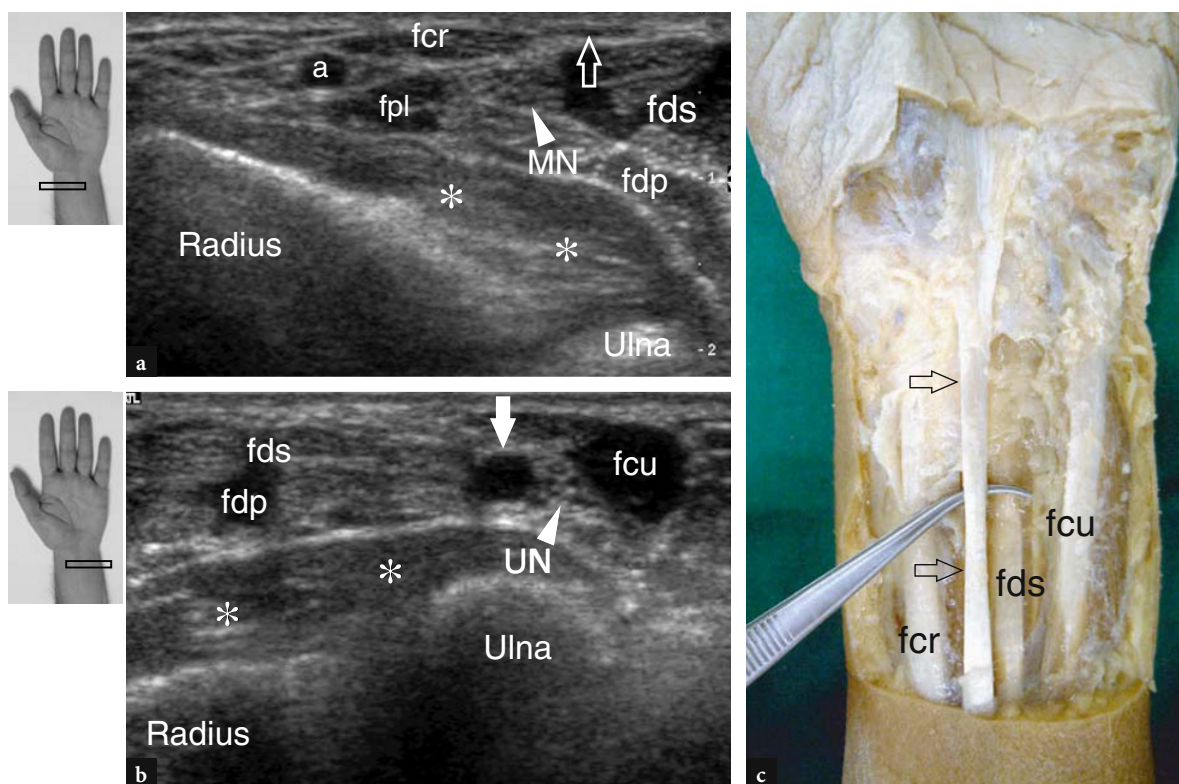
Fig. 10.23 a−c. Ventral wrist structures proximal to the carpal tunnel. Transverse 12−5 MHz US images obtained over the **a** radial and **b** ulnar sides of the proximal wrist (level of radial and ulnar metaphyses) demonstrate the relationship among ventral tendons, nerves and vessels proceeding toward the wrist over the pronator quadratus *(asterisks)*. From lateral to medial, these structures are: the radial artery *(a)*, the flexor carpi radialis *(fcr)* and flexor pollicis longus *(fpl)*, the median nerve *(MN)*, the flexor digitorum superficialis *(fds)* and flexor digitorum profundus *(fdp)*, the ulnar artery *(white arrow)*, the ulnar nerve *(UN)* and the flexor carpi ulnaris *(fcu)*. In **a**, observe the palmaris longus tendon as a very superficial and thin hypoechoic band *(open arrow)* lying medial to the flexor carpi radialis. **c** Gross anatomic view of the ventral wrist shows the relationship of the palmaris longus *(arrows)* with the flexor carpi radialis *(fcr)*, the flexor digitorum superficialis *(fds)* and the flexor carpi ulnaris *(fcu)* tendons. The inserts at the upper left side of the figure indicate probe positioning

a more medial location. Anatomic variations in the number of wrist arteries can be found. The presence of a median artery of the forearm, close to the median nerve, can be readily assessed with US. When evaluating wrist vessels, care should be taken not to apply excessive pressure with the transducer on the artery to avoid its collapse and non-visualization.

Proximal to the carpal and Guyon tunnels, the median and ulnar nerves are recognized based on their peculiar fascicular echotexture. Approaching the wrist, the median nerve becomes more superficial and lateral and then runs toward midline and in a deeper position to enter the carpal tunnel (Jamadar et al. 2001). The palmar cutaneous branch of the median nerve arises from its palmar-radial quadrant approximately 5 cm cranial to the proximal wrist crease (Taleisnik 1973). It remains bound at the main nerve trunk to leave it after approximately

2 cm (Fig. 10.25). After piercing the antebrachial fascia or the transverse carpal ligament and entering the palm, the palmar cutaneous branch of the median nerve supplies the skin of the thenar and midpalmar areas. Awareness of the palmar cutaneous branch is important from the surgical point of vies to avoid inadvertent resection during release of the transverse carpal ligament performed with a too radial approach. Injury of this branch is followed by postoperative sensory disturbances. On short axis planes high-resolution US transducers can image this small nerve division. The ulnar nerve is found at the medial aspect of the distal forearm between the tendon of the flexor carpi ulnaris and the ulnar artery. Because of its close relationship with the ulnar artery, the ulnar nerve can be easily identified by detecting the pulsatility or the presence of color flow signals in the adjacent artery.
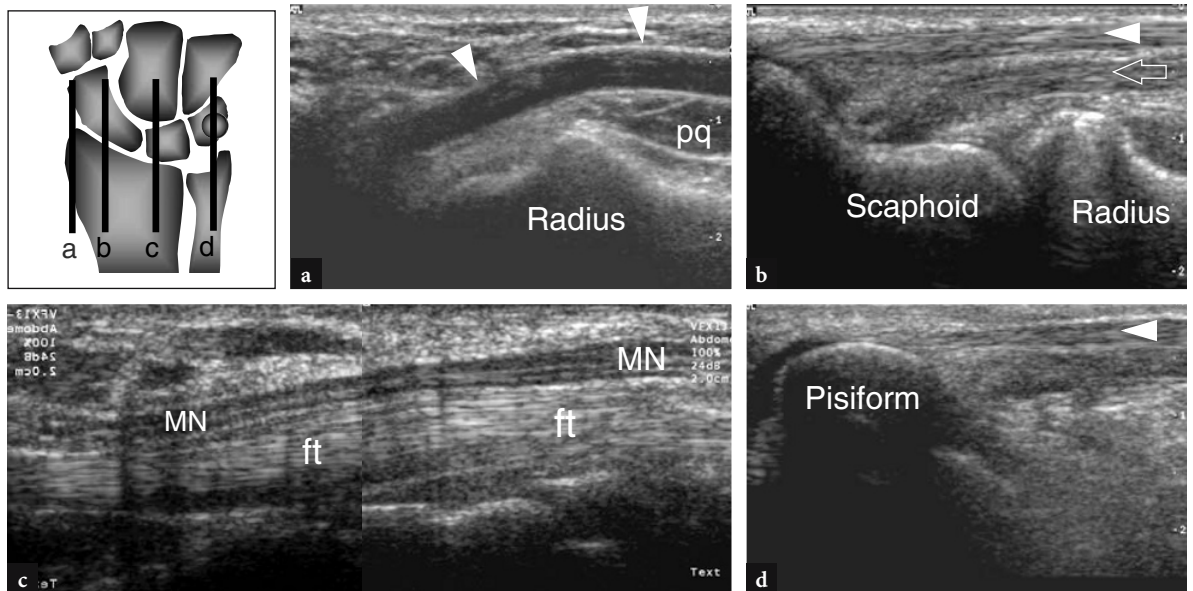
Fig. 10.24 a–d. Longitudinal scanning planes over the ventral wrist obtained with a 12–5 MHz US transducer demonstrate from lateral (**a**) to medial (**d**) according to the reference diagram shown at the upper left side of the figure: **a**, the course of the radial artery (*arrowheads*), which is superficial between the skin and the pronator quadratus *(pq)* and then deepens to enter the anatomic snuff-box; **b**, the diverging course of the flexor carpi radialis (*arrowhead*) and flexor pollicis longus (*arrow*) over the scaphoid bone; **c**, the superficial course of the median nerve *(MN)* relative to the flexor tendons *(ft)* in the carpal tunnel and **d**, the flexor carpi ulnaris tendon (*arrowhead*) which courses superficial to the pisiform
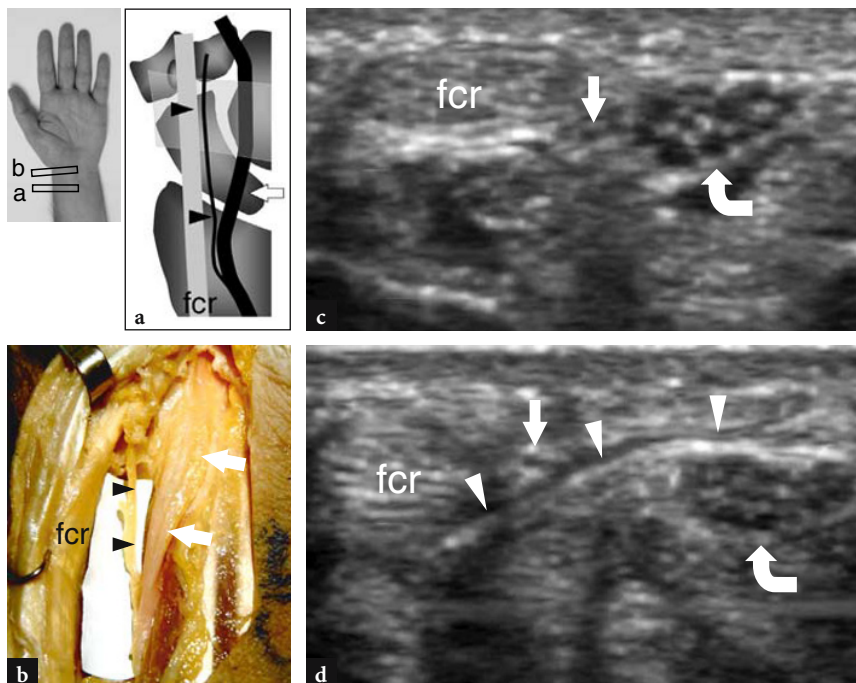
Fig. 10.25 a–d. Palmar cutaneous branch of the median nerve. **a** Schematic drawing of a coronal view through the lateral wrist and **b** corresponding gross anatomic specimen outline the course of the median nerve (*arrows*) and its palmar cutaneous branch (*arrowheads*) relative to the flexor carpi radialis tendon *(fcr)* and the transverse carpal ligament. **c,d** Transverse 15–7 MHz US images obtained **c** at the distal radius and **d** at the proximal carpal tunnel level reveal the palmar cutaneous branch as a small hypoechoic fascicle (*straight arrow*) which leaves the median nerve (*curved arrow*) and pierces the transverse carpal ligament (*arrowheads*) to run between it and the flexor carpi radialis tendon *(fcr)*

10.4.2.2
Proximal Carpal Tunnel

The most useful bony landmarks to identify the proximal carpal tunnel are the pisiform at its ulnar side and the scaphoid at its radial side (Fig. 10.7). At US examination, these bones appear as round hyperechoic structures with posterior acoustic shadowing. Once these landmarks are demonstrated in a single image, the orientation of the probe should be adjusted to optimize the depiction of the soft tissues contained within the tunnel (Fig. 10.26). Tilting the probe back and forth may be helpful to distinguish the hypoechoic median nerve by the adjacent anisotropic tendons. Relative to the flexor carpi radialis, the flexor pollicis longus tendon runs in a deeper location, slightly closer to the midline. Oblique longitudinal US images can depict these tendons in the same plane (Fig. 10.24b). The proximal carpal tunnel is larger in size compared with the distal tunnel. In a comparative US-cadaveric study, US has proved to be accurate in evaluating the different diameters, the outline and the cross-sectional area of the carpal tunnel and the median nerve (Kamolz et al. 2001). The transverse carpal ligament appears as a thin slightly convex band of 1–1.5 mm thickness (Fig. 10.26). Its attachments to the pisiform and the scaphoid are readily detected with US. Because of its curvilinear shape, the anisotropic transverse carpal ligament may appear hypoechoic when the US beam is not perpendicular to it. This is particularly true at its attachments. Even with a careful scanning technique, high-resolution US is unable to depict the lateral division of the transverse carpal ligament which holds the flexor carpi radialis tendon. The nine flexor tendons (four from the flexor digitorum superficialis, four from the flexor digitorum profundus and the flexor pollicis longus) can be imaged inside the carpal tunnel as individual structures (Fig. 10.26). The identification of each of these tendons is easily accomplished based on their anatomic position (radial flexors rest on the radial side of the tunnel, ulnar flexors on the ulnar side) and by their action at dynamic US scanning. Compared with the round cross-sectional profile of the flexor digitorum tendons, the flexor pollicis longus is more oval in shape and its major axis is vertically oriented on transverse planes. At least in part, this may depend on the course of this tendon which diverges radially to reach the thumb. The median nerve courses superficial and parallel to the second and third flexor tendons and medial to the flexor pollicis longus tendon, just deep to the transverse carpal ligament (Fig. 10.26). Its cross-section is usually an ellipse, but its shape may change depending on wrist positions and varies among subjects (Kuo et al. 2001). In addition, even the size of the nerve seems to change relative to the wrist activity (Massy-Westropp et al. 2001). During flexion of the fingers or fist clenching, transverse US images demonstrate passive shifting movements of the median nerve on the underlying gliding flexor tendons (Nakamichi and Takibana 1992).

Some anatomic variants of clinical relevance in the intracanal structures can be identified with US. The presence of anomalous muscles coursing within the carpal tunnel has been reported, includ-
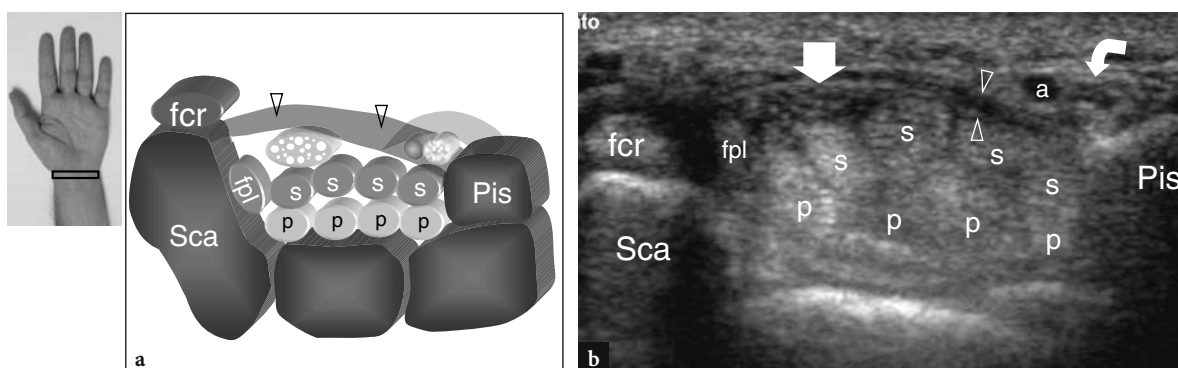
Fig. 10.26 a,b. Proximal carpal tunnel and Guyon tunnel. **a** Schematic drawing and **b** corresponding transverse 12–5 MHz US image show the proximal level of the carpal tunnel delimited by the scaphoid *(Sca)* and the pisiform *(Pis)*. The transverse carpal ligament *(arrowheads)* forms the roof of the carpal tunnel and the floor of the Guyon tunnel. The palmar carpal ligament *(light gray)* forms the volar boundary of the Guyon tunnel. US image demonstrates the tendons of the flexor digitorum superficialis *(s)* and profundus *(p)*, the tendons of the flexor pollicis longus *(fpl)* and flexor carpi radialis *(fcr)* and the median nerve *(straight arrow)* extending through the carpal tunnel, with the nerve lying palmar-radially. At the pisiform level, the ulnar nerve *(curved arrow)* courses medial to the ulnar artery *(a)* within the Guyon tunnel

ing accessory flexor muscles or the proximal extension of lumbrical muscles inserting into the flexor digitorum profundus tendons (Timins 1999). A bifid median nerve (presence of two paired nerves within the carpal tunnel) occurs when the main trunk splits in the distal forearm (Iannicelli et al. 2000, 2001; Propeck et al. 2000). Although the two components of the nerve can diverge proximally, they are most often arranged side by side within the tunnel (Fig. 10.27). The persistent median artery of the forearm is an accessory artery that arises from the ulnar artery at the proximal forearm and accompanies the median nerve along its course throughout the forearm and the carpal tunnel. It can be found in association with either a bifid median nerve or a normal nerve. In the first case, it lies in between the two nerve bundles; in the second, it runs on the ulnar side of the nerve (Figs. 10.28, 10.29). When associated to a bifid nerve, the artery and the nerve bundles may be enveloped by a common epineurium or may course freely, as separate structures. Anatomic studies have demonstrated the median artery in as many as 20% of cadaveric dissections (Rodriguez-Niedenfuhr et al. 1999). The presence of a median artery can be easily assessed with US and should be detailed in the report. In fact, the hand surgeon must be alerted to the presence of these anomalies because the nerve and the artery can be injured during arthroscopic release of the transverse carpal ligament.

10.4.2.3
Distal Carpal Tunnel

The main bony landmarks of the distal carpal tunnel are the tubercle of the trapezium at its radial side and the hook of the hamate at its ulnar side (Fig. 10.7). The trapezium is easily recognized because of its flat palmar surface, while the small curvilinear profile of the hamate hook is located closer to the midline with respect to the pisiform. Due to a more central location of the hamate hook, the distal tunnel is considerably smaller than the proximal one. In addition, the distal transverse carpal ligament is thicker at this level and has a straight appearance. As the tunnel becomes progressively narrower from proximal to distal, the median nerve tends to assume a more flattened appearance distally. Deep to the nerve, the flexor tendons are more difficult to differentiate from each other because they are closely apposed (Fig. 10.30). In addition, they lie in a deeper position, closely related to the volar capsule of the midcarpal joint. By sweeping the transducer on the radial side of the tunnel, the tendon of the flexor carpi radialis can be imaged inside a narrow groove under the tubercle of the trapezium. The flexor pollicis longus tendon is detected immediately medial to it. The overall size of the nerve can be subjectively estimated by comparing its cross-section with the underlying tendons. The fascicular echotexture of the median nerve is more evident proximally, at the entrance of the tunnel, where the nerve runs parallel to the skin and perpendicular to the US beam, than in the distal tunnel where the nerve has an oblique downward course. Tilting probe orientation or slight flexion of the wrist should be performed while evaluating the internal structure of the median nerve in the distal carpal tunnel. After exiting the distal edge of the transverse carpal ligament, the median nerve divides into two or three branches, the common palmar digital nerves, from which the digital nerves arise as terminal divisions for the opposite sides of the fingers (Fig. 10.31).
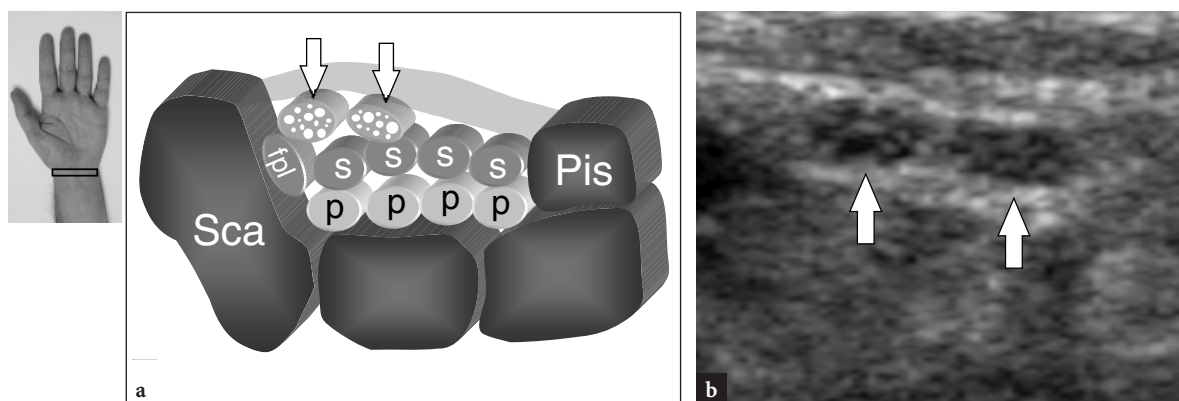
Fig. 10.27 a,b. Bifid median nerve. **a** Schematic drawing and **b** corresponding transverse 12−5 MHz US image over the ventral wrist in an asymptomatic subject reveal the radial and ulnar trunks (*arrows*) of a bifid median nerve. *Sca*, scaphoid; *Pis*, pisiform; *fpl*, flexor pollicis longus tendon; *p* and *s*, the tendons of the flexor digitorum profundus and superficialis
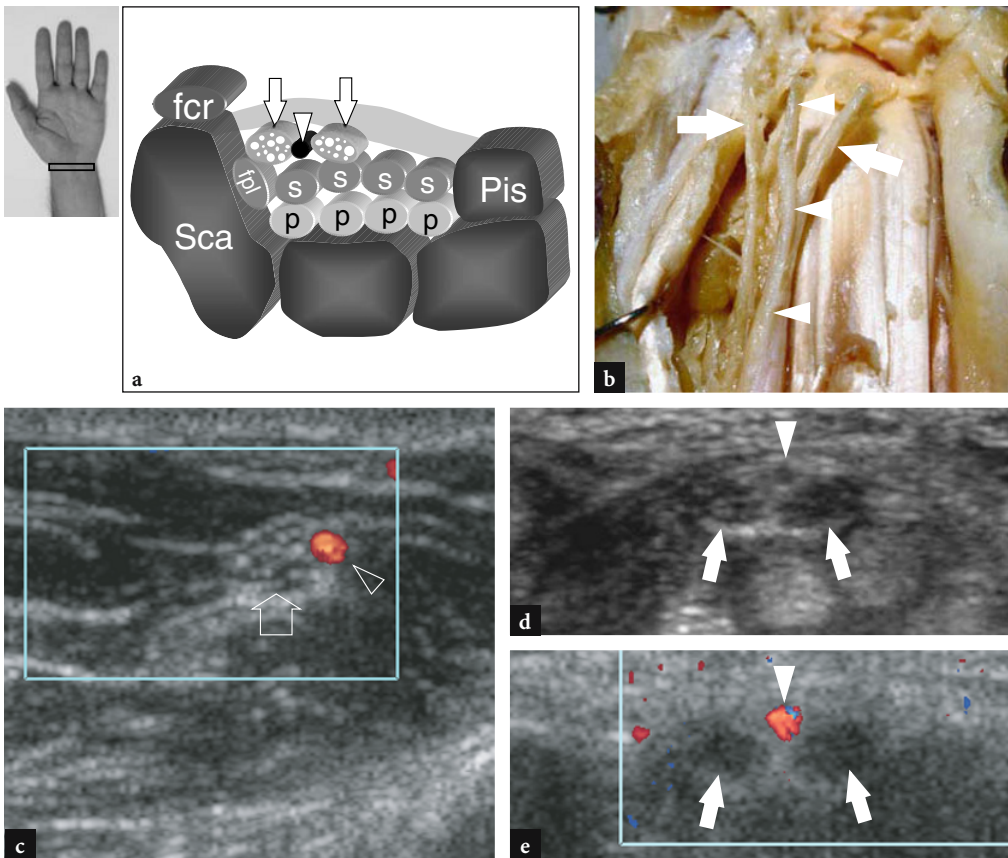
Fig. 10.28 a–e. Persistent median artery of the forearm and bifid median nerve. **a** Schematic drawing in the axial plane and **b** gross anatomic coronal view of the carpal tunnel outline the course of a persistent median artery (*arrowheads*) interposed between the two trunks (*arrows*) of a bifid median nerve. **c** Transverse 12−5 MHz US image obtained at the middle forearm show the relationship of the persistent median artery (*arrowhead*) with the median nerve (*arrow*). Observe that the median nerve is not yet divided at mid-forearm level. Transverse **d** gray-scale and **e** color Doppler 12−5 MHz US images obtained at the proximal carpal tunnel level of the same case shown in **c** demonstrate the median artery (*arrowhead*) located between the radial and ulnar trunks (*arrows*) of a bifid median nerve. Note that the two nerve trunks and the artery are enveloped by a common epineurium. The patient had mild intermittent symptoms related to carpal tunnel syndrome. *Sca*, scaphoid; *Pis*, pisiform; *fcr*, tendons of the flexor carpi radialis; *fpl*, flexor pollicis longus tendon; *p* and *s*, tendons of the flexor digitorum superficialis and profundus
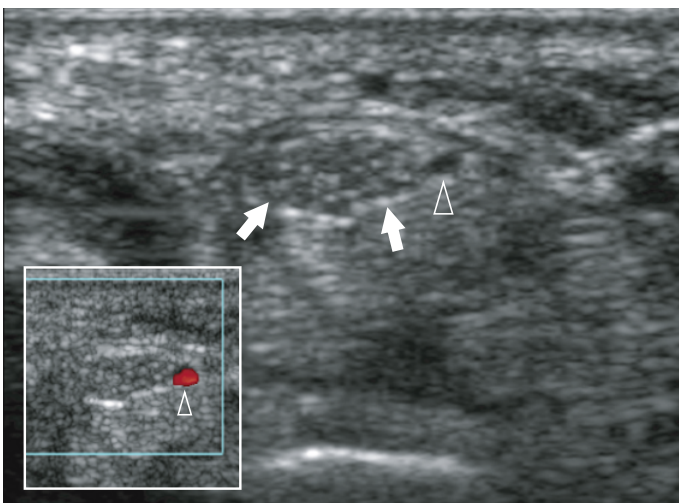
Fig. 10.29. Persistent median artery of the forearm. Transverse gray-scale 12−5 MHz US image of the proximal carpal tunnel in an asymptomatic subject reveals a persistent median artery (*arrowhead*) on the ulnar side of the median nerve (*arrows*). Note the anechoic appearance of the artery relative to the hypoechoic nerve fascicles. In the insert at the lower right side of the figure color Doppler imaging demonstrates flow signals inside the vessel
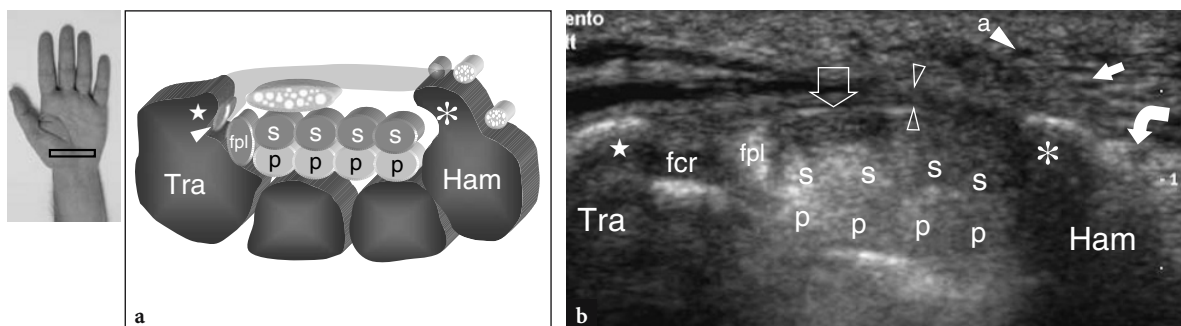
Fig. 10.30 a,b. Distal carpal tunnel. **a** Schematic drawing and **b** corresponding transverse 12−5 MHz US image show the distal level of the carpal tunnel delimited by the trapezium *(Tra)* and the hamate *(Ham)*. The transverse carpal ligament *(open arrowheads)* inserts on the tubercle *(star)* of trapezium and the hook *(asterisk)* of the hamate. US image demonstrates the tendons of the flexor digitorum superficialis *(s)* and profundus *(p)*, the tendons of the flexor pollicis longus *(fpl)* and flexor carpi radialis *(white arrowhead* in **a**, *fcr* in **b**) and the median nerve *(open arrow)*. At the hamate level, the transverse carpal ligament is thicker than at the proximal carpal tunnel (see for comparison Fig. 10.26b) and the ulnar nerve divides into two terminal branches: a deep motor *(curved arrow)* and a superficial sensory *(straight white arrow)* branch. *a*, ulnar artery
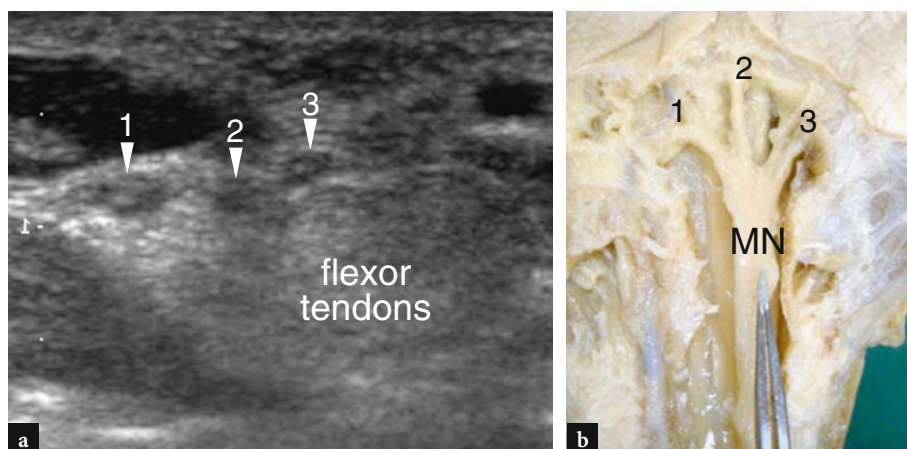
Fig. 10.31a,b. Median nerve beyond the carpal tunnel. **a** Transverse 12−5 MHz US image obtained beyond the distal edge of the transverse carpal ligament with **b** gross anatomic correlation reveals the division of the main trunk of the median nerve *(MN)* into three branches (*1, 2, 3*), the common palmar digital nerves

10.4.2.4
Guyon Tunnel

The Guyon tunnel is located in a medial and superficial position relative to the carpal tunnel. It is delimited by the dorsal aspect of the transverse carpal ligament and the superficial palmar carpal ligament on the radial side, and by the lateral aspect of the pisiform on the ulnar side. The transverse carpal ligament and the pisiform are easily detected with US. On the contrary, the superficial palmar carpal ligament is very thin and difficult to visualize. Once the curvilinear shape of the pisiform is found, care should be taken to identify the ulnar artery as a round, pulsatile hypoechoic structure. The ulnar nerve lies in between these two structures and can be better depicted by means of subtle tilting movements of the probe. It appears as a small structure of 2−2.5 mm in size, containing a few internal hypoechoic fascicles (Fig. 10.32a,b). The most commonly encountered anomalous muscle in the tunnel is the accessory abductor digiti minimi (Timins 1999) (see Sect. 10.5.4.4). Distal to the pisiform, the distal Guyon tunnel can be imaged with very high-resolution transducers. At this level, the ulnar nerve can be seen dividing into two terminal branches: the superficial sensory branch continues to run close to the ulnar artery, whereas the deep
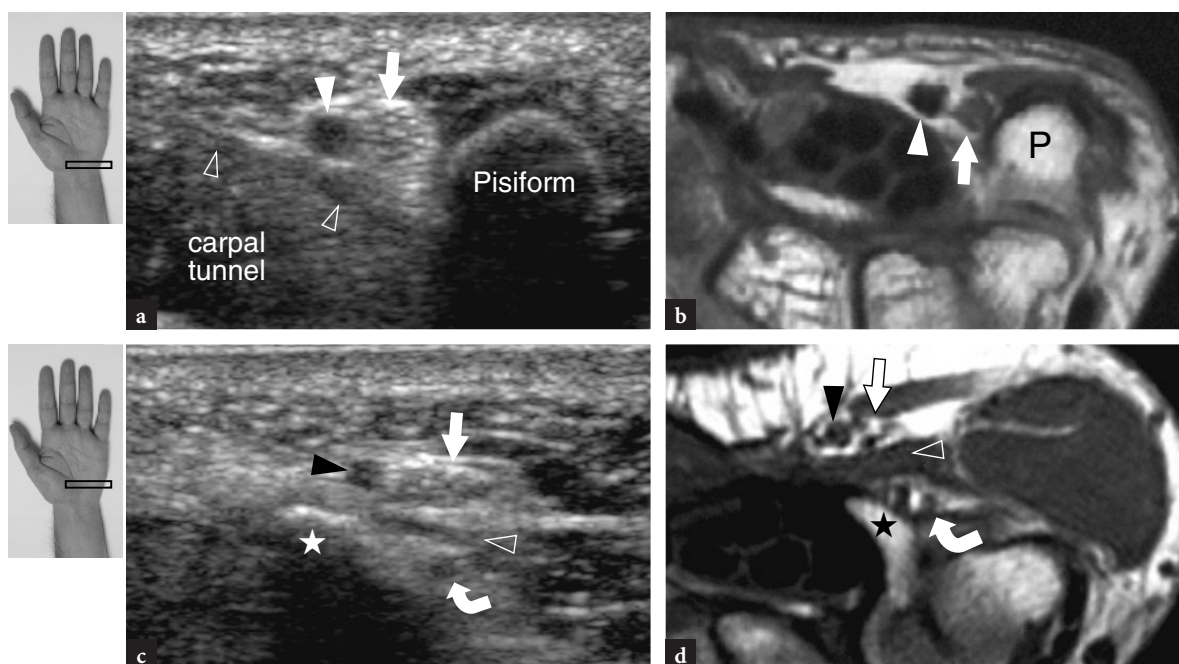
Fig. 10.32 a–d. Guyon tunnel. **a,c** Transverse 15–7 MHz US images with **b,d** corresponding transverse T1w SE MR imaging correlation show **a,b** the proximal Guyon tunnel at the pisiform *(P)* level, and **3092** the distal tunnel indicated by the hamate hook *(star)*. **a,b** High-resolution US demonstrates the main trunk of the ulnar nerve *(white arrow)* located between the ulnar artery *(white arrowhead)* and the pisiform, just superficial to the transverse carpal ligament *(open arrowheads)*. **c,d** More distally, the superficial sensory *(straight arrow)* and deep motor *(curved arrow)* branches of the ulnar nerve are visualized one over the other. Note a slip from the flexor digiti minimi brevis *(open arrowheads)* intervening between the superficial and deep nerve branches and the closer relationship of the deep nerve branch with the outside slope of the hamate hook *(star)*. *Black arrowhead*, superficial ulnar artery. The inserts at the upper left side of the figure indicate probe positioning.

motor branch courses alongside the medial surface of the hamate hook (Fig. 10.32c,d). Similarly, the ulnar artery splits into two branches, superficial and deep, each following the respective nerves bundles.

10.5
Wrist Pathology

10.5.1
Dorsal Wrist Pathology

Tendinitis and tendinopathies of the dorsal wrist are common and account for a high percentage of consultations in hand surgery. They can be related to local causes, particularly overuse due to sport or occupational activities, or may be the result of systemic musculoskeletal disorders. Because the tendons of the dorsal wrist are invested by a synovial sheath, the term "tenosynovitis" is more correct to define most of these conditions. Typical sites of dorsal wrist

tendinopathy include: the radial styloid for the extensor tendons of the first compartment (de Quervain disease); the level in which the extensor carpi radialis brevis and longus are crossed by the abductor pollicis longus and extensor pollicis brevis (intersection syndrome); the area around the Lister tubercle for the extensor pollicis longus tendon; the ulnar head region for the extensor carpi ulnaris (Fig. 10.33a) (DAENEN et al. 2004). Since the extensor tendons tear more commonly in the hand than at wrist, this topic will be more specifically addressed in Chapter 11.

10.5.1.1
De Quervain Disease

De Quervain disease is a typical example of overuse tenosynovitis of the wrist. This condition usually affects patients who perform repetitive movements of the thumb such as typists and piano players. New mothers are also commonly affected as a result of repeated extension and flexion of the wrist with
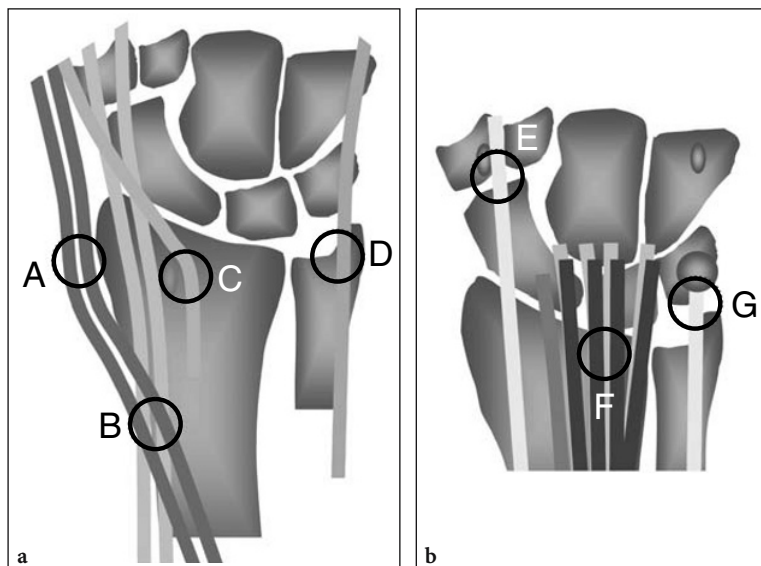
Fig. 10.33 a,b. Schematic drawings illustrate typical sites of overuse tendinopathies in the **a** dorsal and **b** ventral wrist, including: *A*, de Quervain tenosynovitis; *B*, intersection syndrome; *C*, extensor pollicis longus tenosynovitis, *D*, extensor carpi ulnaris tenosynovitis; *E*, flexor carpi radialis tenosynovitis; *F*, flexor digitorum superficialis and flexor digitorum profundus tenosynovitis; *G*, flexor carpi ulnaris tendinopathy

abduction of the thumb against resistance, such as occur while holding the baby's head (Baby Wrist) (ANDERSON et al. 2004). Low grade chronic microtrauma at the level of the radial styloid can lead to localized thickening of the extensor retinaculum of the wrist, narrowing of the first compartment of the extensor tendons and subsequent impingement and inflammation of the extensor pollicis brevis and abductor pollicis longus tendons. Clinically, patients complain of tenderness and pain over the radial styloid exacerbated by wide movements of the thumb and forceful pinching of objects. As already described in Sect. 10.3.1, a useful diagnostic test, the Finkelstein test, is performed by applying passive ulnar deviation of the wrist with the thumb maximally flexed, a maneuver that aggravates the patient's pain. Treatment of de Quervain disease relies on anti-inflammatory drugs and splinting. Resistant cases are treated with more invasive approaches such as local injections and surgical release of the retinaculum. A vertical septum splitting the first compartment seems to predispose to local tendon friction and is encountered more frequently in patients than in cadaver surveys (BAHM et al. 1995). Several authors have described the US appearance of de Quervain disease (GOODING 1988; MARINI et al. 1994; NAGAOKA et al. 2000; TRENTANNI et al. 1997; GIOVAGNORIO et al. 1997). Both longitudinal and transverse US images are performed over the radial styloid. Although lon-

gitudinal planes are more valuable during dynamic scanning, transverse images give a better view of the retinaculum, internal septa and accessory tendons. The affected tendons are typically swollen and, as a whole, they have a more rounded cross-section under the retinaculum than in normal subjects (Figs. 10.34, 10.35). In acute phases, a synovial sheath effusion surrounding the tendons can be demonstrated caudal to the distal edge of the retinaculum, whereas in chronic longstanding disease the extensor tendons may appear hypoechoic or may have a heterogeneous echotexture. A thickened and hypoechoic extensor retinaculum should be accurately searched for at US because its demonstration can indicate the need for surgical decompression. Accessory vertical septa appear as thin vertical hypoechoic bands intervening between the tendons (NAGAOKA et al. 2000). Demonstration of a vertical septum has clinical implications because it acts as a barrier to diffusion of injected steroids and requires opening of both tunnels at surgery (LESLIE et al. 1990). In some cases, the inflammatory process may selectively involve one tendon when a septum is present (Fig. 10.36). In a postoperative setting, high-resolution US can identify complications, such as the volar subluxation of tendons due to an excessive section of the retinaculum (Fig. 10.37). In conclusion, although the clinical diagnosis of de Quervain tenosynovitis is not difficult, US can help to confirm it, detect whether a vertical septum is
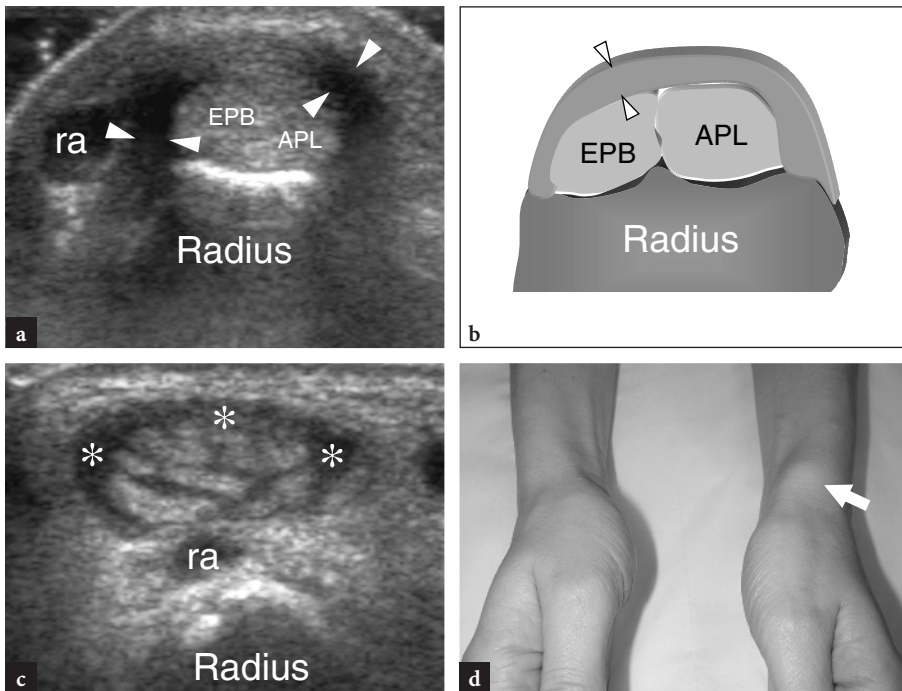
Fig. 10.34a−d. de Quervain disease. **a** Transverse 12−5MHz US image obtained over the radial styloid with **b** corresponding schematic drawing shows marked thickening and hypoechoic appearance of the retinaculum of the first compartment (*arrowheads*). Inside the tunnel, the extensor pollicis brevis *(EPB)* and abductor pollicis longus *(APL)* tendons are increased in size as a result of edematous changes. They cannot be distinguished from one another because are pressed within the confined space of the osteofibrous tunnel and have a more rounded profile with respect to their normal appearance shown in Fig. 10.11a. **c** Short-axis 12−5 MHz US image obtained distal to the retinaculum reveals accessory tendons in the first compartment and mild sheath effusion (*asterisks*). Outside the tunnel, observe the decompressed appearance of the extensor tendons. **d** Photograph of the wrist of the same patient shows localized swelling (*arrow*) over the radial styloid. *ra*, radial artery
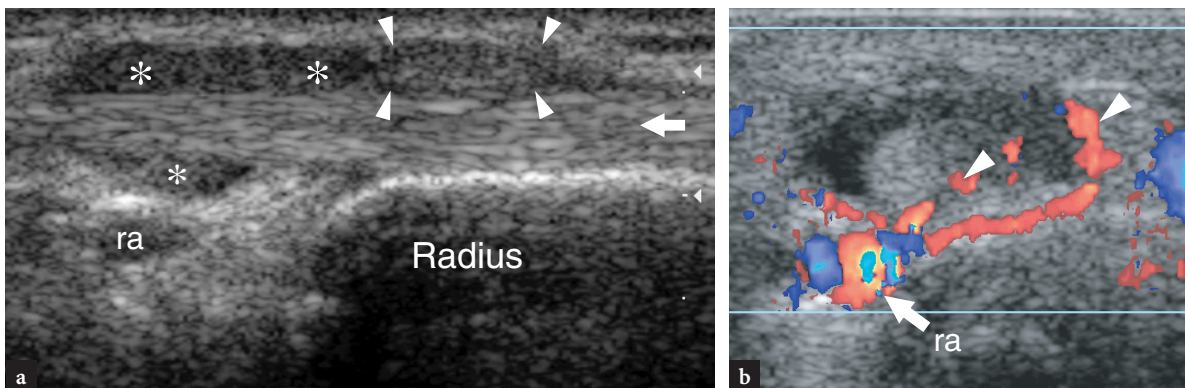
Fig. 10.35 a,b. de Quervain disease. **a** Long-axis 12−5 MHz US image obtained over the first compartment reveals the main signs of disease, including a thickened and hypoechoic retinaculum (*arrowheads*) and synovial hypertrophy and effusion (*asterisks*) in the sheath of the extensor tendons (*arrow*). Note the position of the retinaculum, which lies over the radial styloid to retain the extensor tendons against it, and the cross-sectional appearance of the radial artery *(ra)* while it crosses the first compartment to reach the dorsal wrist. **b** Color Doppler US image shows a hypervascular pattern made of flow signals distributed around the tendon sheath and within the tendon itself (*arrowheads*) due to inflammatory hyperemia. Note the origin of these vessels from the adjacent radial artery *(ra)*
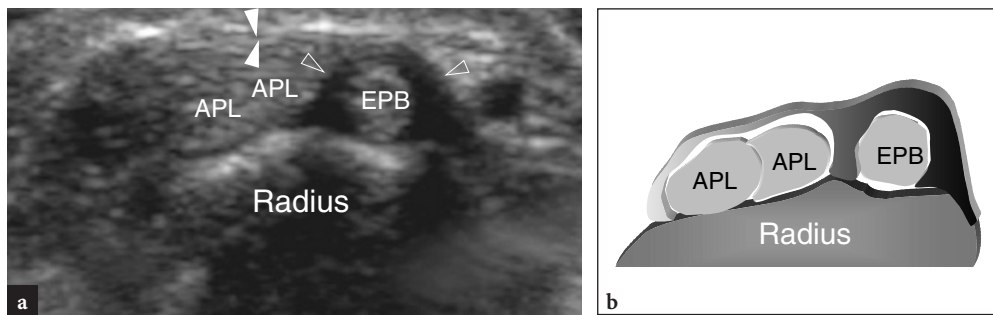
Fig. 10.36 a,b. Incomplete de Quervain disease. **a** Transverse 12−5 MHz US image obtained over the radial styloid with **b** corresponding schematic drawing in a patient with acute clinical symptoms of de Quervain disease demonstrates selective thickening of the dorsal portion of the retinaculum (*open arrowheads*) and the vertical septum (*open arrowheads*) enveloping the extensor pollicis brevis tendon *(EPB)*, whereas the more ventral portion of the retinaculum (*white arrowheads*) and the abductor pollicis longus tendons *(APL)* retain a normal appearance. In such case, the injection of corticosteroids was selectively directed to the sheath of the extensor pollicis brevis
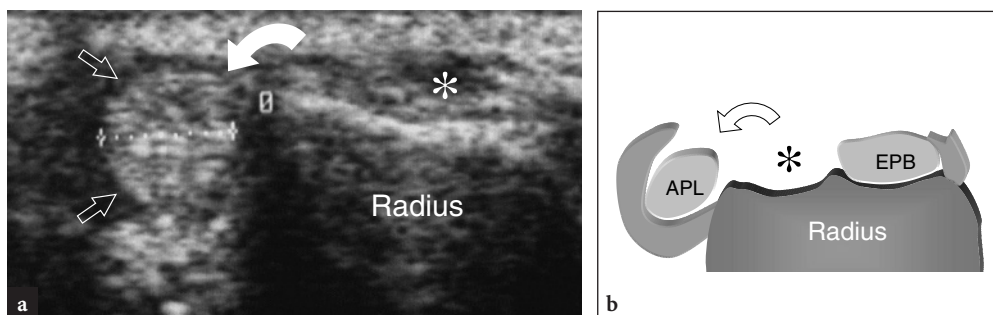
Fig. 10.37 a,b. Postoperative complication in de Quervain disease after surgical release of the retinaculum. Transverse 10−7.5 MHz US image obtained over the radial styloid with **b** corresponding diagram shows palmar dislocation (*curved arrow*) of the abductor pollicis longus tendon (*straight arrows*) following excessive section of the retinaculum of the first extensor compartment. Note the empty groove (*asterisk*) on the radial styloid. The patient, a professional pianist, had considerable limitation in her activity

present, and assess postsurgical complications such as tendon instability.

10.5.1.2
Wartenberg Disease

The neuropathy affecting the superficial terminal branch of the radial nerve at the wrist is known as Wartenberg disease. This fairly common condition may be secondary to trauma or iatrogenic event, such as intravenous infusion, instability of the triangular fibrocartilage and nerve entrapment between the brachioradialis and the extensor carpi radialis longus tendons, most often occurring during activities that require forearm pronation with simultaneous flexion and ulnar deviation of the hand. The increased tension on the nerve causes ischemia, local inflammation and pain. Differentiation of Wartenberg neuropathy from de Quervain tenosynovitis or arthritis of the trapeziometacarpal joint is not clinically straight-

forward. In fact, these conditions may present with pain over the dorsoradial surface of the wrist and distal forearm radiating distally to the dorsum of the hand and thumb. High-resolution US examination is able to depict subtle abnormalities of the superficial cutaneous branch of the radial nerve following stretching or traumatic injures (Fig. 10.38). Therapy for Wartenberg disease depends on both local and causative factors. Corticosteroid injection at the site of tenderness along the nerve is the treatment of choice because it is effective with minimal distress to the patient. Since the superficial terminal branch of the nerve becomes entrapped at end-range pronation, this motion should be avoided.

10.5.1.3
Intersection Syndrome

Intersection syndrome is due to irritation of the two radial extensors of the wrist – the extensor carpi
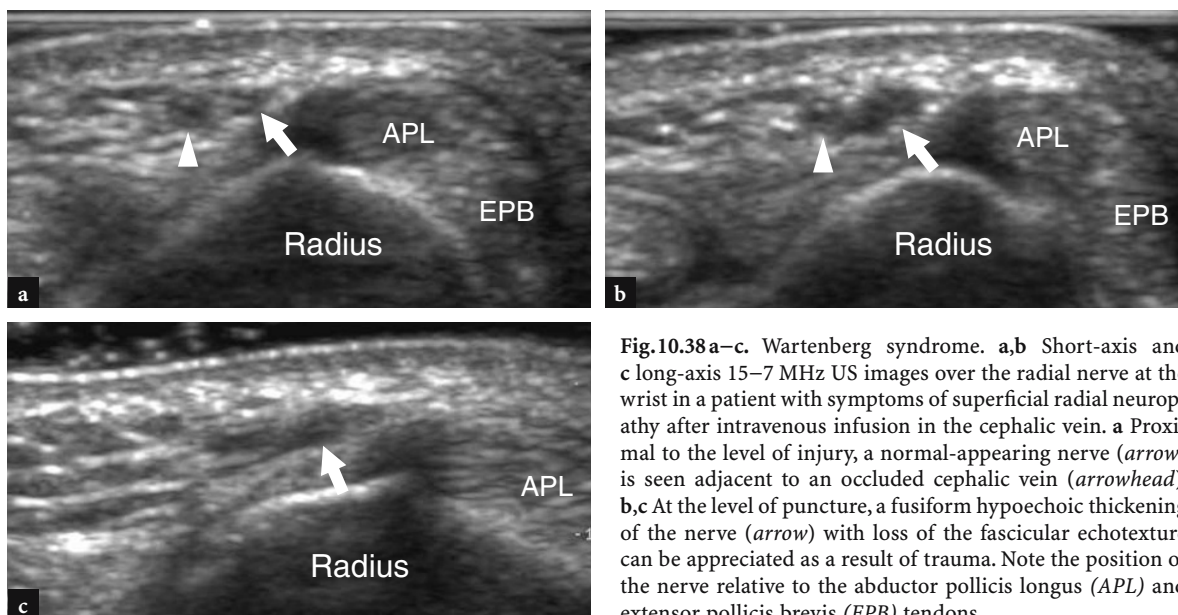
Fig. 10.38 a–c. Wartenberg syndrome. **a,b** Short-axis and **c** long-axis 15−7 MHz US images over the radial nerve at the wrist in a patient with symptoms of superficial radial neuropathy after intravenous infusion in the cephalic vein. **a** Proximal to the level of injury, a normal-appearing nerve (*arrow*) is seen adjacent to an occluded cephalic vein (*arrowhead*). **b,c** At the level of puncture, a fusiform hypoechoic thickening of the nerve (*arrow*) with loss of the fascicular echotexture can be appreciated as a result of trauma. Note the position of the nerve relative to the abductor pollicis longus (*APL*) and extensor pollicis brevis (*EPB*) tendons

radialis longus and the extensor carpi radialis brevis – at the level at which they are crossed by the abductor pollicis longus and extensor pollicis brevis. This condition is usually secondary to occupational repetitive flexions and extensions of the wrist, such as occur in rowers and weightlifters. The clinical diagnosis is not straightforward because intersection syndrome may be easily confused with the more distal de Quervain disease. Wrist splints and local steroid injections are curative in most patients. Intersection syndrome appears at US as an ill-defined hypoechoic area between the two tendon groups, probably corresponding to local soft-tissue edema and tenosynovial fluid, with loss of the hyperechoic cleavage plane between them (Fig. 10.39). A true synovial bursa filled by fluid is a rare finding.

10.5.1.4
Extensor Pollicis Longus Tenosynovitis

As already stated, the extensor pollicis longus tendon (third compartment of the extensor tendons) is a thin tendon that reflects over the medial aspect of the Lister tubercle before reaching the dorsum of the hand. Because of mechanical friction and its small size, the extensor pollicis longus is frequently affected by tenosynovitis that presents with local pain over the Lister tubercle and, less commonly, with local crepitus during thumb movements. This condition can be associated with previous fractures of the distal radius

(DENMAN 1979) and leads to considerable tendon weakness, partial and complete tears if untreated. In extensor pollicis longus tenosynovitis, the synovial sheath effusion is typically found just proximal to the Lister tubercle and after the tendon has crossed the extensor carpi radialis longus (Fig. 10.40). Due to the restricted space under the fascia, the synovial sheath of this tendon may be distended with fluid in the area of the Lister tubercle and over the radial wrist extensors only when the amount of effusion is remarkable.

10.5.1.5
Extensor Carpi Ulnaris Tenosynovitis

Extensor carpi ulnaris tenosynovitis is mostly secondary to instability of the retinaculum of the sixth compartment, as a result of mechanical friction of this tendon against the ulna. The patient typically complains of a localized pain over the dorsum of the ulna. Clinical findings are nonspecific and can mimic disorders of the distal radio-ulnar joint, especially when a snapping sensation is present. Although high-resolution US cannot accurately recognize distal radio-ulnar joint pathology, it can readily measure the tendon size, and is able to identify intrasubstance longitudinal splits related to recurrent tendon subluxation and to evaluate tendon sheath effusion and synovial hypertrophy (Figs. 10.41, 10.42). The relevance of a dynamic examination has to be emphasized in this setting.
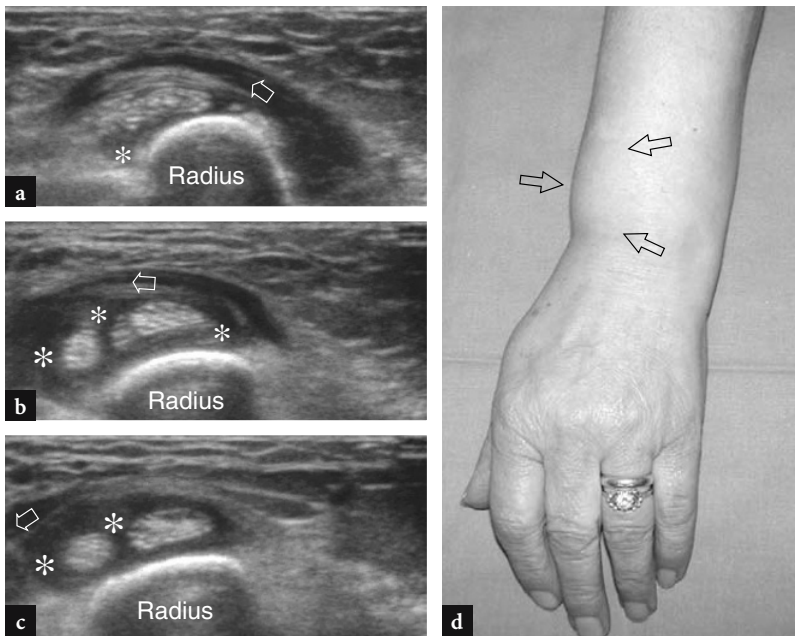
Fig. 10.39 a–d. Intersection syndrome. **a–c** Serial sequence of transverse 12–5 MHz US images obtained from **a** cranial to **c** caudal over the distal dorsal forearm demonstrate tenosynovial effusion (*asterisks*) in the sheath of the extensor carpi radialis longus and brevis at the level in which these tendons are crossed (*arrow*) by the muscle bellies of the abductor pollicis longus and extensor pollicis brevis. Note the loss of the hyperechoic fat plane intervening between these two tendon groups. See Fig. 10.15a for comparison with normal findings. **d** Photograph of the forearm and wrist of the same patient shows soft-tissue swelling (*arrows*) at the radial aspect of the distal dorsal forearm
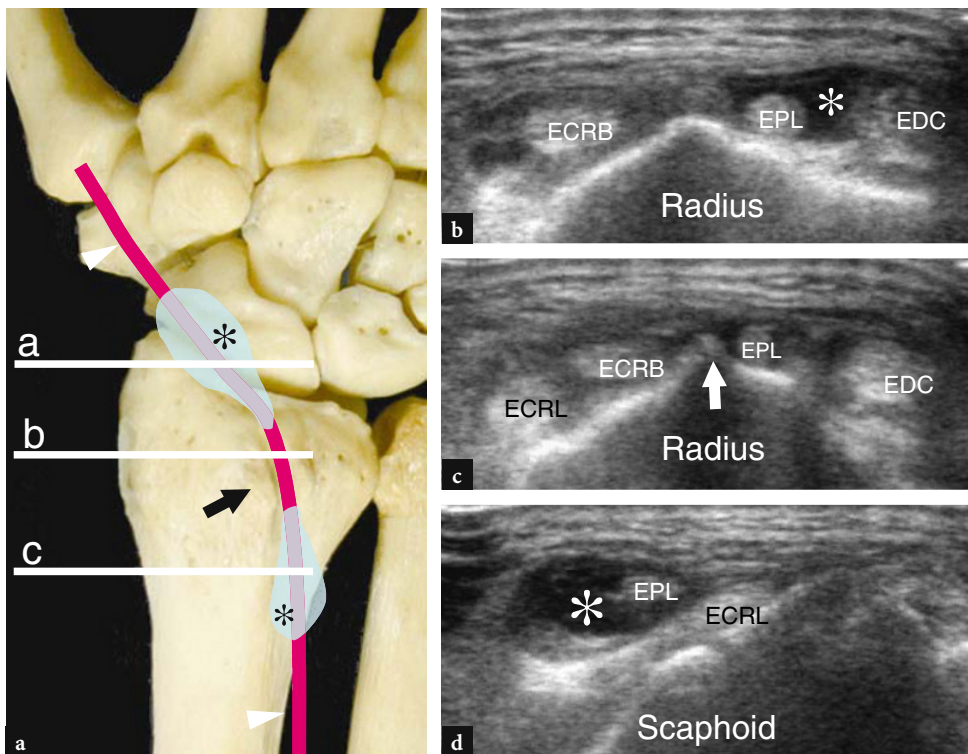
Fig. 10.40 a–d. Extensor pollicis longus tenosynovitis. **a** Dorsal aspect of the wrist bones illustrates the course of the extensor pollicis longus tendon (*arrowheads*) relative to the Lister tubercle (*arrow*) and the typical clepsydra-like distribution of sheath fluid (*asterisks*) in a case of tenosynovitis. The narrow tunnel of the third compartment intrinsically hinders the sheath distension of the extensor pollicis longus at the level of the Lister tubercle except in cases of abundant effusion. Most often, the fluid distributes just proximal to the Lister tubercle and after the tendon has crossed the extensor carpi radialis longus. **b–d** Transverse 15–7 MHz US images over the third compartment of the extensor tendons obtained at the levels (*horizontal white bars*) indicated in a show the typical distribution of fluid (*asterisk*) in the sheath of the extensor pollicis longus tendon *(EPL)* relative to the Lister tubercle (*arrow*) and the extensor carpi radialis brevis *(ECRB)* and longus *(ECRL)*. *EDC*, extensor digitorum tendons
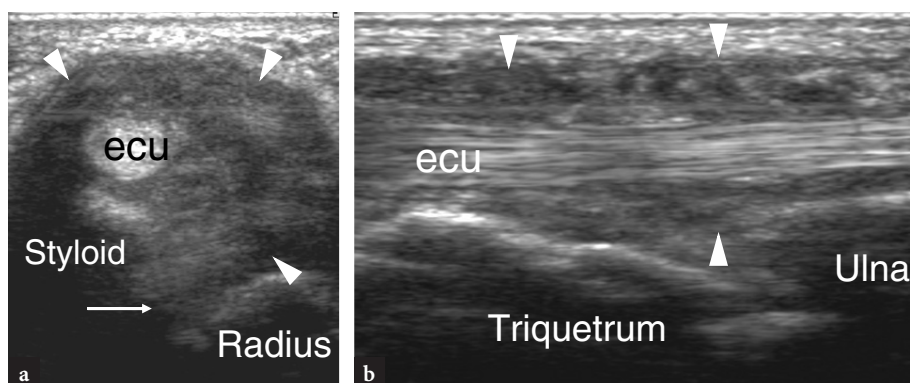
Fig. 10.41 a,b. Hypertrophic tenosynovitis of the extensor carpi ulnaris in a patient with rheumatoid arthritis. **a** Short-axis and **b** long-axis 12–5 MHz US images of the extensor carpi ulnaris tendon (*ecu*) reveal hypoechoic synovial pannus (*arrowheads*) which causes abnormal distention of the synovial sheath. The extensor carpi ulnaris is displaced anteriorly because of loosening of the retinaculum. Note the pannus filling the distal radioulnar joint cavity (*arrow*)
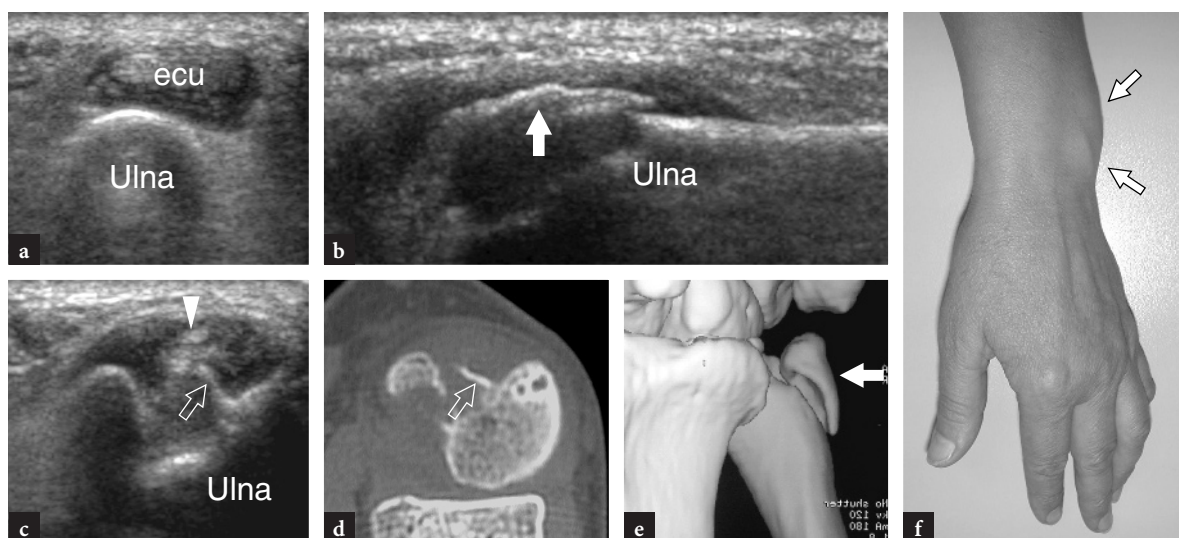
Fig. 10.42 a–f. Post-traumatic partial tear of the extensor carpi ulnaris tendon. The patient presented at US examination with negative radiographic studies and persistent pain and tenderness over the wrist lasting 15 days after the trauma. **a** Transverse and **b** longitudinal 12–5 MHz US images over the dorsal aspect of the ulnar head show a swollen extensor carpi ulnaris tendon (*ecu*) and a radiographically occult fracture of the ulnar styloid (*white arrow*) with displacement of a small fragment of bone. **c** Transverse 12–5 MHz US image obtained at the level of the ulnar fracture with **d** CT scan and **e** 3D reconstructed image correlation reveals fracture of the ulnar styloid (*white arrow*) and a bone fragment (*open arrow*) causing impingement on the adjacent extensor carpi ulnaris tendon (*arrowhead*). Note the tendon thinning at the level of bone impingement suggesting a partial tear. **f** Photograph of the same patient shows marked soft-tissue swelling (*arrows*) at the ulnar side of the wrist

10.5.1.6
Extensor Carpi Ulnaris Instability

The retinaculum most commonly torn at the wrist is that of the sixth osteofibrous tunnel which retains the extensor carpi ulnaris tendon in a correct position during rotation and flexion-extension movements of the forearm. This retinaculum tears as a result of acute trauma, chronic overuse and inflammatory changes in the extensor carpi ulnaris tendon sheath, such as in rheumatoid arthritis. Acute and chronic tears can be observed in sport injuries, including tennis practice, where the player performs a powerful pronation from a supinated position. This causes a sudden contraction of the extensor carpi ulnaris which stabilizes the ulnar

head, and may lead to stripping of the retinaculum. Tear of the retinaculum related to rheumatoid arthritis will be discussed later (see Sect. 10.5.3.2), because this finding is closely related to the involvement of the distal radio-ulnar joint and the extensor carpi ulnaris tendon sheath. Regardless of the cause of retinaculum tear, the extensor carpi ulnaris tendon undergoes anterior (volar) dislocation. The instability of the extensor carpi ulnaris may result in either subluxation, when the flattened tendon moves over the medial aspect of the ulna, or intermittent dislocation, when there may be either spontaneous phases of dislocation and reduction, or permanent dislocations. Because of its high-resolution capabilities and dynamic scanning, US is the ideal imaging tool to confirm the instability of the extensor carpi ulnaris tendon (Fig. 10.43). Permanent dislocation of the extensor carpi ulnaris tendon is uncommon and can be identified by means of transverse planes obtained over the posteromedial aspect of the ulna. The diagnosis of intermittent dislocation is difficult if this possibility is not kept in mind by the examiner. To avoid false negative results, care should be taken not to limit the US examination to the static assessment of the tendon. On the contrary, transverse planes obtained during progressive pronation of the forearm can disclose the progressive displacement of the extensor carpi ulnaris tendon over the ulnar head.

10.5.2
Ventral Wrist Pathology

Similar to the dorsal wrist, tendinopathies of the flexor tendons are commonly encountered, most often at the insertion of the flexor carpi radialis tendon and within the carpal tunnel for the flexor digitorum tendons (Fig. 10.33b) (Daenen et al. 2004). In addition to tendinopathies, compression neuropathy of the median nerve at the carpal tunnel is the leading pathology of the wrist as regards prevalence of disease and clinical relevance. The entrapment of the ulnar nerve at the Guyon tunnel is rare and, in many cases, secondary to other disorders.
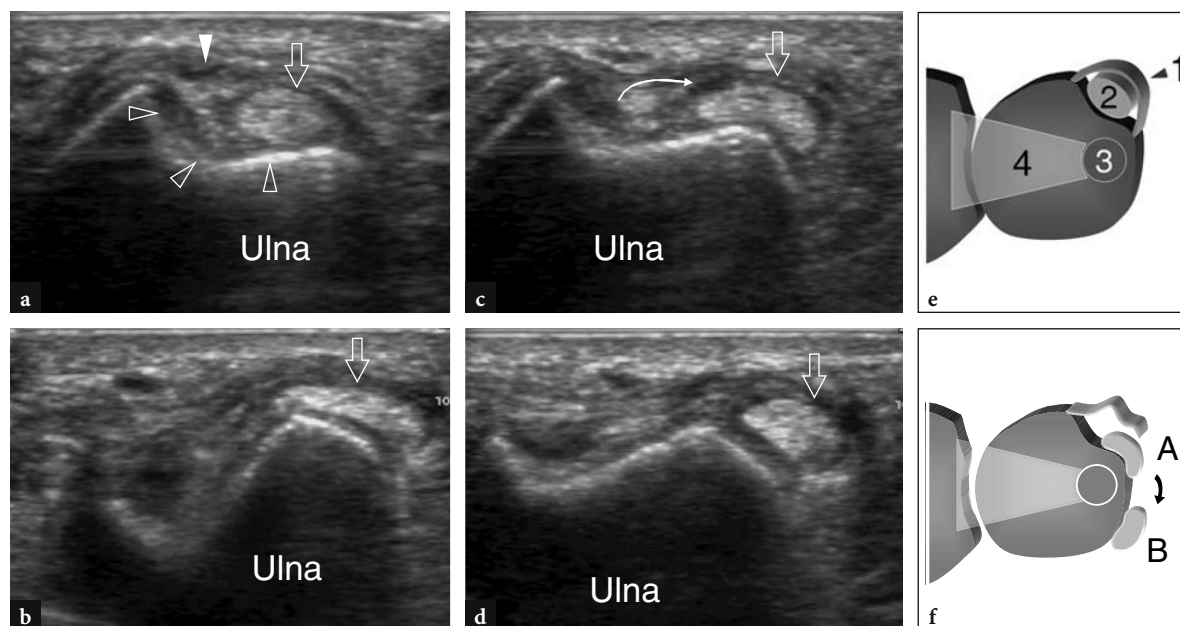
Fig. 10.43 a–f. Extensor carpi ulnaris instability. **a–d** Dorsal transverse 12–5 MHz US images obtained over the distal epiphysis of the ulna during progressive pronation of the forearm. **a** When the wrist is supinated, US shows the groove on the ulnar cortex (*open arrowheads*) for the extensor carpi ulnaris tendon (*arrow*) and an irregular appearance of the retinaculum (*white arrowhead*). **b,c** During progressive pronation, the extensor carpi ulnaris tendon (*open arrow*) subluxes (*curved arrow*) over the internal wall of the groove. Note the flattened appearance of the tendon as a result of tensile forces applied on it. **d** In full pronation, the extensor carpi ulnaris (*arrow*) dislocates out of the groove and exhibits a more rounded appearance. **e,f** Schematic drawings of a transverse view through the ulnar head **e** in the normal state and **f** when the retinaculum is torn. In **e**, the intact retinaculum *(1)* maintains the extensor carpi ulnaris *(2)* within the osteofibrous tunnel. 3, styloid process of the ulna; 4, triangular fibrocartilage. In **f**, the retinaculum tear leads the extensor carpi ulnaris first to sublux *(A)* and then to dislocate *(B)* out of the groove

10.5.2.1
Flexor Carpi Radialis Tenosynovitis

At the proximal wrist, the flexor carpi radialis tendon is held inside a splitting of the transverse carpal ligament bounded posteriorly by the scapho-trapezium-trapezoid joint. More distally, the tendon passes below the tubercle of the trapezium to become deep and insert onto the base of the second metacarpal. Although flexor carpi radialis tenosynovitis was only recently described (Fitton et al. 1968; Parellada et al. 2006), this condition is not widely recognized. Middle-aged women are most frequently affected. They report pain over the radial aspect of the volar wrist and a local lump, often misinterpreted as a volar ganglion. As an additional finding, tingling on the skin of the thenar eminence can be observed due to the close relationship of this tendon with the palmar branch of the median nerve (Kerboull and Le viet 1995). Pathogenesis includes friction inside the carpal tunnel where the tendon curves to reach its posterior insertion and osteoarthritis of the first carpometacarpal joint and scapho-trapezium joint, which are considered the leading causes (Le Viet 1995). In this latter circumstance, tendon inflammation is secondary to the presence of volar osteophytes that cause impingement over the posterior aspect of the tendon during flexion and extension movements of the wrist. Surgery is only indicated if conservative treatment fails. In most cases, US examination is requested to rule out a volar ganglion because of a local swelling (see paragraph Sect. 10.5.4.1). The main US signs include a swollen and irregularly hypoechoic tendon (Fig. 10.44). A synovial effusion can often be found within the tendon sheath as an expression of tenosynovitis (Fig. 10.45). In some cases, longitudinal fissures can be encountered, especially arising from the deep surface of the tendon.

10.5.2.2
Flexor Carpi Ulnaris Tendinopathy

With the exception of the palmaris longus, the flexor carpi ulnaris is the only wrist tendon without a synovial sheath because of its straight course from the forearm to the distal insertion into the pisiform. The term "tendinopathy" is the most appropriate to describe this condition, because fluid cannot be demonstrated surrounding the tendon even in acute clinical settings. The most common disorder affecting the flexor carpi ulnaris tendon is calcifying tendinitis. This disorder predominantly affects young to middle-aged women, presenting with pain located just proximal to the pisiform. In general, the onset of pain is acute and physical examination shows a tender pisiform covered by inflamed warm skin. Symptoms are related to the rupture of intratendinous calcified deposits into the surrounding tissues with secondary acute inflamma-
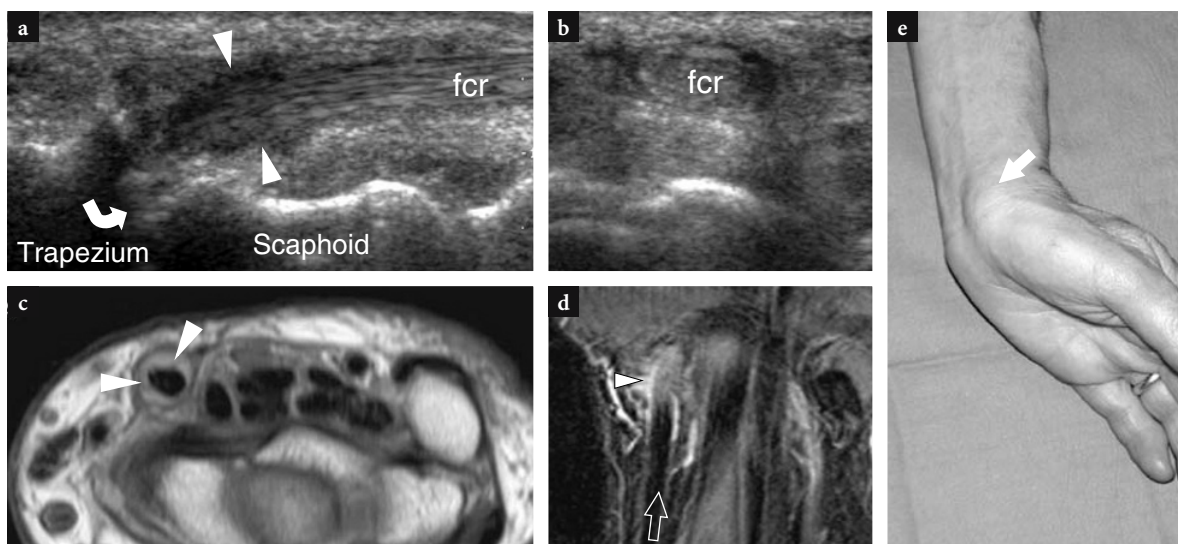
Fig. 10.44 a–e. Flexor carpi radialis tendinopathy. **a** Long-axis and **b** short-axis 12–5 MHz US images of the flexor carpi radialis tendon (*fcr*) show a swollen hypoechoic tendon (*arrowheads*) and bony irregularities (*curved arrow*) at the scapho-trapezium joint level suggestive of osteoarthritis. **c** Transverse Gd+T1w SE and **d** coronal T2w tSE MR images demonstrate hypervascular synovium and mild distention of the sheath (*arrowheads*) of flexor carpi radialis. **e** Photograph of the same patient shows a localized swelling (*arrow*) over the involved tendon, just proximal to the scaphoid. In this case, physical examination presumed that the lump was a volar ganglion
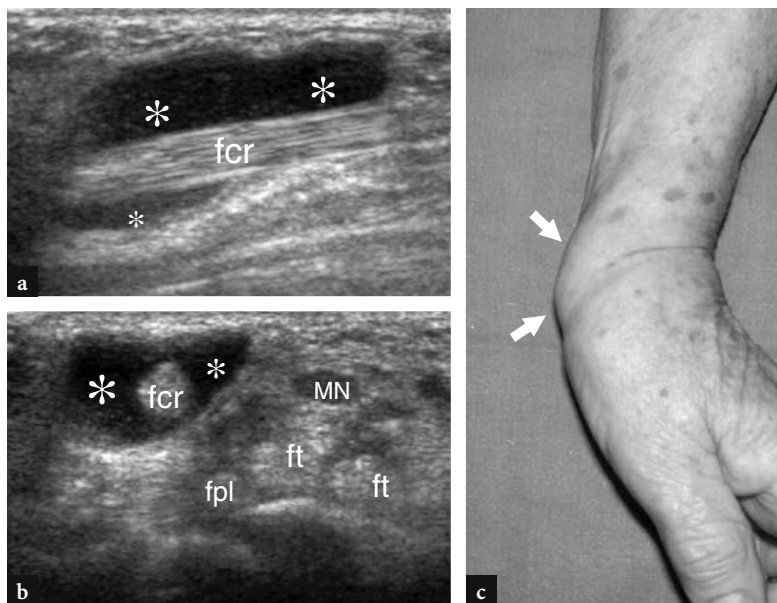
Fig. 10.45 a−c. Acute tenosynovitis of the flexor carpi radialis tendon. **a** Short-axis and (**b**) long-axis 12−5 MHz US images at the wrist demonstrate abnormal distension of the sheath of flexor carpi radialis tendon *(fcr)* by abundant hypoechoic fluid *(asterisks)*, whereas the tendon echotexture is normal. Note the relationship of the flexor carpi radialis with the median nerve *(MN)*, the flexor digitorum *(ft)* and the flexor pollicis longus *(fpl)* tendons. **c** Photograph of the same patient shows the mass effect *(arrows)* of tendon sheath effusion on the radial side of the ventral wrist

tion. Therapy includes anti-inflammatory drugs, ice and immobilization. In cases of severe refractory pain, a brief (1−3 days) course of intramuscular steroids can be indicated. The diagnosis of flexor carpi ulnaris tendinopathy is based on clinical and radiological findings. Standard radiographs obtained in anteroposterior and lateral views can be negative, small calcifications being easily masked by the pisiform. If the diagnosis is suspected, an additional oblique view should be obtained to clearly show the broken calcified deposits (Fig. 10.46a). High-resolution US can easily image the flexor carpi ulnaris tendon due to its straight superficial course. Calcified deposits usually appear as spotty hyperechoic foci located between the tendon and the pisiform. Color and power Doppler imaging can demonstrate signs of hyperemia in cases of acute inflammation (Fig. 10.46b). The pisiform itself can exhibit small cortical erosions related to local inflammation (Fig. 10.46c). If US is the first imaging modality and calcifying tendinitis of the flexor carpi ulnaris is suspected, radiographs should always be performed to confirm the diagnosis.

10.5.2.3
Carpal Tunnel Syndrome

Carpal tunnel syndrome is the most common entrapment syndrome of the upper limb with an estimated prevalence of approximately 125×10^6 new cases per year. This syndrome arises from compression of the median nerve at the wrist. Predisposing factors may be related to anatomic variants (i.e., narrow tunnel, presence of the median artery, abnormal and accessory tendons and muscles), susceptibility of the nerve to pressure (i.e., diabetes, systemic neuropathies), systemic and endocrine disorders (i.e., pregnancy, hypothyroidism, amyloidosis) and space-occupying lesions within the tunnel. Clinically, the patient, usually a late middle-aged woman, relates a history of tingling, numbness and burning pain localized in the thumb, index, middle finger and radial half of the ring finger, typically exacerbated by prolonged strenuous manual work. The dominant arm is more commonly affected. Night pain (brachialgia paresthetica nocturna) is the usual symptom that, at least in part, can be explained by local edema and prolonged wrist flexion during sleeping. In general, symptoms resolve after repeated hand movements. In early carpal tunnel syndrome, gross morphologic abnormalities of the median nerve do not occur. Later on, the nerve becomes swollen and exhibits changes in shape and histology with progressive demyelinization and fibrosclerosis. In chronic longstanding disease, permanent sensory and motor deficit in the territory of innervation of the median nerve can arise. Wasting of hand muscles is best appreciated at the volar aspect
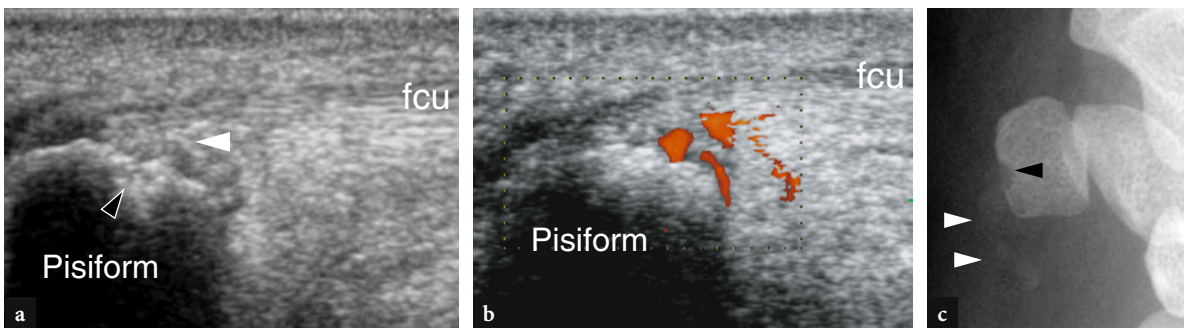
Fig. 10.46 a–c. Flexor carpi ulnaris tendinopathy. **a** Longitudinal gray-scale and **b** power Doppler 10−5 MHz US images over the flexor carpi ulnaris tendon (*fcu*). Since this tendon is not invested by a synovial sheath, fluid and pannus cannot be demonstrated around it in the setting of acute tendinitis. Instead, some hyperechoic spots (*white arrowhead*) can be detected between the tendon and the palmar aspect of the pisiform. A focal irregularity of the pisiform cortex (*black arrowhead*) reflects a superficial bone erosion. Power Doppler imaging reveals blood flow signals between the tendon and the pisiform as a sign of acute local inflammation. **c** Corresponding ulnar oblique radiograph of the wrist confirms the calcifications and the osseous erosion

of the thenar eminence, causing a typical deformity of the hand, commonly referred to as "ape hand" (Fig. 10.47). Depending on the severity of symptoms and presence of atrophic changes in the muscles of the thenar eminence, treatment includes night splinting, intracanal steroid injections and surgical resection of the transverse carpal ligament.

An early diagnosis is essential to prevent permanent muscle damage and functional sequelae. In general, it relies on clinical and electrodiagnostic findings and, at least in typical cases, does not require an imaging study. However, the progressive refinement of US transducers has enhanced the ability to depict the median nerve in the carpal tunnel and high-resolution US is currently considered a low-cost, rapid and accurate modality to assess nerve compression in both static and dynamic states (CHEN et al. 1997). The main US findings in carpal tunnel syndrome include changes in shape and echotexture of the median nerve and abnormalities in the transverse carpal ligament and the soft-tissue structures within the tunnel. Although the median nerve exhibits discrete morphologic abnormalities in many patients with carpal tunnel syndrome, some cases with early onset
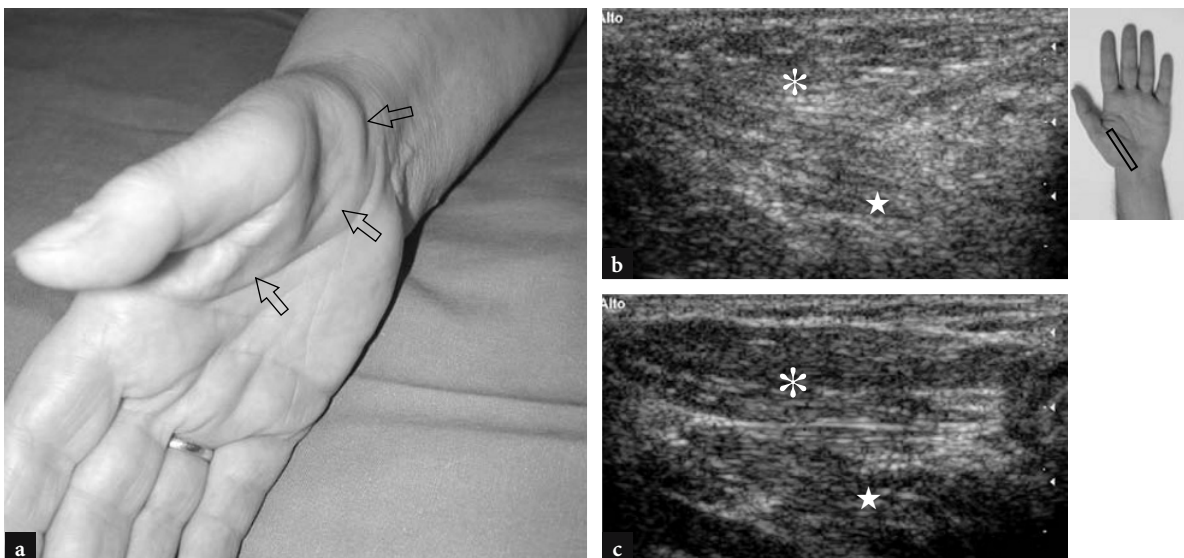
Fig. 10.47 a–c. "Ape hand" deformity in the right hand of a patient with severe median neuropathy at the carpal tunnel level. **a** Photograph of the palmar aspect of the hand reveals a skin depression (*arrows*) due to loss in bulk of the intrinsic muscles at the thenar eminence. **b** Transverse 12−5 MHz US image at the dorsal aspect of the hand demonstrates a hyperechoic appearance of the abductor pollicis brevis (*asterisk*) and opponens pollicis (*star*) related to neurogenic fatty atrophy. **d** Contralateral healthy side. The insert at the upper right side of the figure indicates probe positioning

of symptoms do not show any detectable change at US examination. Accordingly, the examiner should be aware that a normal nerve does not exclude the diagnosis of median neuropathy. When abnormalities are present, the compressed nerve appears swollen at the proximal tunnel and flattened at the distal tunnel regardless of the cause of compression (Buchberger et al. 1991, 1992) (Figs. 10.48, 10.49). An abrupt nerve caliber change at the entrance of the carpal tunnel, commonly referred to as the "notch sign", is typically appreciated (Lee et al. 1999). During scanning, this finding increases the diagnostic confidence of the examiner. In some cases, the notch sign may occur at a distal site, where the nerve passes below the distal edge of the retinaculum to exit the carpal tunnel (inverted notch sign). In this instance, the nerve and its divisional branches are swollen in the palm and flattened at the distal tunnel level (Fig. 10.50), whereas no shape change is usually appreciated at the distal radius and the proximal tunnel levels. An inverted notch sign indicates a distal compression and should be referred to the neurologist (to recommend functional tests with more sophisticated techniques, such as short segment and palmar stimulations, avoiding overly proximal routine electrophysiologic testing) and to the hand surgeon.

Since the nerve shape varies through the tunnel, some indexes have been introduced with US to better quantify abnormal findings in nerve morphology: among these, a nerve cross-sectional area ≥ 9 mm^2 (Duncan et al. 1999) or ≥ 10 mm^2 (Buchberger et al. 1992; Chen et al. 1997) calculated at the proximal
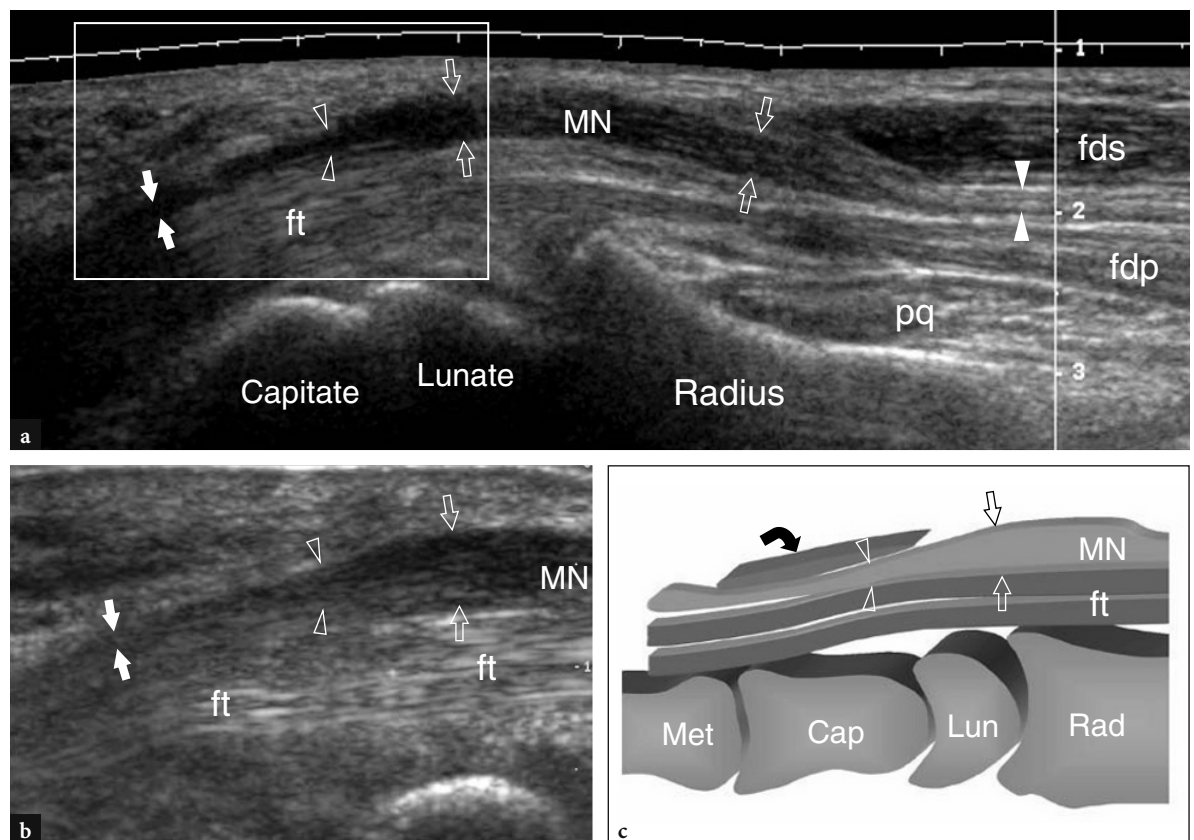
Fig. 10.48 a–c. Carpal tunnel syndrome. **a** Long-axis extended field-of-view 12−5 MHz US image of the median nerve through the distal forearm and the wrist demonstrates the median nerve *(MN)*, which appears increasingly swollen and hypoechoic *(open arrows)* with absent fascicular pattern as it progresses toward the carpal tunnel. Observe the normal size of the nerve at the forearm *(white arrowheads)* between the flexor digitorum superficialis *(fds)* and profundus *(fdp)*. At the proximal carpal tunnel level, an abrupt change in nerve size, the notch sign *(open arrowheads)*, indicates the compression point. More distally, at the distal carpal tunnel, the nerve remains flattened and hypoechoic *(white arrows)*. *pq*, pronator quadratus muscle; *ft*, flexor tendons. **b** Long-axis 12−5 MHz US image of the median nerve showing the notch sign at a higher magnification. The field-of-view of this image is indicated in **a** by a white box. **c** Corresponding schematic drawing illustrates the main nerve shape abnormalities in carpal tunnel disease. Note the swelling portion *(arrows)* of the median nerve *(MN)* at the distal radius, proximal to the level of compression *(arrowheads)* and the nerve flattening deep to the transverse carpal ligament *(curved arrow)*
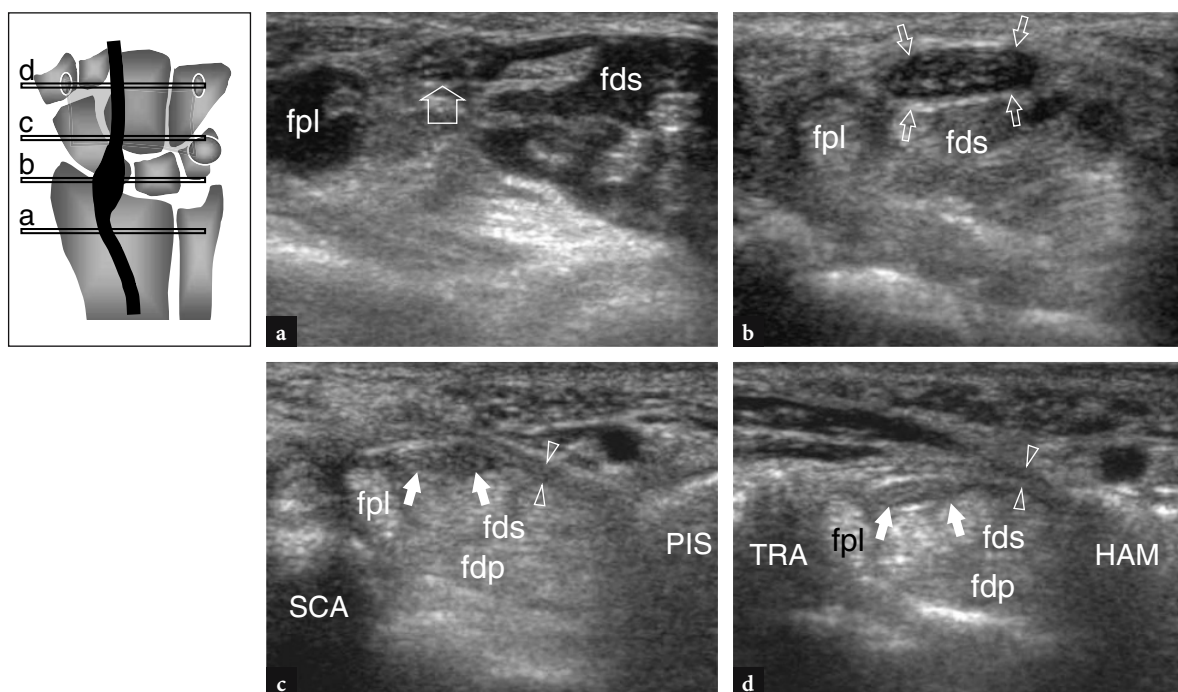
Fig. 10.49 a–d. Carpal tunnel syndrome. Serial transverse 12–5 MHz US images obtained **a** at the distal radius, **b** just behind the transverse carpal ligament, **c** at the proximal tunnel (scaphoid-pisiform level) and **d** at the distal tunnel (trapezium-hamate level) according to the reference diagram shown at the upper left side of the figure. **a** A normal-appearing median nerve (*arrow*) is seen between the flexor pollicis longus *(fpl)* and the flexor digitorum superficialis *(fds)* muscles. **b** Progressive enlargement of the median nerve (*arrows*) and hypoechoic changes in the epineurium occur just behind the proximal edge of the transverse carpal ligament. This is the point of maximum nerve swelling. Note the relationship of the nerve with the flexor pollicis longus *(fpl)* and flexor digitorum superficialis tendons. **c** By comparing this image with **b**, a sudden change in the cross-sectional area of the median nerve (*arrows*) can be clearly identified at the point where the nerve gets deep to the transverse carpal ligament (*arrowheads*). *fdp*, flexor digitorum profundus; *SCA*, scaphoid; *PIS*, pisiform. **d** At the distal tunnel, the nerve area does not change significantly in comparison with that seen in **c**, whereas the transverse carpal ligament (*arrowheads*) appears thicker. *TRA*, trapezium; *HAM*, hamate

carpal tunnel (scaphoid-pisiform level) by means of the ellipse formula [(maximum AP diameter) × (maximum LL diameter) × (π/4)] is reported to be the best diagnostic criterion for the diagnosis (Fig. 10.51a). Nevertheless, there is no consensus in the literature as to what size of the median nerve has to be considered abnormal. A nerve cross-sectional area ≥15 mm^2 has also been proposed by other authors as the threshold value (Lee et al. 1999). These authors found a correlation between the nerve area and the severity of electrophysiologic findings and used 15 mm^2 as the cut-off value to separate patients with severe disease in whom surgical decompression is indicated. In our experience, we found the point of maximum nerve swelling more commonly located behind the proximal edge of the transverse carpal ligament rather than at the proximal carpal tunnel level. Therefore, the greater difference in nerve cross-sectional area seems to be more reliably obtained by comparing the distal forearm level (pronator quadratus level) with the distal end of the radius. Using these landmarks, the cross-sectional area of the median nerve is approximately the same in normal states, whereas it may be greater than 2 in patients with carpal tunnel syndrome. In addition to proximal median nerve enlargement a distal flattening ratio >3, calculated at the distal tunnel by dividing the transverse diameter of the nerve by its anteroposterior diameter, has also been proposed as an additional finding of carpal tunnel syndrome (Buchberger et al. 1991, 1992). This latter finding, however, was not confirmed in later studies (Nakamichi and Tachibana 2000; Sarria et al. 2000) (Fig. 10.51b,c).

In addition to shape changes, high-resolution US can identify fine echotextural changes in the compressed median nerve, which becomes uniformly hypoechoic with loss of the fascicular pattern as a probable result of intraneural edema or fibrosis (Martinoli et al.
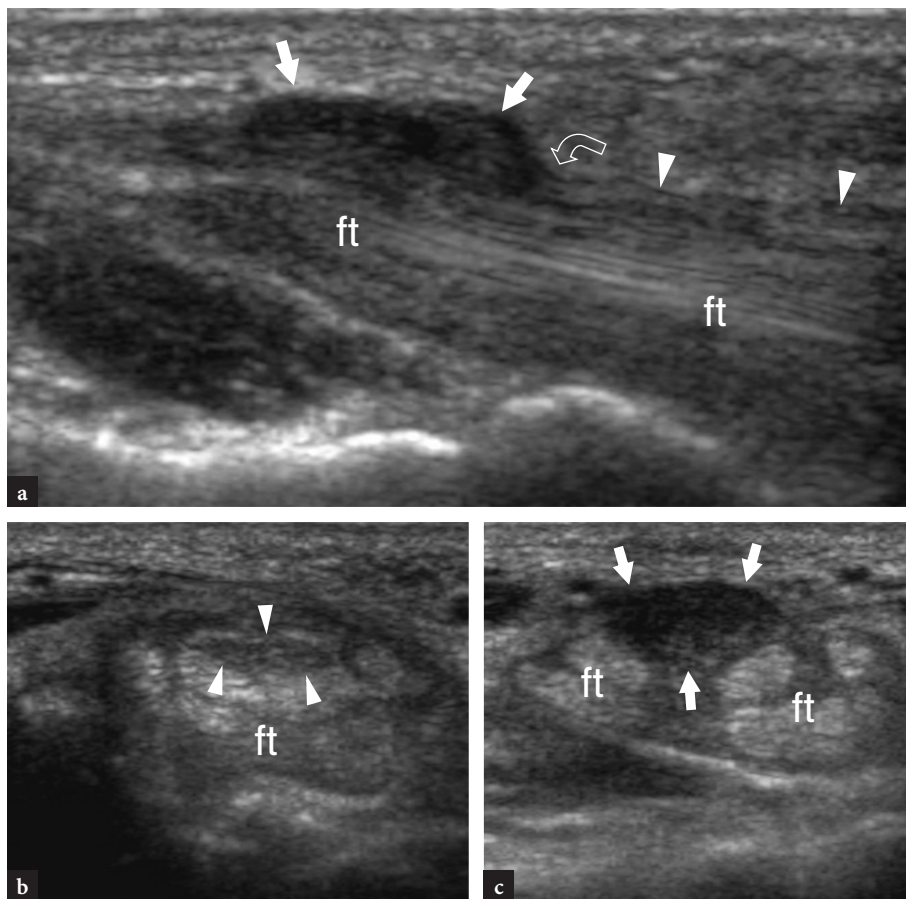
Fig. 10.50 a−c. Carpal tunnel syndrome. **a** Long-axis 12−5 MHz US image of the median nerve (*arrowheads*) at the distal carpal tunnel and in the palm reveals a focal swelling (*arrows*) of the nerve just ahead the distal edge (*curved arrow*) of the transverse carpal ligament, the so-called inverted notch sign. No change in nerve size and echotexture could be appreciated at a more proximal level. **b,c** Correlative transverse 12−5 MHz US images obtained **b** at the distal tunnel and **c** in the palm show a normal-appearing nerve (*arrowheads*) behind the retinaculum which becomes abnormally enlarged and hypoechoic with loss of the fascicular echotexture just after exiting the tunnel. *ft*, flexor tendons. The patient, an architectural professional designer, had bilateral carpal tunnel disease and considerable limitation in her professional activity
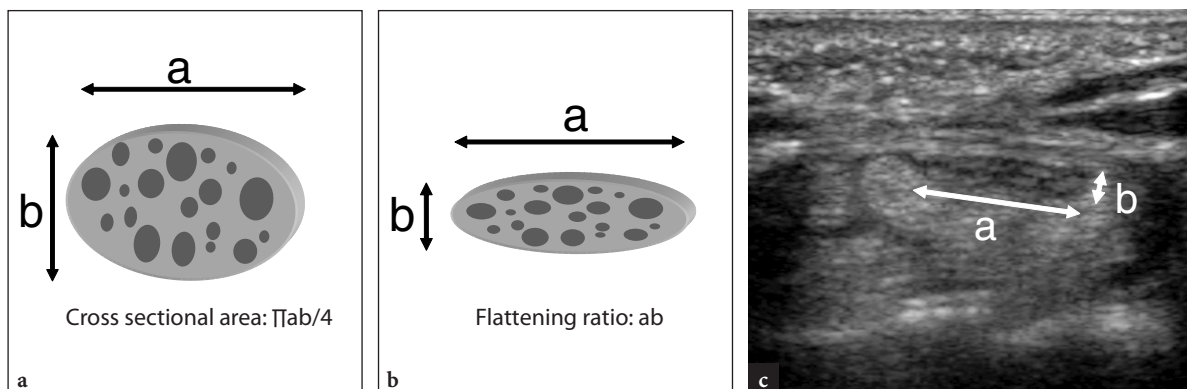
Fig. 10.51 a−c. Quantitative indexes in carpal tunnel syndrome. **a** Nerve cross-sectional area. This measure is calculated at the point of maximum nerve swelling by the transverse *(a)* and anteroposterior *(b)* diameters of the nerve using the ellipse formula [abπ/4]. **b,c** Flattening ratio. This measure is determined at the distal carpal tunnel by dividing the transverse diameter *(a)* of the nerve by its anteroposterior diameter (*b*). In **c**, the measurement of nerve diameters for calculating the flattening ratio is shown in a transverse 12−5 MHz US image of the distal carpal tunnel. The threshold values for these measurements are reported in Sect. 10.5.2.3

1996) (Figs. 10.48, 10.49). When evaluating the fascicular echotexture, care should be taken to place the nerve axis perpendicular to the US beam to avoid artifacts related to the oblique course of the fascicles. In addition, color and power Doppler imaging can show hyperemic blood flow in the longitudinal perineural plexus and within intraneural branches, related to disturbances in the intraneural microvasculature as well as to the inflammatory process (Martinoli et al. 2000). Reduced transverse sliding of the nerve beneath the retinaculum during flexion and extension of the index finger may also be seen, but this latter sign is too subjective and hard to quantify (Chen et al. 1997; Nakamichi and Tachibana 1995).

In carpal tunnel disease, the increased intracanal pressure may often lead to an increased convexity of the transverse carpal ligament that is normally straight or slightly convex. The bulging of the ligament can be appreciated with US and is measured at the distal tunnel (hamate-trapezium level) (Fig. 10.52). Once the tubercle of the trapezium and the hook of the hamate are identified, a line is drawn tangential to them. Then, the distance between this line and the most anterior portion of the transverse carpal ligament is calculated: a distance ≥4 mm reflects an excessive anterior bulging and can be considered an ancillary pathologic sign (Buchberger et al. 1991, 1992).

Besides assessing the median nerve and the transverse carpal ligament, extrinsic causes for nerve entrapment can also be identified with US. Most patients with carpal tunnel syndrome are affected by tenosynovitis of flexor tendons (Fig. 10.53). This condition may be secondary to a variety of causes and can be identified with US based on the presence of hypoechoic halos surrounding the flexor tendons due to fluid effusion and thickened synovium. In general, the synovial sheath effusion facilitates visualization and differentiation of the individual flexor tendons within the carpal tunnel. Dynamic scanning in transverse planes obtained during repetitive flexion and extension movements of the fingers may aid the differentiation between tendons and echogenic synovium. To avoid false negative results, scanning should be extended at more proximal and distal levels relative to the carpal tunnel because most synovial fluid may accumulate outside the tunnel where there is least resistance to sheath distension (Fig. 10.54). Comparison with the opposite uninvolved wrist may also be useful in the case of subtle findings.

A variety of space-occupying lesions can be encountered within the carpal tunnel. Ganglion cysts appear as lobulated anechoic masses with well-defined margins (Fig. 10.55). They usually arise in the deep portion of the tunnel from the wrist joints and dislocate both

median nerve and flexor tendons against the transverse carpal ligament. Amyloidosis can be a complication of longstanding renal disease (Ikegaya et al. 1995; Lanteri et al. 1997; Takahashi et al. 2002). At US, it appears as an ill-defined solid hypoechoic mass arising over the radiocarpal and midcarpal joints that dislocates the intracanal structures (Fig. 10.56). Accessory muscles can also be found inside the carpal tunnel (see also Sect. 10.5.4.4). They are related to either the proximal insertion of a lumbrical muscle, the distal insertion of a belly of the flexor digitorum muscles or are real accessory muscles. In all cases, anomalous muscles appear at US as hypoechoic masses with internal elongated hyperechoic lines reflecting muscular septa. Anomalous bone projecting inside the tunnel, such as an exuberant callus or a displaced lunate, appear as bright hyperechoic structures with posterior acoustic shadowing. A persistent median artery can occasionally be associated with carpal tunnel syndrome. In some patients, symptoms may arise suddenly as a
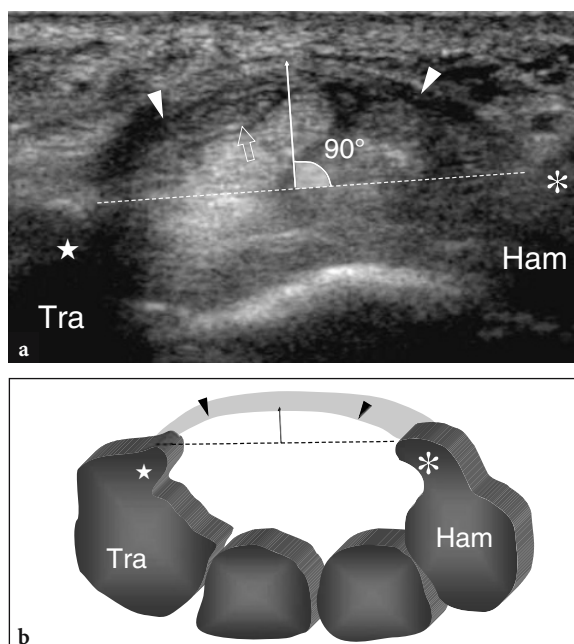
Fig. 10.52 a,b. Quantitative indexes in carpal tunnel syndrome. **a** Transverse 12–5 MHz US image with **b** schematic drawing correlation shows the method for calculating the bulging of the transverse carpal ligament. A line (*dashed line*) is drawn to join the tubercle (*star*) of the trapezium *(Tra)* and the hook (*asterisk*) of the hamate *(Ham)*. Then, a perpendicular (*continuous white line*) to this line is drawn to reach the most prominent portion of the transverse carpal ligament (*arrowheads*). When this latter line measures ≥4 mm, it indicates abnormal bulging of the ligament. In **a**, observe the median nerve (*open arrow*) compressed against the convex transverse carpal ligament in a patient with tenosynovitis of the flexor tendons
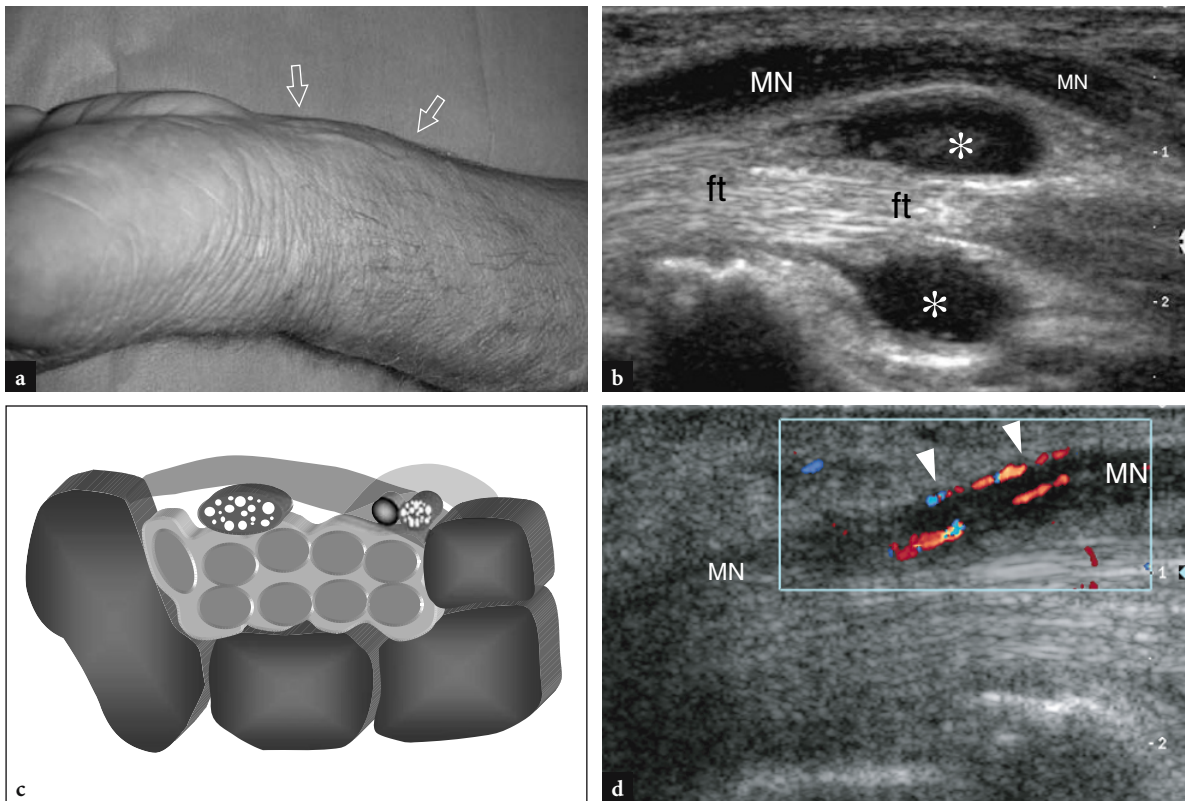
Fig. 10.53 a–d. Carpal tunnel syndrome in tenosynovitis of the flexor tendons. **a** Photograph demonstrates soft-tissue swelling (*arrows*) at the palmar aspect of the left wrist in a manual laborer presenting with inability to clench the fist and burning pain in the volar aspect of the wrist and palm. **b** Long-axis 12–5 MHz US image of the median nerve at the distal radius demonstrates abnormally increased fluid effusion (*asterisks*) surrounding flexor tendons (*ft*), resulting in palmar displacement and compression of the median nerve *(MN)* at the entrance of the tunnel. **c** Correlative schematic drawing shows sheath fluid (*intermediate gray*) surrounding the flexor tendons in the carpal tunnel. The increased content of the tunnel causes secondary median nerve compression. **d** Long-axis color Doppler US image of the median nerve *(MN)* demonstrates blood flow signals (*arrowheads*) from the longitudinal perineural plexus and the intranervous branches as a result of hyperemic changes related with the inflammation
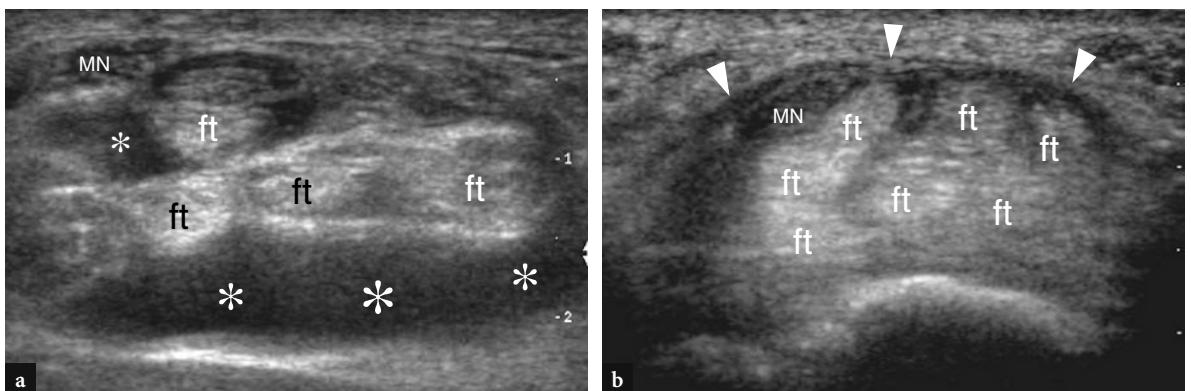
Fig. 10.54 a,b. Carpal tunnel syndrome in tenosynovitis of flexor tendons. Same case as illustrated in Fig. 10.53. **a,b** Transverse 12–5 MHz US images obtained **a** at the distal radius and **b** at the proximal carpal tunnel level. Note that an abundant anechoic effusion (*asterisks*) in the sheath of flexor tendon *(ft)* is better demonstrated at the distal radius rather than inside the carpal tunnel. This finding is related to a lesser degree of sheath compliance within the restricted space of the tunnel. In **b**, carpal tunnel disease is mostly indicated by the abnormal bulging of the transverse carpal ligament (*arrowheads*). *MN*, median nerve
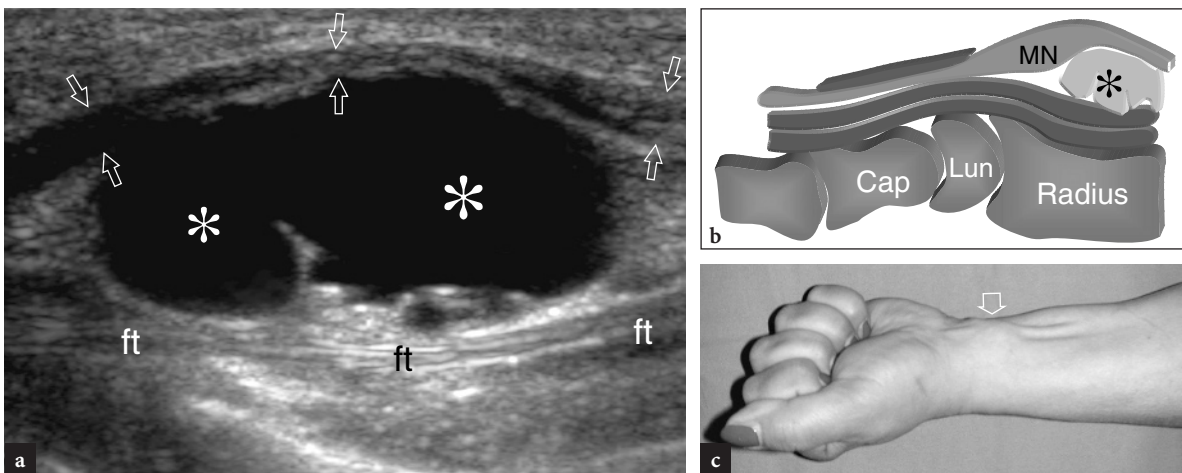
Fig. 10.55 a–c. Carpal tunnel syndrome caused by ganglion cyst. **a** Longitudinal 12−5 MHz US image over the distal radius with **b** diagram correlation reveals a large bilobed ganglion cyst (*asterisks*) displacing the median nerve (*arrows* in **a**, *MN* in **b**) toward the skin and the flexor tendons *(ft)* downwards. **c** Photograph demonstrates the lump (*arrow*) caused by the cyst on the ventral wrist. The lump became more prominent while clenching the fist
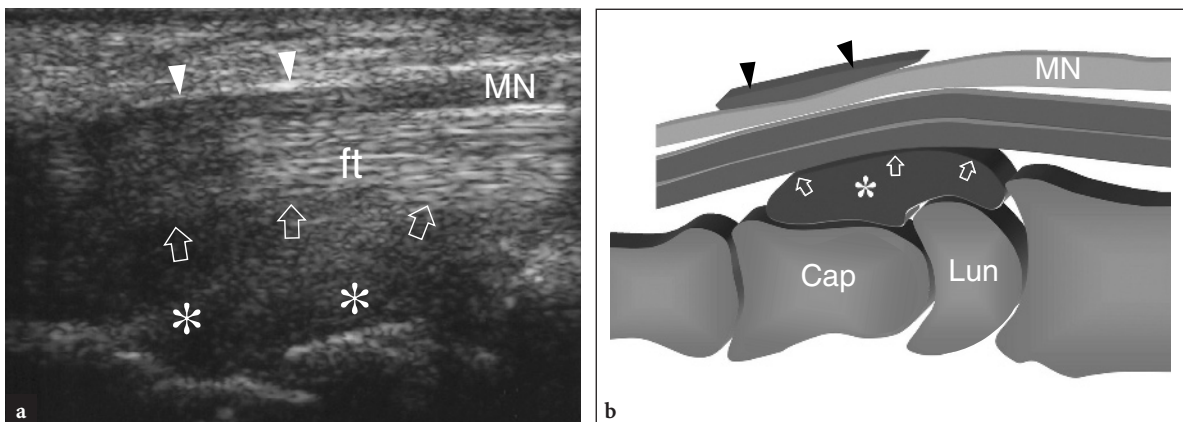
Fig. 10.56a,b. Carpal tunnel syndrome in amyloid arthropathy. **a** Longitudinal 12−5 MHz US image through the carpal tunnel with **b** diagram correlation shows the bulk of amyloid substance (*asterisks*) contained in the deep portion of the tunnel that compresses the flexor tendons *(ft)* and the median nerve *(MN)* against the flexor retinaculum (*arrowheads*). The patient had chronic renal failure and underwent long-term hemodialysis

result of acute thrombosis of this artery, a condition that requires thrombolitic treatment more than surgical excision (Fig. 10.57). US and color Doppler techniques make the diagnosis by showing lack of pulsatility and absence of internal flow in the occluded artery (FUMIERE et al. 2002). Other masses that can cause carpal tunnel syndrome include lipomas and pigmented villonodular synovitis.

The conservative treatment of carpal tunnel syndrome includes wrist splints during sleep, nonsteroidal anti-inflammatory drugs and local corticosteroid injections adjacent to the tunnel. If such treatment fails or progressive sensory loss and muscle weak-

ness and atrophy become apparent, surgical decompression of the transverse carpal ligament is recommended. Surgery may be performed with an open or endoscopic technique by dividing the retinaculum in proximity to its ulnar insertion on the hook of the hamate to avoid incidental damage to the branches of the median and ulnar nerves. After surgical release of the retinaculum, the appearance and mobility of the median nerve may improve and the cleft in the transverse carpal ligament can be seen with US (Fig. 10.58). Typically, the median nerve lies in a more superficial position at the proximal carpal tunnel level and the resected bands of the transverse carpal ligament are
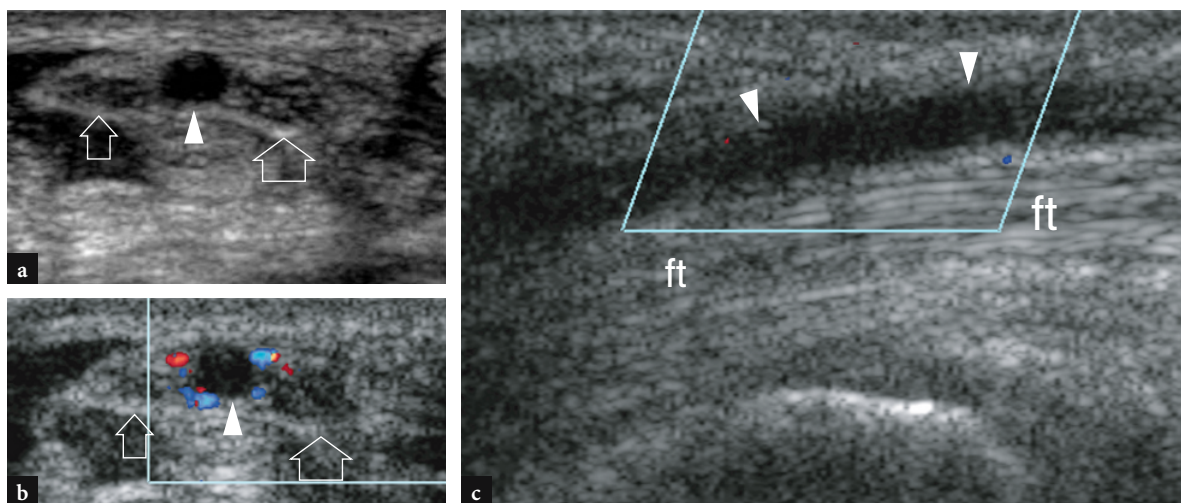
Fig. 10.57 a–c. Carpal tunnel syndrome in thrombosis of the persistent median artery. Transverse **a** gray-scale and **b** color Doppler 12−5 MHz US images over the proximal carpal tunnel demonstrate a bifid median nerve (*arrows*). Between the two nerve trunks, an enlarged hypoechoic median artery (*arrowheads*) free of endoluminal color Doppler signals is found suggesting vessel occlusion. In **b**, note the residual color flow in small perivascular collaterals distributed all around the thrombosed artery. **c** Longitudinal color Doppler 12−5 MHz US image over the artery (*arrowheads*) confirms the absence of intravascular blood flow. *ft*, flexor tendons. The patient was a baker who injured his artery in the palm as a result of repetitive microtrauma while making bread. The thrombosis extended from the proximal edge of the transverse carpal ligament down to the palm, where the vessel was reopened by the superficial palmar arch. After thrombolisis, the artery returned to be patent
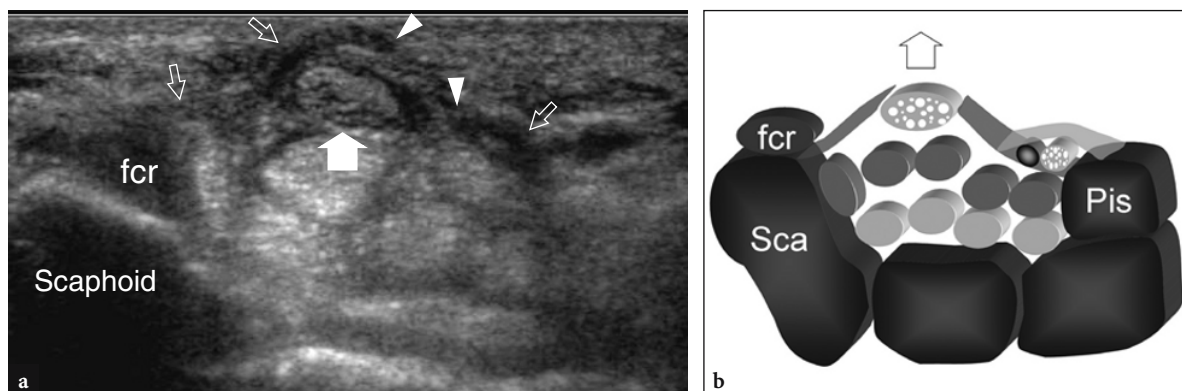
Fig. 10.58 a,b. Postoperative carpal tunnel. **a** Transverse 12−5 MHz US image over the proximal carpal tunnel with **b** diagram correlation reveals a wavy appearance of the radial and ulnar portions (*open arrows*) of the transverse carpal ligament. The borders of the sectioned ligament are indicated by *arrowheads*. After release of the transverse carpal ligament, the median nerve (*arrow*) returns to a normal size and appearance and moves anteriorly due to lack of any ligament constriction. Note the abnormal ventral position of the median nerve relative to the flexor carpi radialis tendon (*fcr*). After surgery, the patient had good functional recovery and complete relief of pain

disposed obliquely on each side of the nerve. High-resolution US can be used in patients with unrelieved or recurrent symptoms to rule on incomplete sectioning of the transverse carpal ligament (early complication) or scarring involving the nerve (late recurrences) (CHEN et al. 1997). In the case of incomplete section of the ligament, the notch sign continues to be appreciated in the median nerve although at a more distal

level than observed preoperatively (Fig. 10.59). On the other hand, postsurgical scarring tissue in the carpal tunnel appears as an irregular hypoechoic mass with ill-defined margins encasing the median nerve.

In conclusion, when carpal tunnel syndrome is suspected on clinical grounds based on the patient's history and the physical examination, high-resolution US can be a useful means to: confirm the diagnosis by
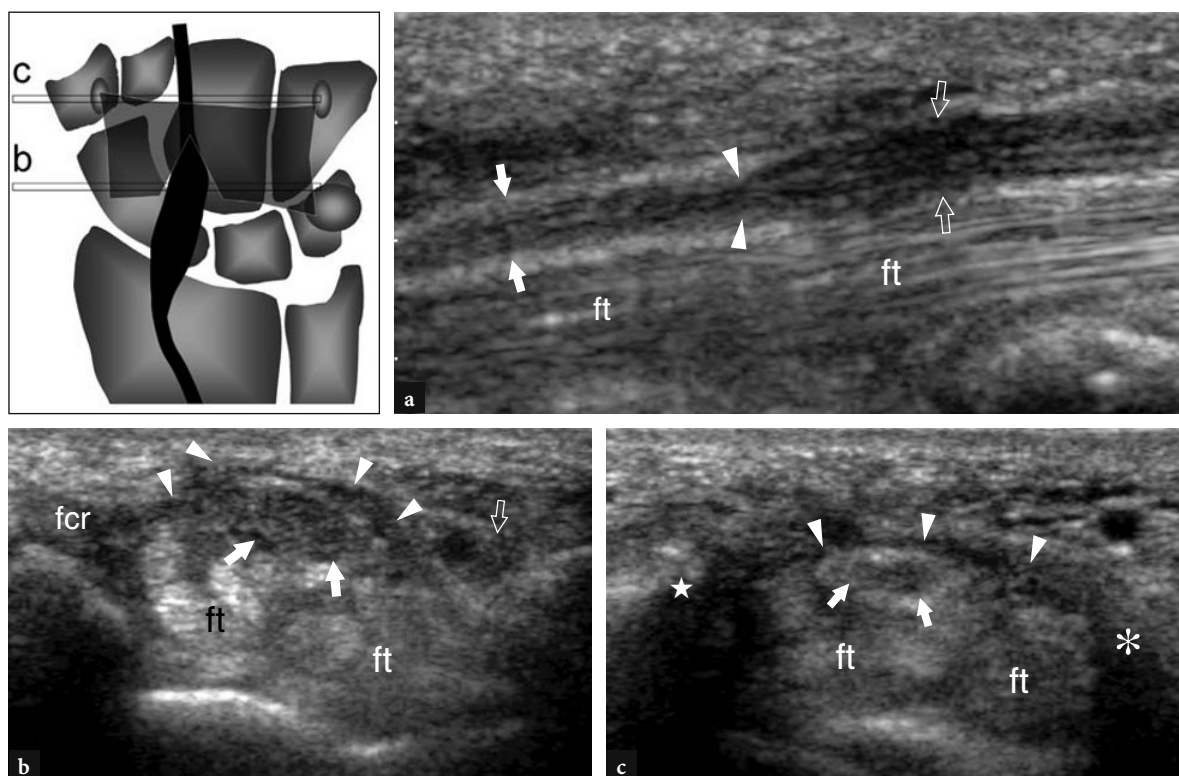
Fig. 10.59 a–c. Complication after carpal tunnel release. **a** Longitudinal 12–5 MHz US postoperative image through the carpal tunnel demonstrates a persistent notch sign (*arrowheads*) in the median nerve at the level of distal tunnel. Note the change in nerve caliber and shape between the proximal (*open arrows*) and distal (*white arrows*) tunnel. **b,c** Transverse 12–5 MHz US images obtained **a** at the proximal tunnel (scaphoid-pisiform level) and **b** at the distal tunnel (trapezium-hamate level) according to the reference diagram shown at the upper left side of the figure. **b** Although the transverse carpal ligament (*arrowheads*) is sectioned and has a wavy appearance, the median nerve (*arrows*) remains thickened and hypoechoic with loss of the fascicular echotexture. **c** More distally, the nerve (*arrows*) is still compressed by the intact distal portion of the ligament (*arrowheads*). Note the continuity of the transverse carpal ligament between the tubercle of the trapezium (*star*) and the hamate hook (*asterisk*). This finding suggests an incomplete sectioning of the transverse carpal ligament. The patient complained of persistent symptoms after surgery. After US examination, he was operated on again with good clinical success. *fcr*, flexor carpi radialis tendon; *ft*, flexor digitorum tendons

showing changes in nerve shape and echotexture; rule out anatomic variants, such as a bifid median nerve or the presence of a median artery of the forearm, which may contraindicate arthroscopic access; assess the cause of compression. Detection of a space-occupying mass within the carpal tunnel usually suggests an open surgical approach. When compared with electrodiagnostic studies, US has proved to be nearly equivalent in the diagnosis. It has been suggested as initial test of choice for patients suspected of having carpal tunnel syndorme (Wong et al. 2004)

10.5.2.4
Guyon Tunnel Syndrome

Compared with carpal tunnel and cubital tunnel syndrome, ulnar neuropathy at the Guyon canal is rare.

The clinical symptoms of Guyon tunnel syndrome may vary depending on the site of compression of the ulnar nerve. From a pathophysiologic point of view, the Guyon tunnel can be divided in three anatomic zones (Gross and Gelberman 1984). Zone I corresponds to the proximal portion of the tunnel (pisiform level) and houses the main trunk of the nerve with sensory and motor fibers. Zones II and III are located more distally (hamate level): zone II corresponds to the deep portion of the tunnel where the motor branch of the nerve is held; zone III is superficial and contains the sensitive branch of the ulnar nerve. Depending on the site of compression within these different zones, the patient may have either mixed symptoms or a purely motor or sensory syndrome. The leading cause for Guyon tunnel syndrome is represented by ganglion cysts (Elias et

al. 2001), which account for approximately 30–40% of cases of this syndrome. These ganglia originate from either the hamate-triquetrum or the piso-triquetrum joints, to which they are usually connected through a tortuous pedicle, and expand inside the Guyon tunnel. These lesions are readily diagnosed by high-resolution US (Fig. 10.60). They typically appear as well-delineated anechoic masses free of internal flow signals. The relationship of the mass with the ulnar nerve and the ulnar artery is best appreciated on transverse US scans. Usually, the origin of the ganglion cannot be established with certainty because its pedicle is almost never well depicted with US. In the preoperative planning, additional modalities should be performed, such as MR imaging and CT arthrography after injection of contrast material into the radiocarpal and eventually midcarpal joint, to assess the origin and extension of the mass in detail. Among other cases of Guyon tunnel syndrome, injures to the ulnar artery causing thrombosis and pseudoaneurysm formation, and anomalous muscles within the tunnel, such as the accessory abductor digiti minimi

(see Sect. 10.5.4.4), may also lead to ulnar nerve compression by squeezing the nerve.

10.5.2.5
Nerve Trauma

In a traumatic setting, acute injuries to wrist nerves are usually the result of penetrating injuries. The diagnosis of these lesions is straightforward on physical examination and US may have a complementary role in obtaining further confirmation of the clinical diagnosis and accurately assessing the precise site of the nerve lesion. In complete tears, the severed nerve is interrupted by an irregular hypoechoic area intervening between the nerve stumps related to hematoma and, later on, to fibrosclerosis. Typically, local pressure obtained with the probe over the lesion site can elicit acute pain (US Tinel sign). The US appearance of partial tears may be different depending on the nerve size. In small nerves, such as the divisional branches of ulnar nerve and the radial nerve, par-
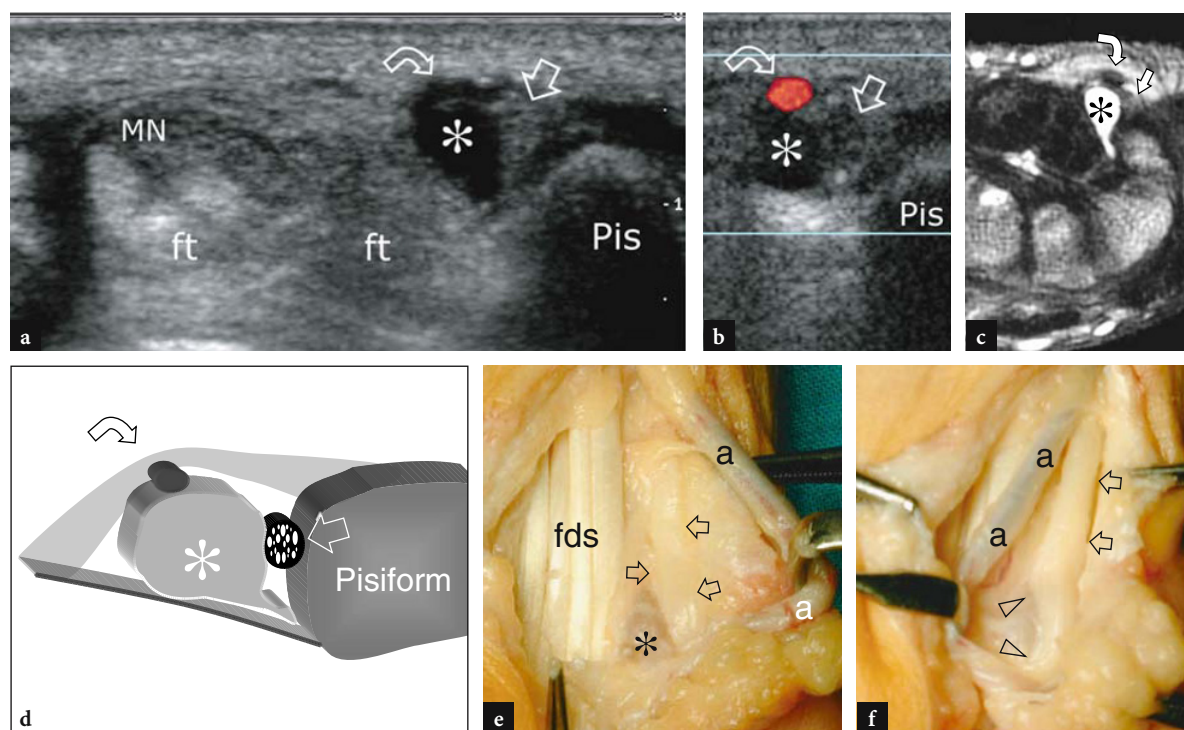
Fig. 10.60 a–f. Guyon tunnel syndrome in a pisotriquetrum ganglion. Transverse **a** gray-scale and **b** color Doppler 12–5 MHz US images with **c** T2w tSE MR imaging and **d** diagram correlation demonstrate an oval hypoechoic ganglion cyst *(asterisk)* which displaces the ulnar artery *(curved arrow)* and compresses the ulnar nerve *(straight arrow)* against the pisiform *(Pis)*. Note the position of the median nerve *(MN)* and the flexor tendons *(ft)* in the carpal tunnel. **e,f** Gross operative views of the same case obtained **e** before and **f** after resection of the ganglion cyst *(asterisk)* show the ulnar nerve *(arrows)*, the flexor digitorum superficialis tendon *(fds)* and the ulnar artery *(a)*. In **f**, observe the concave profile *(arrowheads)* of the ulnar nerve at the point where the cyst was removed, suggesting nerve entrapment

tial tears appear as a fusiform nerve swelling with hypoechoic echotextural changes (fusiform neuroma) in the absence of defects in nerve continuity. In large nerves, such as the median and the ulnar nerve, partial tears are best depicted in transverse planes showing the complete interruption of some fascicles whereas other fascicles retain a normal appearance (Fig. 10.61). With very high-frequency probes, a careful US assessment on short-axis planes can establish the percentage of affected fascicles. In most cases, an estimate of the fascicular involvement, i.e., whether less or more than 50% of fascicles are affected, can reliably be made. The wrist area where the median and ulnar nerves are particularly exposed to penetrating injures is located proximal to the carpal tunnel, where these nerves course superficially, just under the skin. The examiner should keep in mind that the flexor carpi radialis tendon is often affected in traumatic injures to the median nerve. Similarly, if the ulnar nerve is injured, the flexor carpi ulnaris tendon and the ulnar artery are rarely spared. Then, a nerve lesion should be suspected

if an open injury is followed by loss of tendon function. As a rule, the tendons of the middle and ring fingers lie more superficial than those of the index and little fingers and are, therefore, more likely to be involved by lacerations on the ventral wrist. In chronic nonoperated tears of the median and ulnar nerves, a hypertrophied neuroma usually develops at the level of nerve section, possibly causing a lump on the ventral wrist (Figs. 10.62, 10.63). Another typical site of nerve lesion by occupation-related extrinsic causes is the area of the hamate hook where the divisional branches of the ulnar nerve course in close apposition to the bone. Chronic external pressure caused by repetitive stress on the ulnar aspect of the volar wrist by crutches or repetitive use of tools during manual work or sporting activities, such as biking, may be the cause of a ulnar neuropathy involving the superficial or deep branch of the nerve at this site (Fig. 10.64). In these cases, a fusiform nerve thickening can be appreciated just over the hamate hook. Galeazzi fracture-dislocation may also lead to secondary ulnar neuropathy.
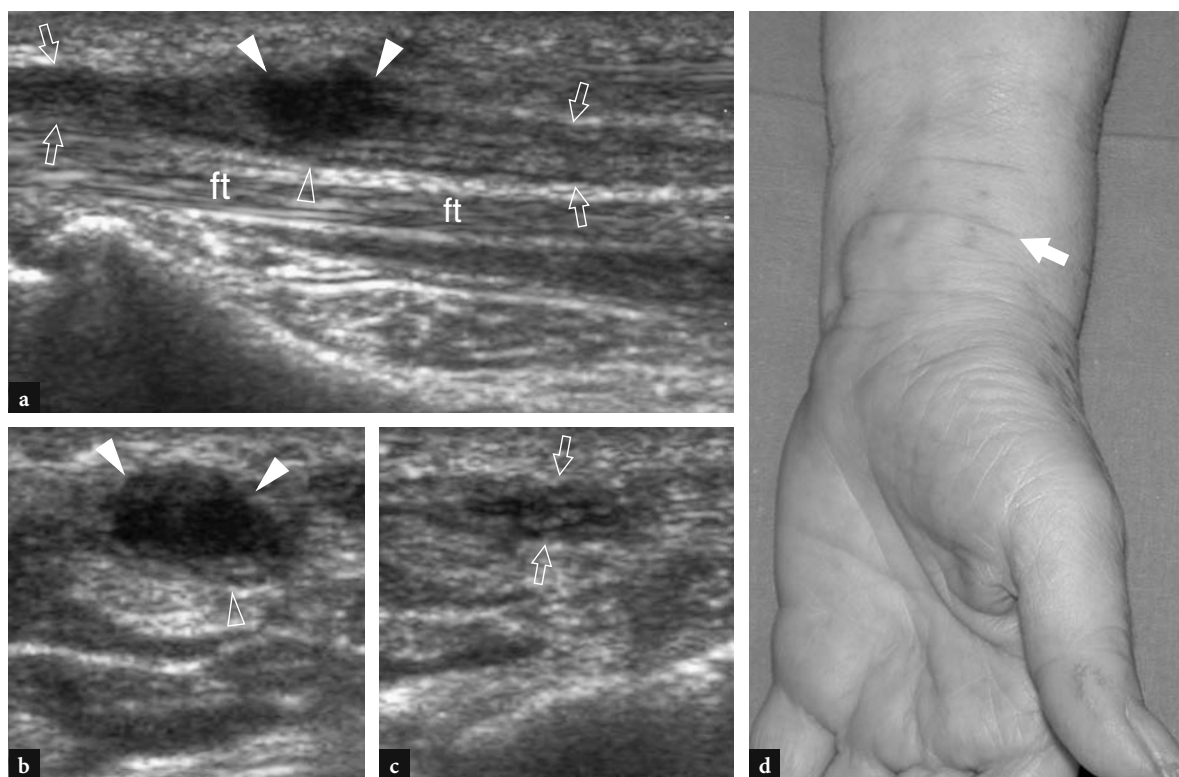
Fig. 10.61 a–d. Partial tear of the median nerve by a knife wound. **a** Long-axis 12–5 MHz US image of the median nerve (*arrows*) at the radial metaphysis reveals a solid hypoechoic neuroma (*white arrowheads*) developing from the severed superficial fascicles of the nerve, whereas the deep fascicles (*open arrowhead*) proceed unaffected. **b,c** Short-axis 12–5 MHz US images of the median nerve obtained **b** at the level of neuroma and **c** just proximal to it. Note the hypoechoic neuroma (*white arrowheads*) and some spared fascicles (*open arrowhead*) along the deep portion of the median nerve (*arrows*). **d** Photograph of the ventral wrist in the same case shows the scar (*arrow*) on the skin produced by the knife. The patient inflicted the wound on herself in an attempted suicide

Fig. 10.62 a,b. Post-traumatic neuroma of the median nerve. **a** Longitudinal 12−5 MHz US image over the distal forearm with **b** photographic correlation shows a hypertrophic traumatic neuroma (*arrowheads*) within the median nerve (*white arrows*) caused by a glass wound. The neuroma appears as a bulging hypoechoic irregular mass (*arrowheads*) with undefined margins due to adhesions. In the photograph, note the coexistent atrophy of the thenar eminence muscles (*open arrow*). The patient had associated injures of the flexor digitorum superficialis muscle and flexor carpi radialis tendon and presented with complete functional deficit of the median nerve. US was not able to quantify the grade of nerve damage within the neuroma
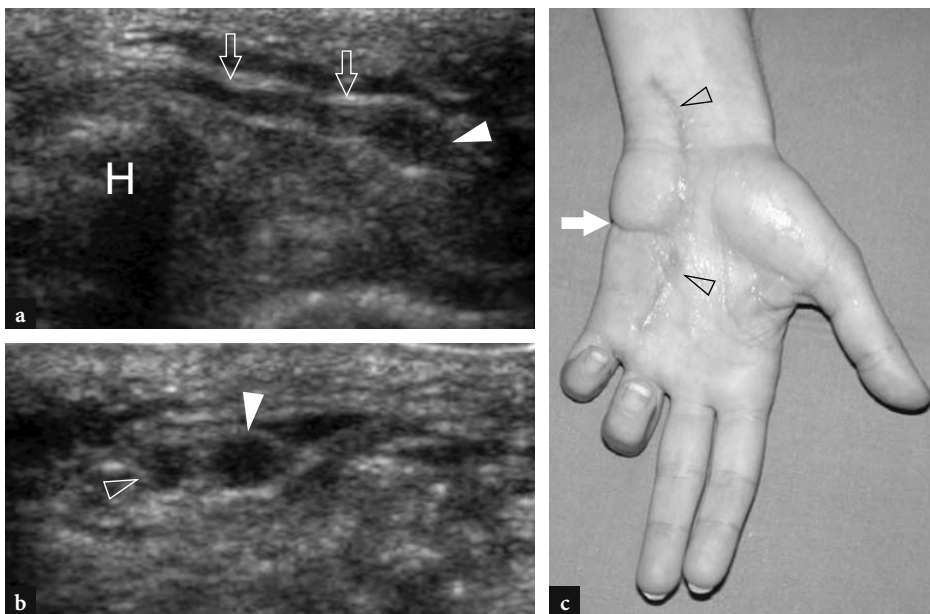
Fig. 10.63 a−c. Complete tear of the ulnar nerve by a wound from a rotating saw. **a** Longitudinal and **b** transverse 12−5 MHz US images obtained distal to the hamate hook *(H)* demonstrate complete tear of the superficial branch of the ulnar nerve. In **a**, note the wavy course of the proximal nerve stump (*arrows*) ending in a hypoechoic neuroma (*arrowhead*). In **b**, two adjacent neuromas are found connected with the proximal (*white arrowhead*) and distal (*open arrowhead*) stumps of the severed nerve. The patient had concurrent tear of the flexor tendons for the fourth and fifth fingers. **c** Photograph shows the cut line (*arrow*) in the hypothenar eminence and the subsequent operative access (*arrowheads*). Ulnar nerve suture failed and flexor tenorraphy led to finger retraction
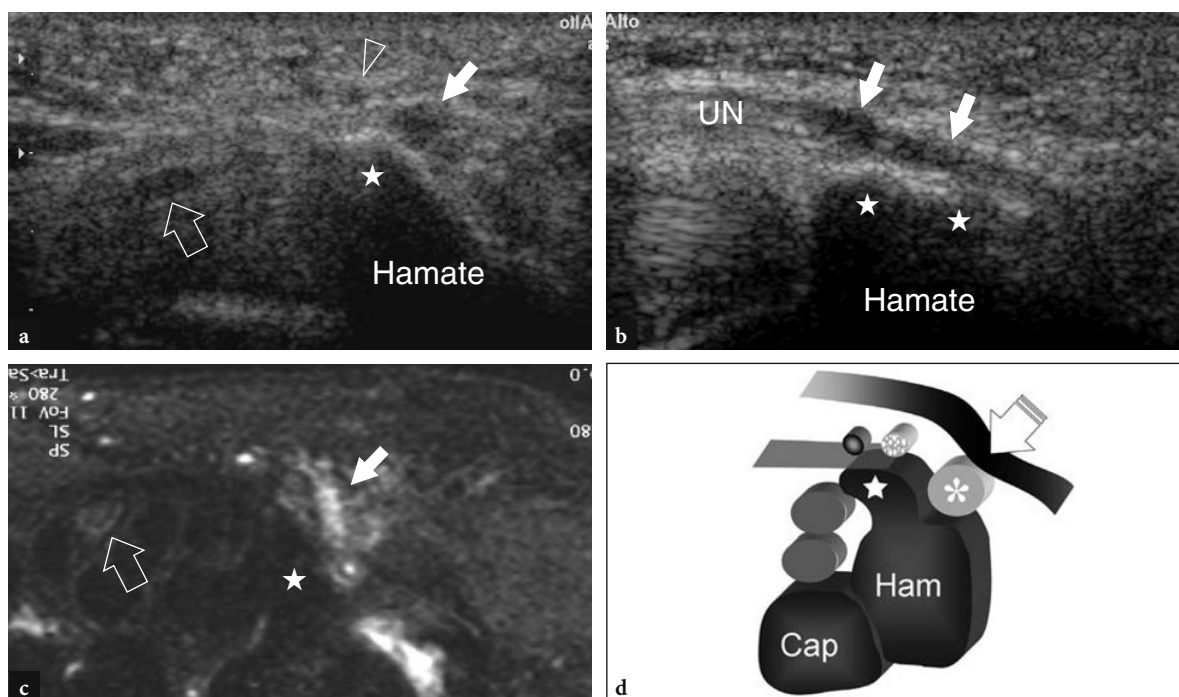
Fig. 10.64 a–d. Selective injury of the motor branch of the ulnar nerve at the hamate level in a patient with dorsal interosseous atrophy and normal sensitivity over the fourth and fifth fingers. **a** Transverse and **b** longitudinal 12–5 MHz US images obtained in the hamate hook area with **c** fat-suppressed T2w tSE MR imaging correlation demonstrate fusiform hypoechoic swelling (*white arrows*) of the deep branch of the ulnar nerve *(UN)* where it passes in close proximity to the hamate hook (*stars*). Note the larger size of the deep branch compared with the superficial branch (*arrowhead*). These branches should be similar in size in normal conditions. *Void arrow*, median nerve. **d** Schematic drawing illustrates the mechanism of injury due to direct compression of the nerve (*asterisk*) against the hamate (*star*) by external compression (*void arrow*). In this particular case, the patient walked on crutches and leaned her body weight over the palm of hands, thus compressing the ulnar nerve against the hamate

10.5.2.6
Vessel Trauma

Because of their superficial location and close proximity to the carpal bones, the vessels of the hand and wrist are particularly predisposed to direct trauma. Microtrauma to the vessel wall may cause intimal thickening with fibrin deposits that may lead to thrombosis and formation of pseudoaneurysms. The ulnar artery and its branches are typically affected at the Guyon tunnel (Hammer syndrome). The involvement of the superficial branch is more common because this small artery can be pinched between the skin and the hamate hook as the result of repeated local trauma. This often occurs in manual workers and in some recreational activities, such as biking (DE FAUCAL et al. 1991; KLEIN et al. 1991). Patients complain of a localized pain at the ulnar side of the palmar wrist as the consequence of ischemic changes in the ring and little fingers due to microembolisms and vasospasms. High-resolution US demonstrates an enlarged artery

with absent or diminished pulsatility and thickening of the arterial wall. The clot filling the lumen appears as a hypoechoic structure. Focal pressure with the probe can be painful and does not affect vessel size. Color and power Doppler imaging can enhance diagnostic confidence by showing no flow signals in the artery. Small collaterals can be demonstrated all around the thrombosed artery as a network of irregular vessels joining the two ends of the thrombus. Retrograde flow can be encountered in the arterial palmar arches in cases of occlusion of the radial or ulnar artery. As a result of a similar compression mechanism, the superficial branch of the radial artery can be severed against the tubercle of the trapezium (Fig. 10.65). Also, the radial artery may be damaged at operation for removal of a palmar ganglion which may encircle the vessel. Repetitive microtrauma to the ulnar artery can cause weakening of the vessel wall up to formation of pseudoaneurysms. The mass effect of the pseudoaneurysm and its stiffness may lead to ulnar nerve compression. The clinical diagnosis may
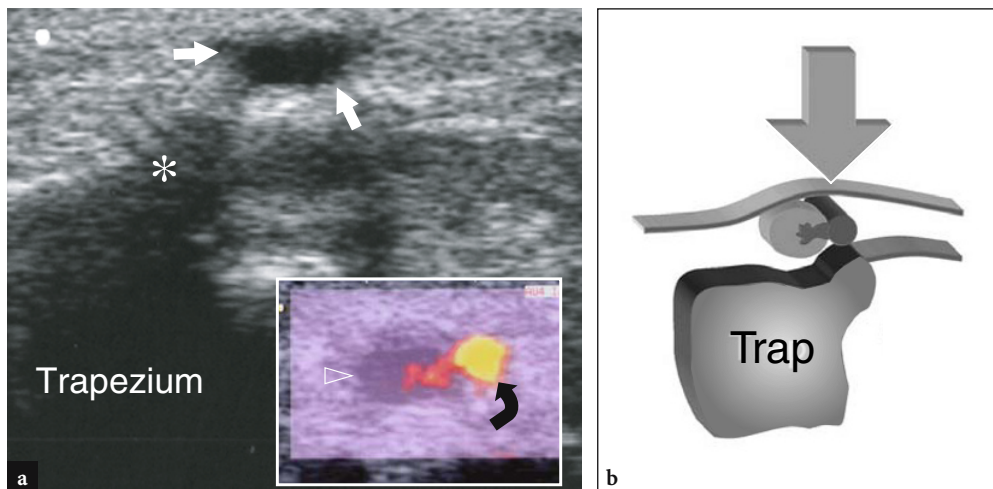
Fig. 10.65 a,b. Pseudoaneurysm of the palmar branch of the radial artery. **a** Transverse 12−5 MHz US image obtained at the radial volar aspect of the wrist with **b** diagram correlation shows a small hypoechoic mass (*white arrows*) overlying the tubercle (*asterisk*) of the trapezium. In the insert at the lower right side of the figure color Doppler imaging demonstrates the palmar branch of the radial artery (*curved arrow*) adjacent to the mass and flow signals reaching the center of the lesion (*open arrowhead*). In this patient the pseudoaneurysm resulted from chronic local trauma due to use of a wheelchair

be difficult in these cases because the patient with an aneurysm of the ulnar artery can have a mixture of neurologic and vascular symptoms. US demonstrates the hypoechoic sac of the aneurysm in continuity with the artery. Color and power Doppler imaging can be useful to confirm residual internal flow and to assess collateral vessels.

10.5.3
Bone and Joint Disorders

10.5.3.1
Synovitis

US has proved to be an accurate means to detect and quantify effusions in the distal radio-ulnar, radiocarpal, midcarpal and carpometacarpal joints (Koski 1992). Because the thickness of para-articular tissues is lower in the dorsal wrist, a dorsal approach is usually more adequate to assess these joint spaces. Fluid distention of the distal radio-ulnar joint is best depicted on transverse US images obtained at a more proximal level than the joint line, where the capsule has a greater compliance to distension (Fig. 10.66). Longitudinal US images are rarely useful to investigate the distal radio-ulnar joint. On the other hand, these are the best planes to assess the dorsal recesses of the radiocarpal and midcarpal joints (Fig. 10.67). Effusions in the radiocarpal, midcarpal and carpometacarpal recesses are, in fact, well depicted on

midsagittal US images. At these levels, transverse US images are most useful to distinguish between deep intra-articular fluid and superficial sheath effusions of the extensor tendons. Coronal US scans may also be useful to investigate the radiocarpal joint at the level of the radioscaphoid space during passive radial and ulnar deviation of the wrist.

Similar to other joints in the body, differentiation between effusion and synovial pannus may not be easy at wrist due to their similar hypoechoic echotexture. As a general rule, the pannus appears more echogenic and pressure applied on it with the probe causes only a partial collapse of the recess, whereas free fluid is easily squeezed away from the field-of-view of the US image. Owing to the superficial position of the wrist joints, color and power Doppler systems can be helpful for this purpose by revealing blood flow inside the synovial membrane. One should be aware that the hyperemia is dependent on the degree of inflammation and that a less active "fibrous" pannus may appear completely free of color flow signals.

10.5.3.2
Rheumatoid Arthritis

A variety of arthritides can affect the wrist joints, the most important of which are rheumatoid arthritis and psoriatic arthritis. Rheumatoid arthritis, is characterized by bilateral and symmetric synovitis. The first manifestation of arthritis is serous syno-
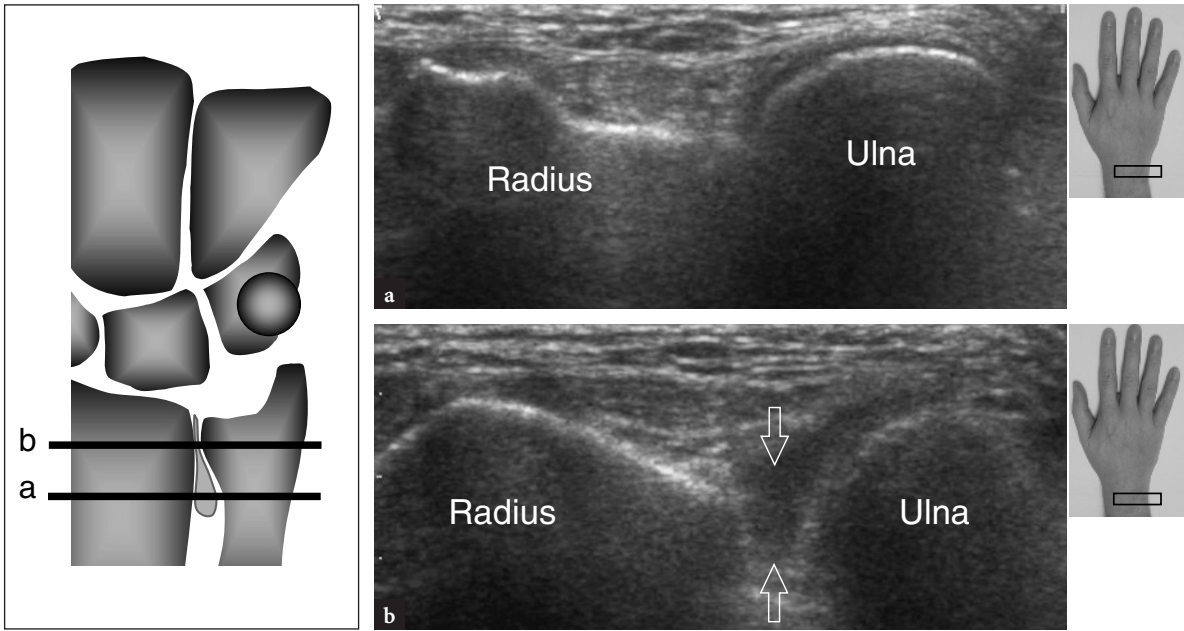
Fig. 10.66 a,b. Distal radio-ulnar joint synovitis. **a** Distal and **b** proximal transverse 12–5 MHz US images obtained over the dorsal aspect of the distal radio-ulnar joint at the levels (*horizontal black bars*) indicated in the diagram on the left show the proximal recess distended by fluid (*arrows*). No effusion is seen at the level of the articular cartilages. The inserts at the upper right sides of the figure indicate probe positioning
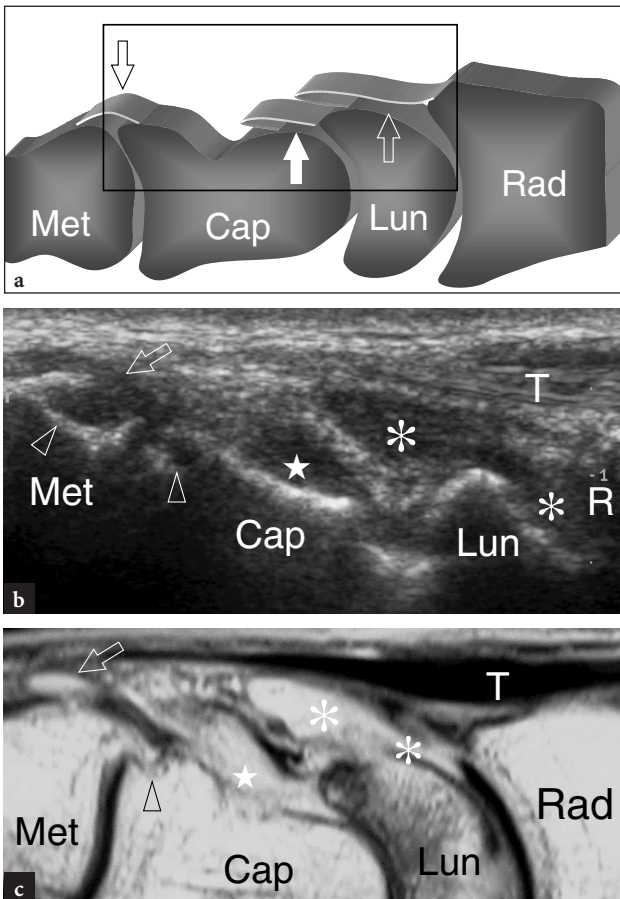
Fig. 10.67 a–c. Synovitis of the wrist joints. **a** Schematic drawing of the dorsal aspect of the wrist illustrates the position of the recesses of the radiocarpal (*open white arrow*), midcarpal (*white arrow*) and carpometacarpal (*open black arrow*) joints. **b,c** Corresponding longitudinal **b** 12–5 MHz US and **c** T2w tSE MR images in a patient with advanced rheumatoid arthritis demonstrate synovitis of the radiocarpal (*asterisks*), midcarpal (*star*) and carpometacarpal (*open arrow*) joints. The field-of-view of the US and MR images are indicated in **a** by a black box. Based on the shape of carpal bones, US is able to depict the distension of each individual recess of the wrist joints. Note the small bone erosions (*arrowheads*) at the distal pole of the capitate. *Met*, metacarpal; *Cap*, capitate; *Lun*, lunate; *Ras* in **a,c** and *R*, in **b**, radius; *T*, extensor tendons

vitis with moderate hyperplasia of the synovial membrane and hyperemia of the para-articular structures. Later in the course, the synovial membrane becomes markedly thickened and hypervascular, leading to formation of synovial pannus which causes bone erosions and disintegration of the articular cartilages. The pannus leads to progressive damage of the joint capsule and ligaments and subsequent joint instability. The diagnosis of rheumatoid arthritis relies on clinical features, serologic tests (Waaler-Rose and Latex tests) and radiographic findings. However, serology can be negative in patients with overt disease (seronegative arthritides) and radiography may demonstrate only late changes when erosions are present. Because an early diagnosis is critical for establishing aggressive therapy and preventing destructive joint changes, additional imaging modalities, such as MR imaging, are used. MR imaging is an accurate means to evaluate the para-articular soft tissues, to detect intra articular effusion and synovial pannus and to show cartilaginous damage and bone erosion (Sugimoto et al. 2000). However, this modality is expensive and not always adequate to ensure follow-up of chronic disorder.

In recent years, increasing attention has been directed to the role of US in the assessment of rheumatoid arthritis of the wrist and hand (Koski 1992; Koski and Hermunen 2001; Lund et al. 1995; van

Vugt et al. 1997, 1998; de Flaviis et al. 1988). US findings of arthritic joints depend on the stage and severity of the disease. At early stages, high-resolution US can detect the presence and location of intra-articular effusions in the recesses of the wrist joint, thus allowing differentiation between joint and para-articular involvement (Fig. 10.68). In advanced disease, high-resolution US shows widening of the joint cavity and synovial pannus appearing as a hypoechoic structure partially or completely filling the joint space. At color Doppler imaging, the hyperemic pattern of the synovium correlates well with the disease activity and can be used as a parameter to follow up the patients (Fig. 10.69). When necessary, synovial biopsy (van Vugt et al. 1997) and intra-articular injection of corticosteroid (Koski and Hermunen 2001) can be effectively guided with US in the appropriate joint space.

Loss of definition and thinning of the articular cartilages may reflect the chondrolytic process of arthritis. The examiner should keep in mind that US allows only a partial evaluation of the hyaline cartilages of the radiocarpal and midcarpal joints due to the vertical orientation of many joint surfaces relative to the probe. In addition, the articular cartilages of the distal radioulnar joint cannot be depicted with US. At certain sites, however, dynamic scanning can improve their demonstration. This is true for the dorsal cartilages of the radiocarpal and midcarpal joints, such as the
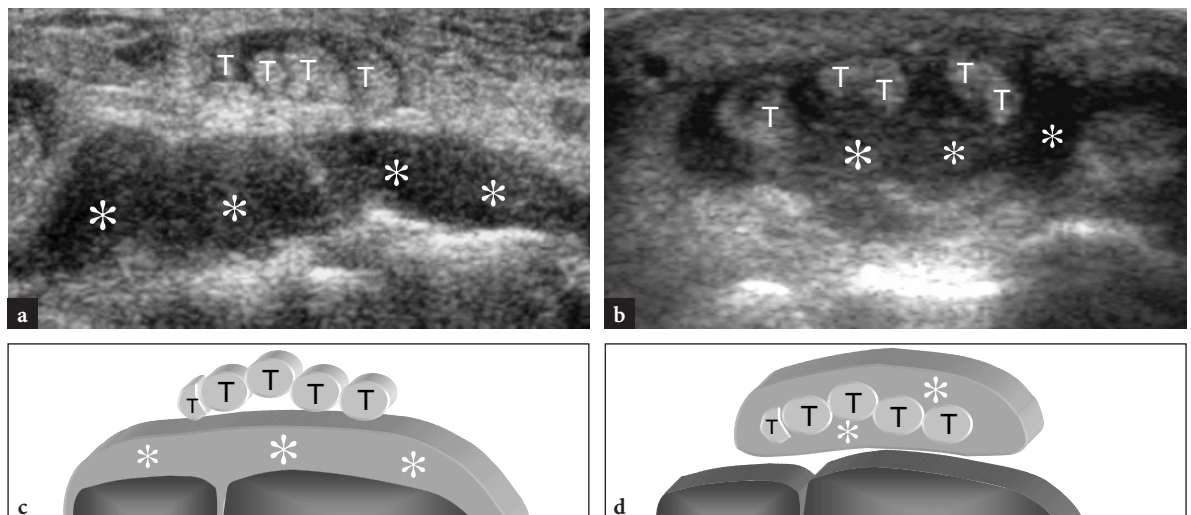
Fig. 10.68 a–d. Distinguishing joint synovitis versus extensor tenosynovitis with US. **a,b** Transverse 12–5 MHz US images obtained over the dorsal wrist in two patients with rheumatoid arthritis each presenting with tenderness and swelling over the dorsal right wrist. In **a**, the synovial effusion (*asterisks*) is closely apposed to the wrist bones because the inflammatory process involves the dorsal recesses of the wrist joints, whereas the overlying extensor tendons *(T)* are spared. In **b**, the effusion (*asterisks*) occurs all around the extensor tendons *(T)* as an expression of tenosynovitis, while the dorsal recesses of the wrist joints are normal. **c,d** Diagram correlations
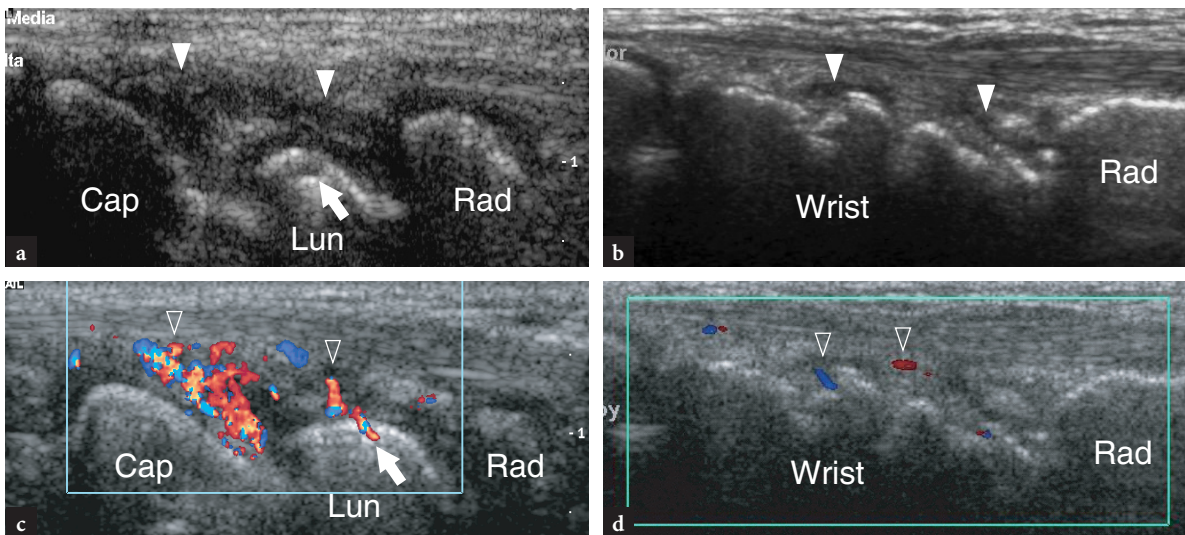
Fig.10.69 a−d. Distinguishing active versus inactive rheumatoid pannus with color Doppler imaging. **a,b** Longitudinal **a** gray-scale and **b** color Doppler 12−5 MHz US images over the dorsal wrist in a child with juvenile rheumatoid arthritis show active pannus (*white arrowheads*) as a marked thickening of the synovial membrane characterized by a hypervascular pattern (*open arrowheads*) at color Doppler imaging. Note a small erosion on the posterior pole of the lunate filled by active pannus and containing color flow signal inside. **c,d** Longitudinal **c** gray-scale and **d** color Doppler US images over the dorsal wrist in a patient with chronic rheumatoid disease reveal "fibrous" pannus as a thin hypoechoic area (*arrowheads*) overlying the carpal bones. Note the indistinct outline of the carpal bones related to extensive erosions and joints destruction following chronic articular involvement. *Cap*, capitate; *Lun*, lunate; *Rad*, radius
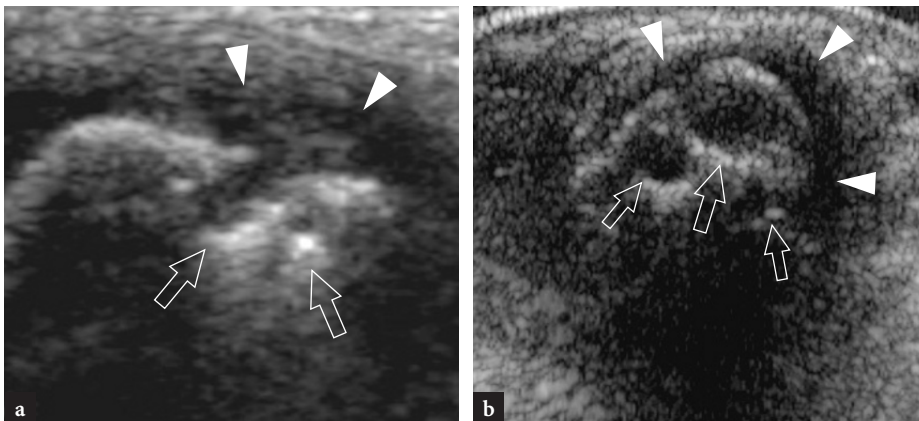
Fig.10.70 a,b. Bone erosions. **a,b** Transverse 12−5 MHz US images over the ulnar head in two patients with longstanding rheumatoid arthritis reveal bone erosions (*arrows*) as small regular defects of the cortical outline. Note the synovial pannus (*arrowheads*) located inside and around them

dorsal cartilage of the lunate, while scanning with the hand flexed. Again, the scaphoid cartilage can be better depicted when coronal planes over the radial aspect of the wrist are obtained with ulnar deviation. In chronic arthritis, bone erosions appear as areas of focal cortical discontinuity and as oval or round well-defined defects of the cortex (Fig. 10.70). Erosions can be seen filled by pannus that, in active synovitis, can show hyperemic flow coming from the inner bone (Fig. 10.69a,b). The sites more commonly involved by erosive arthri-

tis are the dorsal aspect of the posterior horn of the lunate and the ulnar styloid. At these levels, erosions may be the result of synovitis of the distal radio-ulnar and radiocarpal joint, as well as of the involvement of the extensor carpi ulnaris tendon. As the destructive process progresses and the erosions grow in size and become more numerous, the carpal bones become indistinct and difficult to differentiate from one another. In patients with chronic disease, subluxation of joints follows weakening and rupture of ligaments,
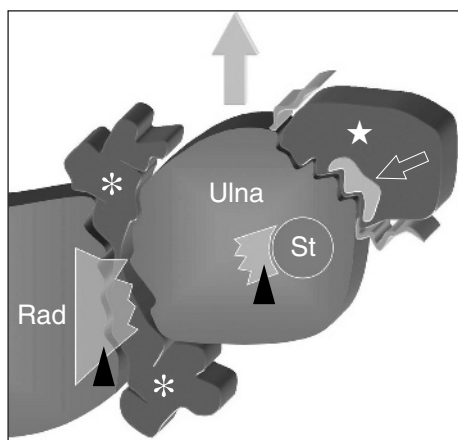
Fig. 10.71. Caput ulnae syndrome in rheumatoid arthritis. Schematic drawing of a transverse view through the distal radio-ulnar joint outlines the rupture of the triangular fibrocartilage (*arrowheads*) and marginal erosions at the distal radio-ulnar joint level due to intra-articular pannus (*asterisks*). As a result, the ulna subluxes dorsally (*gray arrow*). Pannus (*star*) inside the extensor carpi ulnaris tendon (*open arrow*) sheath leads to cortical erosions, tear of the retinaculum and tendon thinning and splitting. *St*, styloid of the ulna; *Rad*, radius

tears of tendons with a para-articular course and disintegration of the articular surfaces of bones. Functional insufficiency of the triangular fibrocartilage, secondary to chronic radiocarpal and distal radio-ulnar joint synovitis, may lead to dorsal dislocation of the ulnar head (Fig. 10.71). This latter finding associated with erosions and irregularities of the bony contours and

inflammation of the adjacent sheath of the extensor carpi ulnaris tendon can lead to dislocation and longitudinal splitting of the extensor carpi ulnaris tendon and possible tears of the extensor digitorum of the ring and little fingers, the so-called caput ulnae syndrome (Fig. 10.72). Final stages of wrist involvement by rheumatoid arthritis are characterized by ankylosis that appears as a continuous hyperechoic line at the surface of wrist bones reflecting bone fusion.

Once the diagnosis of rheumatoid arthritis is made, the examiner should also accurately evaluate the integrity of para-articular tendons, because in longstanding tenosynovitis the cytokine-mediated lytic action of the pannus and the presence of enzymes in the synovial fluid can lead to their secondary damage. When involved by the disease process, tendons become swollen and may exhibit a heterogeneous fibrillar structure because of chronic biochemical and mechanical damage (Fig. 10.73). Then, they may appear thinner (reflecting a partial tear) or completely interrupted and retracted (reflecting a complete tear) (Fig. 10.74). In patients with rheumatoid arthritis, the extensor tendons of the little and ring fingers most commonly rupture at wrist (Fig. 10.75). As stated before, this seems to be secondary to repetitive friction over the irregular bony surface of the dorsally displaced ulnar head. Early US detection of tendon involvement is critical because it can indicate the need for tenosynovectomy, which is effective to prevent further tendon damage and complete tears. When partial and complete tears cannot be differentiated based on clinical
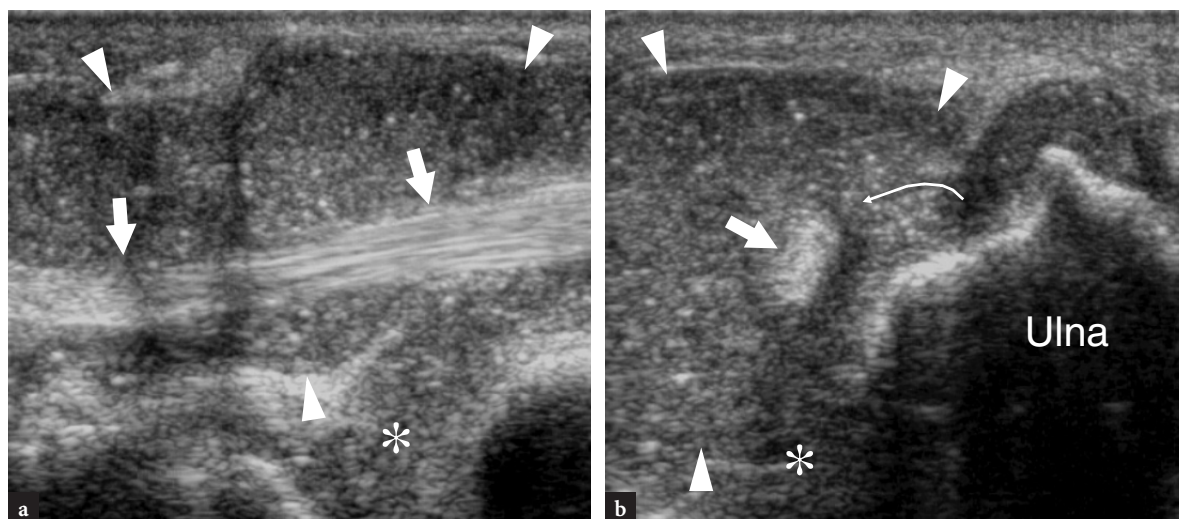
Fig. 10.72 a,b. Caput ulnae syndrome in rheumatoid arthritis. **a** Longitudinal and **b** transverse 12–5 MHz US images over the extensor carpi ulnaris tendon (*straight arrows*) reveal synovial pannus inside the distal radio-ulnar joint (*asterisk*) and the extensor carpi ulnaris tendon sheath (*arrowheads*). The tendon is dislocated (*curved arrow*) out of its ulnar groove due to the tear of the retinaculum. See Fig. 10.20b for comparison with normal findings
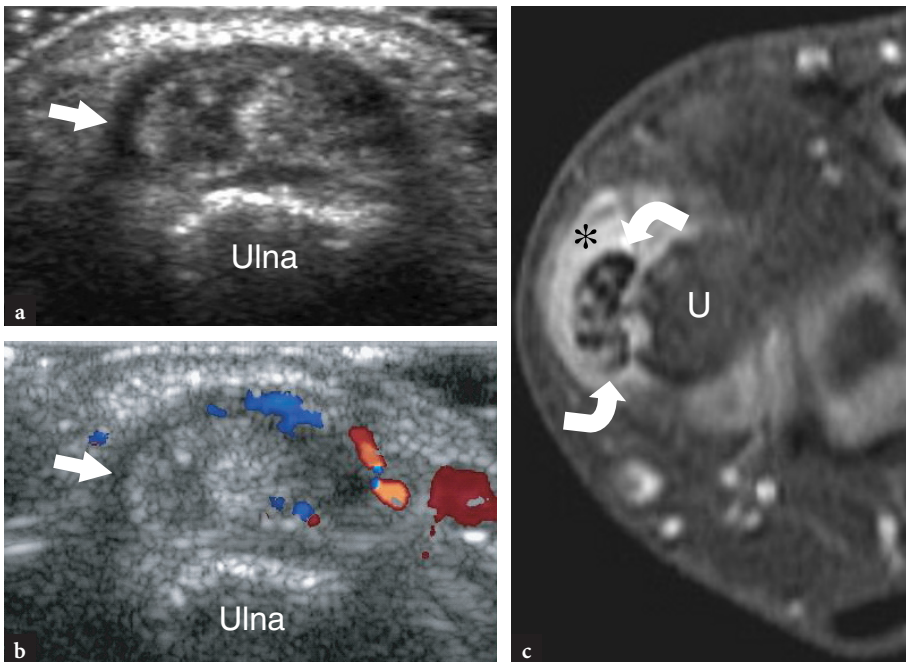
Fig. 10.73 a–c. Longitudinal splits of the extensor carpi ulnaris tendon in rheumatoid arthritis. Transverse **a** gray-scale and **b** color Doppler 12–5 MHz US images over the ulnar head demonstrates a swollen and heterogeneous extensor carpi ulnaris tendon (*arrow*) with intrasubstance hypoechoic clefts suggesting longitudinal fissuration. At color Doppler imaging, increased signals of flow are visible at the synovial sheath level relative to inflammatory hyperemia. **c** Correlative transverse fat-suppressed T2w MR image reveals mild sheath effusion (*asterisk*) and intratendinous areas of increased signal intensity consistent with a partial tear of the extensor carpi ulnaris tendon (*curved arrows*).*U*, ulna
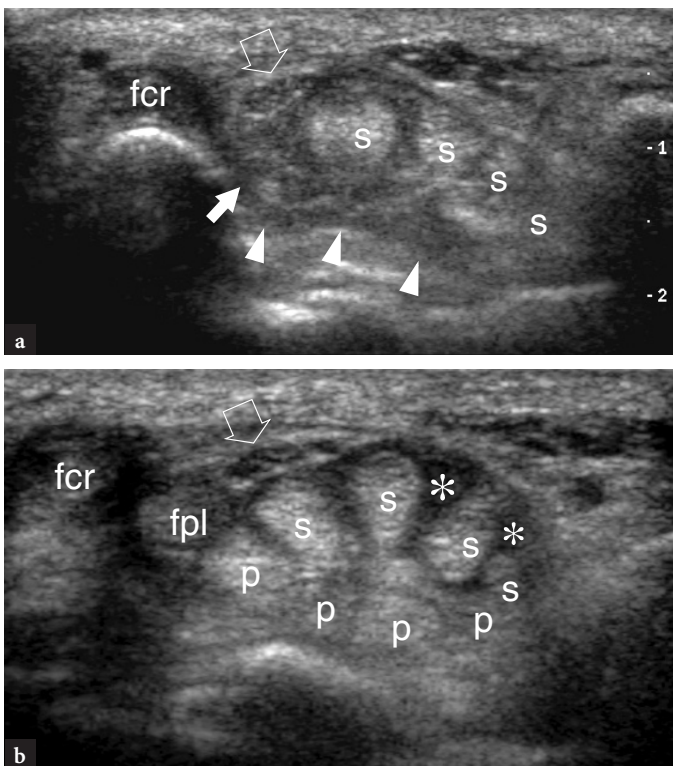
Fig. 10.74 a,b. Multiple flexor tendon tears in rheumatoid arthritis. **a** Transverse 12–5 MHz US image of the right carpal tunnel in patient with the deficit of finger flexion more evident at the distal phalangeal level demonstrates the absence of flexor pollicis longus (*white arrow*) and flexor digitorum profundus (*arrowheads*) tendons. The residual tendons of the flexor digitorum superficialis *(s)* are intact but swollen. **b** Corresponding transverse 12–5 MHz image of the left carpal tunnel demonstrates flexor tenosynovitis (*asterisks*) without signs of tendon discontinuity. In particular, note the flexor digitorum profundus *(p)* and the flexor pollicis longus *(fpl)* tendons which are not detectable in **a**. *Open arrow*, median nerve; *fcr*, flexor carpi radialis
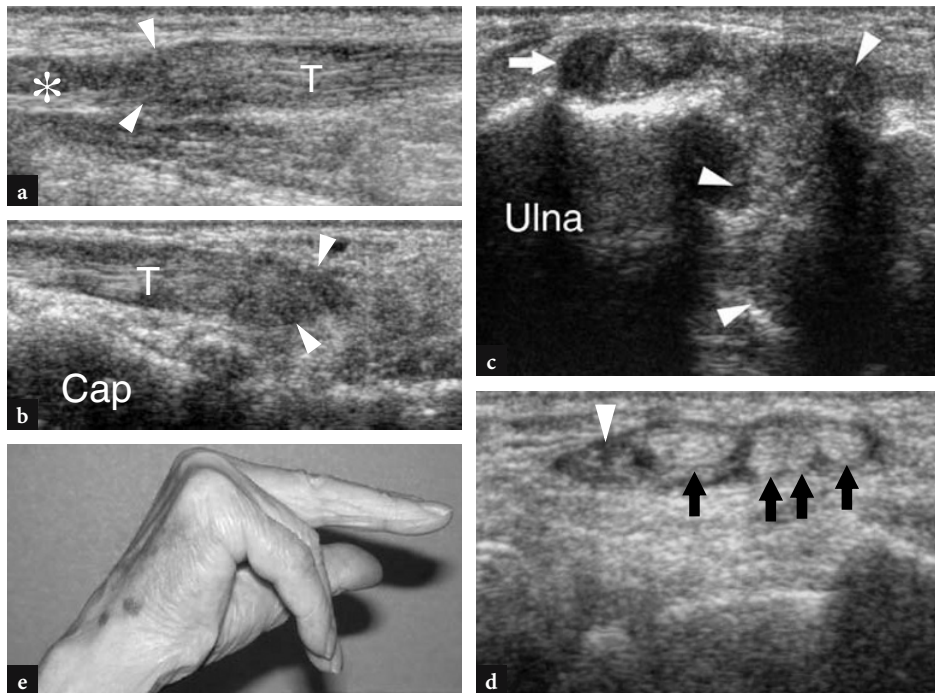
Fig. 10.75 a–e. Complete extensor tendon tear in rheumatoid arthritis. **a,b** Longitudinal 10−5 MHz US images over the dorsal wrist obtained **a** at the distal end of the forearm and **b** over the carpal bones reveal the proximal and distal torn ends (*arrowheads*) of the tendon for the fifth finger *(T)* of the extensor digitorum. A small effusion (*asterisk*) within the tendon sheath is found at the level of the tear. *Cap*, capitate. **c,d** Transverse 12−5 MHz US images obtained **c** at the level of the distal radio-ulnar joint and **d** over the carpal bones. In **c**, US shows synovial pannus which fills the distal radio-ulnar joint space (*arrowheads*) and communicates with the sheath (*arrow*) of the extensor carpi ulnaris tendon. In **d**, the medial tendons of the fourth compartment for the ring and little fingers are no longer detectable. Observe the residual normal tendons for the middle and index fingers and the extensor indicis proprius (*black arrows*). The sheath contains synovial pannus and small amount of hypoechoic fluid. **e** Photograph demonstrates failure of active extension of the ring and little fingers

findings alone, dynamic US evaluation can be useful to give direct demonstration of the lack of tendon movements. In complete ruptures, high-resolution US has a value in accurately locating the proximal retracted end of the torn tendon (Fornage 1989) and in excluding any nerve compression, such as that of the posterior interosseous nerve at the elbow, which can possibly mimic tendon ruptures.

Another typical complication related to the inflammatory process in rheumatoid arthritis is tendon instability that occurs secondary to loosening or rupture of the retinacula. This condition affects the extensor carpi ulnaris tendon and derives from involvement of the distal radio-ulnar joint by the pannus with secondary tearing of the triangular fibrocartilage and upward displacement of the ulnar head, or by weakening of the tendon sheath. The ventral displacement of the extensor carpi ulnaris can be seen during supination or palmar flexion of the wrist and requires dynamic scanning for proper assessment. Longitudinal splitting can complicate the intermittent snapping of the tendon over the irregularly eroded cortex of the ulna.

10.5.3.3
Scapholunate Dissociation

The scapholunate ligament plays an essential role as a stabilizer of the proximal carpal row during wrist motion, maintaining the scaphoid in a correct position and preventing its palmar tilt. Ligament tears result in scapholunate diastasis, palmar flexion of the scaphoid, dorsal flexion of the lunate and proximal repositioning of the capitate. Longstanding ruptures lead to degenerative changes at the capitate-lunate and radio-scaphoid joints, the so-called SLAC wrist (Scapho-Lunate Advanced Collapse), a painful condition that greatly reduces the range of motion of the wrist. Some authors have reported the US appearance of the normal scapholunate ligament (Griffith et al. 2001) and the range of normal scapholunate intervals in different degrees of ulnar and radial deviation. Due to its anatomic position, only the dorsal and ventral components of this ligament can be examined by means of transverse dorsal and ventral imaging planes. In this study, the dorsal

component was completely visible in 48% of cases, partially visible in 30%, barely visible in 8% and not detectable in 15%. The scapholunate ligament appears as a hyperechoic fibrillar structure bridging the hyperechoic cortex of the two bones (Jacobson et al. 2002). The mean thickness of its dorsal band is 1.1 mm and the mean interosseous distance is 4.2 mm. Because of its deep location, the thin ventral component of the ligament is barely visible. Considering the high percentage of poorly visualized dorsal ligaments, its non-visualization at US does not indicate injury. Although the measurement of the interosseous distance is hampered by technical reasons (unclear landmarks for caliper positioning), a clear increase in its size during scanning with ulnar deviation of the wrist should alert the examiner to suggest further imaging modalities to confirm a possible tear (Fig. 10.76). Complications of failed surgical repair of the scapholunate ligament can seldom be demonstrated with US.

10.5.3.4
Triangular Fibrocartilage Tears

The triangular fibrocartilage of the wrist can be depicted with US using a palmar approach with transverse and oblique sagittal images (Chiou et al. 1998). In these planes, it appears as a triangularly shaped homogeneous hyperechoic area of >2.5 mm (confidence level 95%) in thickness, somewhat similar to the knee menisci and the glenoid labrum. In arthrographically proven pathological cases, tears of the triangular fibrocartilage can be appreciated with US as either a focal thinning (<2.5 mm) or a localized hypoechoic cleft within it (Fig. 10.77). Some authors have reported a sensitivity of 68.4% and a specificity of 96.4% for the US diagnosis of triangular fibrocartilage tears (Chiou et al. 1998). In our own experience, we encountered difficulties in accurately assessing the thickness of the triangular fibrocartilage in both normal and pathologic states as well as in reliably assessing its tears.
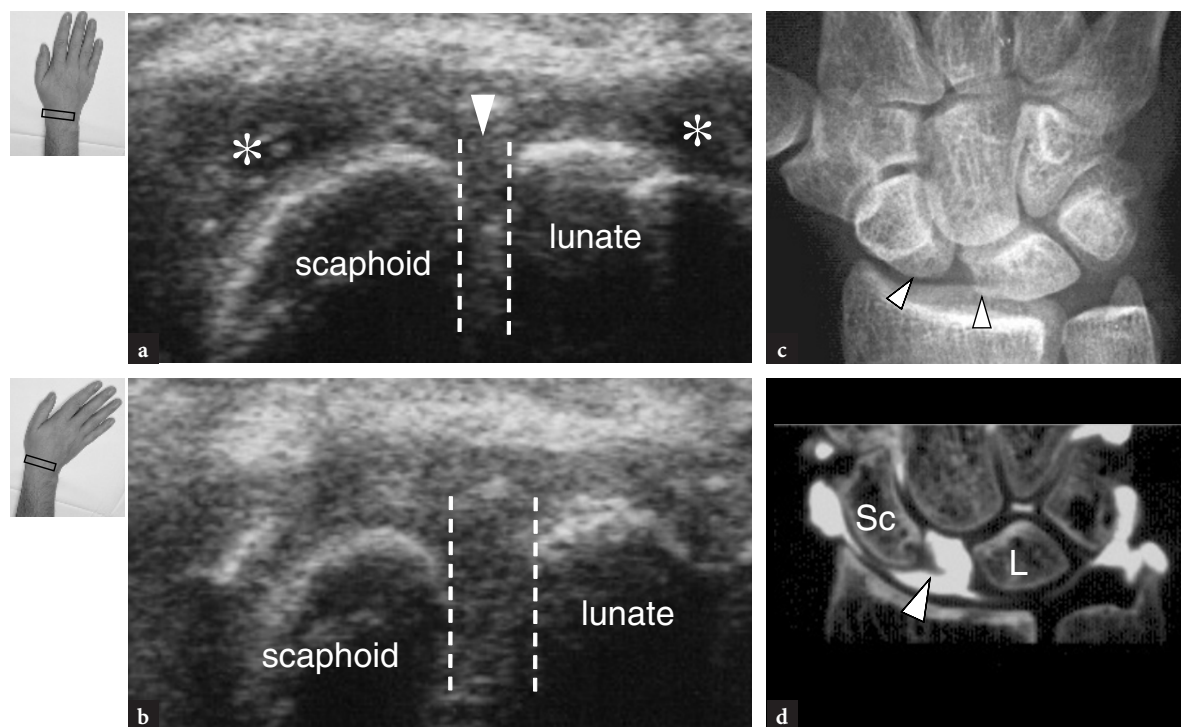
Fig. 10.76 a–d. Scapholunate dissociation. **a,b** Transverse 12–5 MHz US images obtained over the dorsal aspect of the proximal carpal row in a patient who sustained a twisting trauma of the wrist. **a** In neutral position, fluid is observed in the radiocarpal joint recesses (*asterisks*). Note the absence of the scapholunate ligament (*arrowhead*) with respect to the normal findings shown in Fig. 10.18b. The dashed lines demarcate the distance between the scaphoid and the lunate. **b** During ulnar deviation of the wrist, widening of the scapholunate distance can be appreciated. This can be considered an indirect sign of ligament tear. **c** Radiograph shows a broadened scapholunate distance (*arrowheads*) and a foreshortened scaphoid. **d** CT arthrography following contrast medium injection into the radiocarpal joint demonstrates the passage of contrast material inside the midcarpal joint thus confirming the ligament tear. Note the lateral end of the scapholunate ligament (*arrowhead*). *Sc*, scaphoid; *L*, lunate. The inserts at the upper left side of the figure indicate wrist and probe positioning
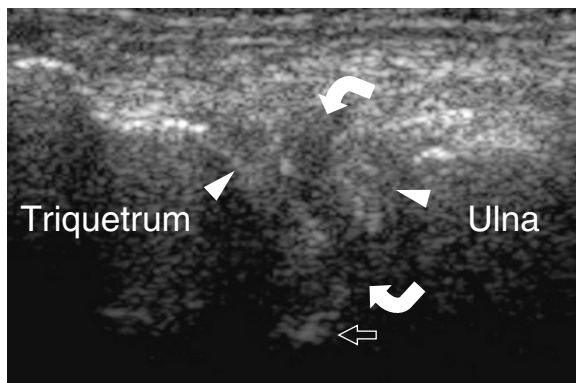
Fig. 10.77. Triangular fibrocartilage tear. Coronal 12−5 MHz US image over the ulnar aspect of the wrist in a patient with a proved communicating tear of the triangular fibrocartilage at CT arthrography demonstrates a well-defined hypoechoic cleft (*curved arrows*) within the hyperechoic fibrocartilaginous tissue lying between the triquetrum and the ulna, consistent with a tear. *Open arrow*, distal radius

In addition, US seems inadequate to differentiate traumatic and degenerative lesions, which can have therapeutic and legal implications. Although results in progress from some groups are encouraging in this field (Keogh at al. 2004), we believe that additional efforts should be made to establish the ultimate role of US in evaluating lesions of this structure.

10.5.3.5
Ligament Calcifications

Calcification of wrist ligaments can follow traumatic injuries or result from crystal pyrophosphate depo-

sition disease. In this disorder, wrist calcifications can be found within the triangular fibrocartilage and within intrinsic and extrinsic wrist ligaments, such as the scapholunate and lunotriquetral ligaments. US is not considered the best modality to detect crystal depositions and a definite diagnosis of crystal pyrophosphate deposition disease basically relies on standard radiographs and analysis of the synovial fluid. Nevertheless, the examiner must be aware of these findings as they can be detected incidentally during a routine examination of the wrist (Fig. 10.78). The appearance of ligament calcifications is that of hyperechoic spots embedded within the involved structure. Once US has suggested the diagnosis and the finding is believed clinically useful, an anteroposterior radiograph should be obtained to confirm it.

10.5.3.6
Occult Fractures and Dislocations of Carpal Bones

It is undisputed that the diagnostic investigation of wrist fractures and dislocations relies on clinical findings and standard radiographs and not on US findings. Nevertheless, the anatomic complexity of the wrist area often means some wrist fractures and dislocations are unnoticed on standard radiographs. In this setting, high-resolution may have an ancillary role in detecting occult fractures, bony avulsions and dislocations during a conventional US examination of the wrist. For this reason, bone surfaces should be accurately analyzed during a routine US examination, because even small irregularities can suggest the correct diagnosis. The US appearance of traumatic
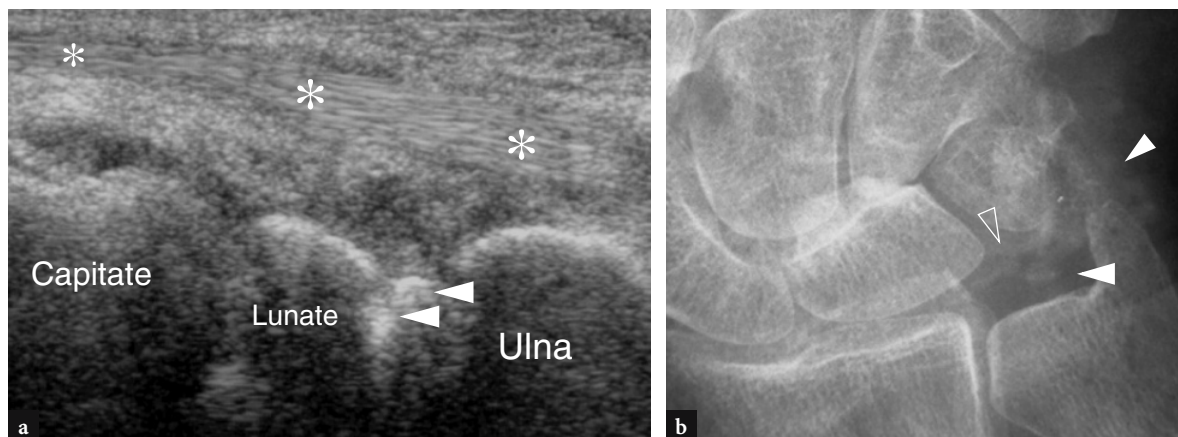
Fig. 10.78 a,b. Wrist ligament calcifications in crystal pyrophosphate deposition disease. **a** Longitudinal oblique 12−5 MHz US image over the middle third of the wrist reveals bright hyperechoic spots (*arrowheads*) inside the lunotriquetral ligament. *Asterisks*, extensor tendons. **b** Anteroposterior radiograph confirms calcifications inside the ligament (*open arrowhead*) and in the adjacent triangular fibrocartilage (*white arrowheads*)

lesions of wrist bones includes a step-off deformity or a focal interruption of the cortical continuity in fractures and a disruption of the normal relationship between two adjacent bones in dislocations. When the occurrence of a fracture is suspected at US examination, further imaging studies with additional radiographic views, CT and MR imaging must be obtained depending on the specific situation to confirm the diagnosis as well as to assess the number and position of the fragments in fractures or the relation of bony ends in dislocations.

The scaphoid is the most common site of occult fractures in the wrist area, with up to 20–25% of cases unnoticed at the initial evaluation (WAIZENEGGER et al. 1994). When the diagnosis is delayed, scaphoid fractures have high rates of complications such as pseudoarthrosis, avascular necrosis of the proximal pole of the bone and secondary radiocarpal osteoarthritis with chronic pain and impaired function. A variety of diagnostic modalities, such as additional radiographic views, bone scan, CT and MR imaging, have been advocated for early detection of scaphoid fractures. The choice between an addi-

tional radiograph obtained after 10 days and more expensive modalities depends on the specific clinical situation, equipment availability and economic factors. High-resolution US can evaluate the scaphoid cortex by means of longitudinal images obtained over its palmar and lateral aspects. With both lateral and palmar approaches, care should be taken to align the transducer to the long axis of the scaphoid. Longitudinal images over the lateral aspect of the bone demonstrate a small ridge at the middle third of the lateral face reflecting the scaphoid tubercle. This tubercle separates the proximal articular facet from the distal nonarticular portion of the bone and should not be misinterpreted as a fracture (Fig. 10.79). Several studies have reported the main US findings in cases of scaphoid fracture (HODGKINSON et al. 1993; HERNETH et al. 2001). Two scanning technique have been proposed. In the first, color Doppler imaging is used to measure the distance between the radial artery and the scaphoid cortex using a lateral approach (HODGKINSON et al. 1993). The superficial displacement of the artery due to post-traumatic local edema is assessed in comparison with the unaffected side. A
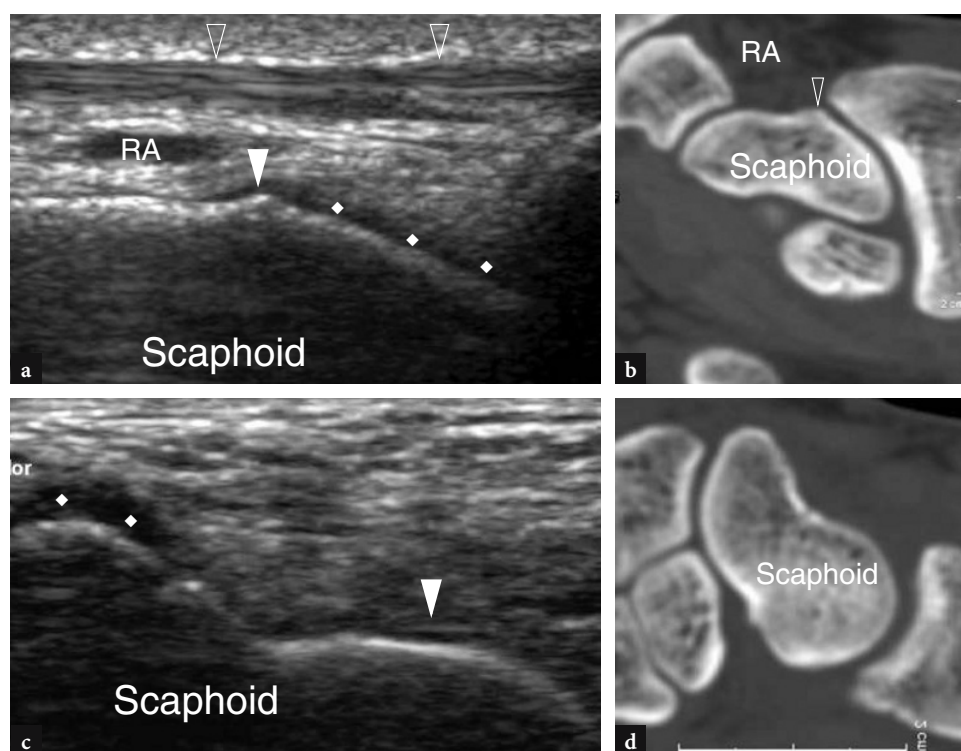
Fig. 10.79 a–d. Normal US appearance of the scaphoid bone. **a** Coronal 15–7 MHz US image over the lateral aspect of the scaphoid reveals the tubercle (*white arrowhead*) and the cartilage covering its radial face (*rhombi*). The radial artery (RA) and the extensor tendons of the first compartment (*open arrowheads*) pass superficial to the bone. **b** Longitudinal 12–5 MHz US image over the palmar aspect of the scaphoid displays the cartilage covering the distal (*rhombi*) and proximal (*arrowhead*) articular faces of the bone. **c,d** Corresponding 2D reformatted CT images

scaphoid index has also been introduced to reduce the variability in the normal scaphoid-radial artery distance. For threshold values ≥30%, a 100% sensitivity and 74% specificity were reported for this index. With progressive advancements in transducer technology, some authors also described the ability of US to detect scaphoid fractures based on detection of a focal interruption of the hyperechoic bony cortex (HERNETH et al. 2001; HAUGER et al. 2002) (Fig. 10.80). A meticulous scanning technique with transverse and longitudinal US scans over the ventral, lateral and dorsal aspects of the scaphoid in both neutral and ulnar deviation

positions is required for this study. Based on cortical disruption as the only diagnostic key, US proved to have 100% sensitivity, 98% specificity and 98% accuracy for the depiction of fractures of the waist of the scaphoid (HAUGER et al. 2002). As an additional feature, some authors interpreted an echogenic line parallel to the cortex as an expression of periosteal elevation (HERNETH et al. 2001). We believe this latter sign cannot be reliably differentiated from the acoustic interface between fluid and cartilage. However, based on cortical discontinuity and/or periosteal elevation, these authors showed an 87% overall accuracy of US
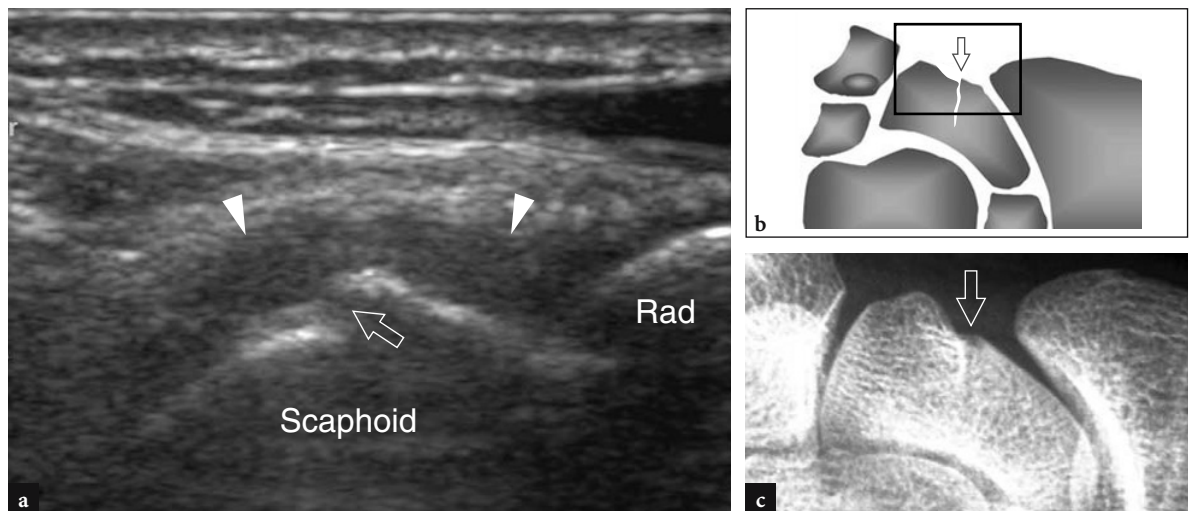
Fig. 10.80 a−c. Scaphoid fracture. **a** Coronal 12−5 MHz US image over the lateral aspect of the wrist with corresponding **b** diagram and **c** anteroposterior radiographic correlation displays a fracture of the waist of the scaphoid as a step-off deformity of the hyperechoic cortical line (*open arrow*). Note a perilesional hypoechoic halo (*arrowheads*) surrounding the fracture site, consistent with a local hematoma. *Rad*, radius
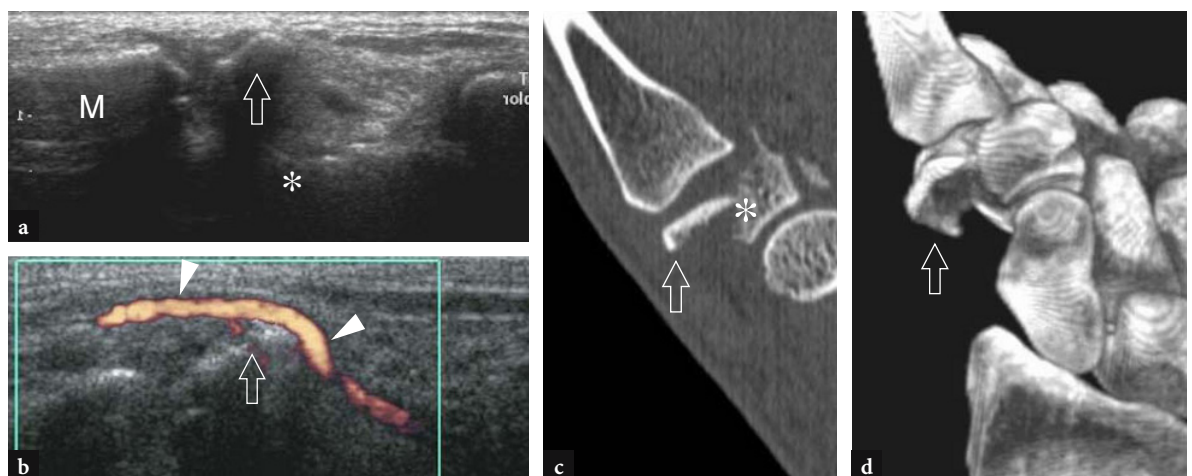
Fig. 10.81a−d. Occult trapezium fracture. Coronal **a** gray-scale and **b** power Doppler 12−5 MHz US images obtained over the lateral aspect of the distal wrist with corresponding **c** reformatted 2D CT coronal image and **d** 3D CT image reveal the lateral dislocation of the distal fracture fragment (*arrow*) of the trapezium (*asterisk*) with secondary displacement of the adjacent radial artery (*arrowheads*). *M*, first metacarpal

for depicting occult fractures compared with 73% for scaphoid radiographic views or clinical examination (Herneth et al. 2001). The use of US to assess the stability of the fracture ends by real-time dynamic examination has also been investigated (Dias et al. 1994).

Other carpal fractures occasionally recognized with US are trapezium fractures and hamate fractures after dorsal dislocation of the fourth and fifth metacarpals. Small avulsion fractures of the dorsal triquetrum may also occur as the result of wrist injuries in hyperflexion and hyperextension. These latter fractures are very difficult to detect on standard radiographs unless tangential views are obtained. High-resolution US identifies the avulsed bone as a small hyperechoic fragment surrounded by a hypoechoic halo due to perilesional inflammatory edema (Fig. 10.81). Local pain enhanced by pressure with the probe is confirmatory of the diagnosis. After osteosynthesis for wrist fractures, US can also recognize postsurgical complications related to the inappropriate positioning or displacement of orthopedic hardware. The conflict of screws and metallic plates with superficial soft tissues may be responsible for tendon impingement and tears. In such cases, US is a valuable tool to identify the severed structures and the hardware material as the cause of impingement (Figs. 10.82, 10.83).

The diagnosis of dislocation of carpal bones may be challenging on plain films. Dislocations affect mostly the lunate which, being free from tendon attachments, is prone to volar dislocation, a condition commonly referred to as perilunate dorsal dislocation of the wrist. Even if radiographic examination can recognize the displacement of the lunate, in some cases this condition goes unnoticed at the first examination and US can be required to assess

the cause of edema and functional inability of the wrist. Longitudinal and transverse US images over the carpal tunnel reveal the volar displacement of the bone which puts on view its concave articular facet, not detectable in normal states as it articulates with the capitate (Fig. 10.84). Direct compression of the flexor tendons and the median nerve by the displaced lunate can be depicted with US as well.

10.5.4
Wrist Masses

Clinically, a variety of pathologic conditions can present as space-occupying lesions around the wrist (Garcia and Bianchi 2001; Seboun et al. 1989). Once the lesion is identified at physical examination, US can be used to confirm its presence, evaluate its margins and internal echotexture (solid vs cystic) and rule out possible anatomic variants mimicking disease. Although the actual nature of a wrist mass cannot always be established based on US findings alone, there are instances in which a specific diagnosis can be made or at least may be strongly suspected. These instances include: ganglion cysts, neurogenic tumors, anomalous bone and accessory muscles.

10.5.4.1
Ganglion Cysts

Ganglia, the most common space-occupying lesions of the hand and wrist, are cystic masses, filled with viscous fluid and lacking a true synovial lining, that derive from degeneration of periarticular soft tissues (Steiner et al. 1996). They present clinically as tender or slight painful masses close to joint
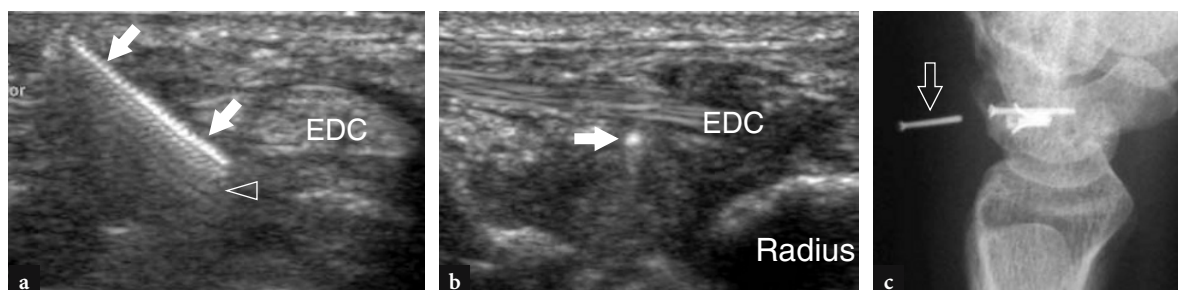
Fig. 10.82a−c. Failed surgical repair of the scapholunate ligament. **a** Transverse and **b** longitudinal 12−5 MHz US images over the proximal wrist in a patient with reported pain and clicking after surgical treatment for a complete scapholunate ligament tear. In the soft tissues of the dorsal wrist, US depicts a bright linear structure (*arrows*) with serrated appearance and posterior reverberation artifact (*open arrowhead*) just deep to the extensor digitorum tendons *(EDC)*, consistent with a displaced screw. **c** Lateral radiograph confirms the US finding
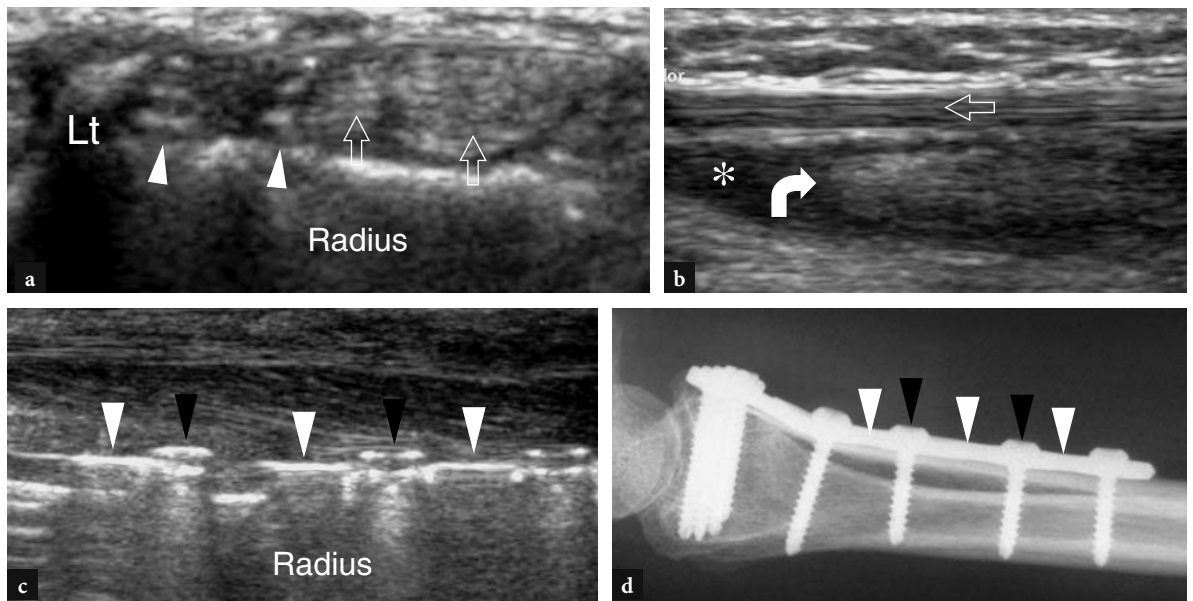
Fig. 10.83 a–d. Extensor pollicis longus tear caused by a screw. **a** Transverse 12−5 MHz US image of the dorsal wrist obtained at the level of the Lister tubercle (*Lt*) in a patient previously operated on for a Colles fracture demonstrates the absence of the extensor pollicis longus tendon. At the level of the third compartment and just medial to it, two hyperechoic foreign bodies (*arrowheads*) corresponding to screw tips can be appreciated. Note the intact adjacent extensor tendons of the fourth compartment (*open arrows*). **b** Longitudinal 12−5 MHz US image over the dorsal distal forearm shows the proximal stump of the retracted extensor pollicis longus tendon (*curved arrow*) as a fusiform irregularly hypoechoic structure surrounded by fluid collection (*asterisk*). Note the normal extensor carpi radialis brevis tendon (*open arrow*). **c** Longitudinal 12−5 MHz US image over the ventral distal forearm with **d** lateral radiographic correlation displays the metallic plate (*white arrowheads*) and the back of the screws (*black arrowheads*)

Fig. 10.84 a–d. Perilunate dorsal dislocation of the wrist in patient with tenderness and swelling over the wrist and inability to flex the fingers after a fall. The report of the initial radiographic study was negative. **a** Longitudinal 7.5−10 MHz US image over the proximal carpal tunnel shows the median nerve (*MN*) and the flexor tendons (*ft*) compressed by the displaced lunate (*L*). Within the carpal tunnel, the lunate is prominent (*asterisk*) and assumes a crescent-shaped profile (*arrowheads*) due to the volar rotation of its concave articular surface. This finding indicates lunate dislocation. **b** Corresponding reformatted 2D CT image and **c** oblique lateral radiograph display the loss of articular relationship between lunate and capitate (*Cap*). **d** Schematic drawing illustrates the mechanism of dislocation

surfaces. Most patients presenting with ganglia are completely asymptomatic and reach medical attention because of cosmetic deformity. Although the operative resection of hand and wrist ganglia is usually thought easy to perform, a recent survey on the postsurgical outcome revealed postoperative pain, limitation of function and local recurrence in 28% of cases (FAITHFULL and SEETO 2000). US demonstrates wrist ganglia as well-defined anechoic structures with posterior acoustic enhancement, located close to a joint (BIANCHI et al. 1994; HOGLUND et al. 1994; PAIVANSALO and JALOVAARA 1991; DE FLAVIIS et al. 1987; CARDINAL et al. 1994; BREIDAHL and ADLER 1996; OSTERWALDER et al. 1997). Most ganglia occur on the dorsal aspect of the wrist (Fig. 10.85). Chronic old ganglia may present a more echogenic appearance due to thickening of their wall and internal septa (Fig. 10.86). The dorsal occult ganglion is a small, painful ganglion occurring at the dorsal aspect of the wrist that cannot be palpated at physical examination (BERGHOFF and AMADIO 1993; HO et al. 2001). In general, dorsal ganglia develops

within the capsule, superficial to the scapholunate ligament (Fig. 10.85). They are often painful as a result of a simple pressure phenomenon exerted by the cyst within the capsule. In fact, large ganglia expanding outside the ligaments within the superficial soft-tissues of the dorsal wrist, and thus forming reservoirs which reduce the intracystic pressure, are less painful. Another possible explanation is the direct compression exerted by the emerging ganglion on the posterior interosseous nerve. In fact, the terminal branch of the posterior interosseous nerve travels on the ulnar side of the Lister tubercle between the extensor pollicis longus and the fourth compartment and then passes in close relationship with the scapholunate ligament. Ventral ganglia are usually located on the radial aspect of the wrist: they originate from the scaphotrapezium joint and typically expand toward the distal epiphysis of the radius where they may compress and displace the radial artery and the superficial sensory branch of the radial nerve (URAYAMA et al. 1998) (Fig. 10.87). These ganglia should be distinguished from pseudoaneurysms
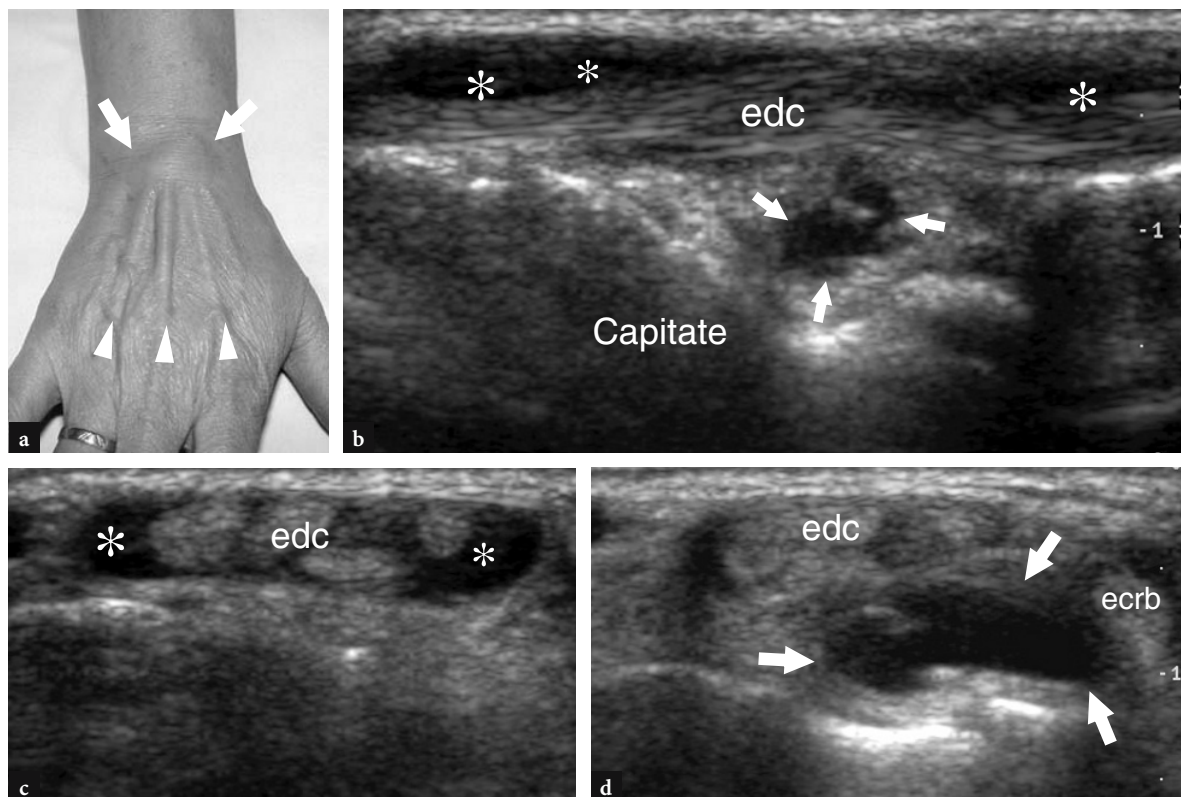
Fig. 10.85a–d. Occult dorsal ganglion. **a** Photograph shows a lump (*arrows*) over the fourth compartment of the extensor digitorum tendons (*arrowheads*) suggesting acute tenosynovitis. **b** Longitudinal and **c,d** transverse 12–5 MHz US images over the lump demonstrates double pathology by revealing fluid sheath distension (*asterisks*) in the fourth compartment of the extensor tendons and a deep ganglion cyst (*arrows*) in relation with the dorsal carpal ligaments. The ganglion expanded between the extensor digitorum *(edc)* and the extensor carpi radialis brevis *(ecrb)* tendons
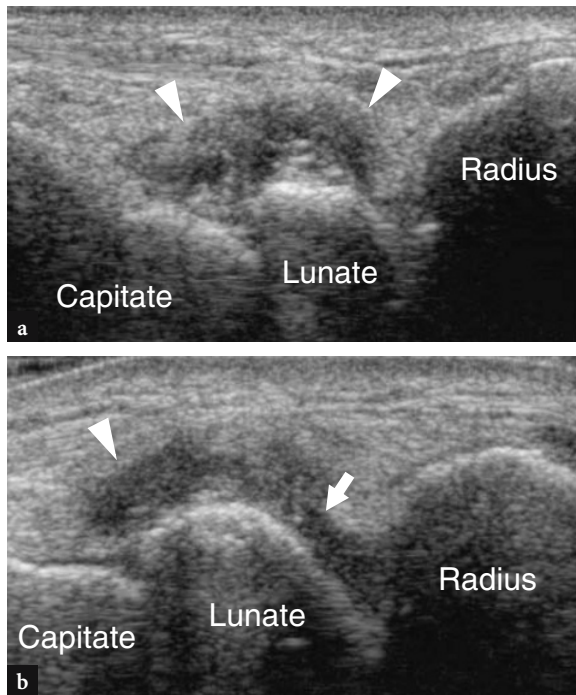
Fig. 10.86 a,b. Old dorsal ganglion. Longitudinal 10−5 MHz US images obtained with the dorsal wrist **a** extended and **b** slightly flexed exhibit a hypoechoic mass (*arrowheads*) with internal echoes located at the typical site of a dorsal ganglion. The internal appearance is that of an old collapsed ganglion with thickened walls and septations. In **b,** note the pedicle (*arrow*) connecting the ganglion with the radiocarpal joint. Care should be taken not to confuse this finding with a mild distension of the dorsal recess of the radiocarpal joint
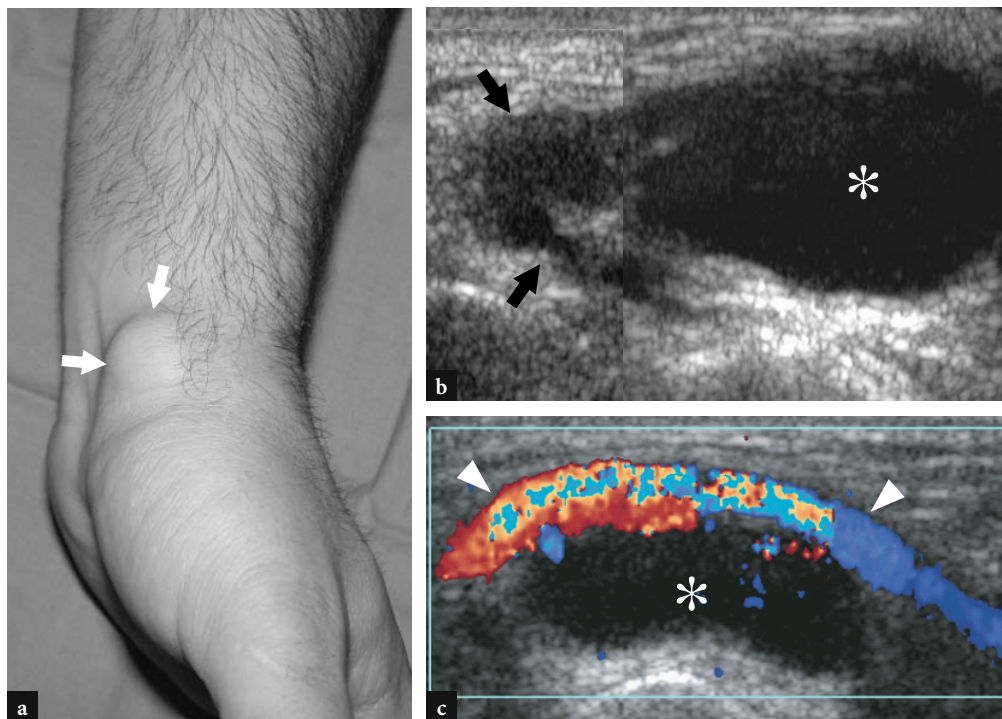
Fig. 10.87 a–c. Ventral ganglion. **a** Photograph of the radial aspect of the wrist in a young man during forced wrist dorsiflexion demonstrates a localized painless mass (*arrows*) on the volar wrist. **b,c** Longitudinal **b** gray-scale and **c** color Doppler 12−5 MHz US images obtained over the mass show a multilobed anechoic cyst (*asterisk*) closely adherent to the radial artery (*arrowheads*). The ganglion communicates with the scapho-trapezium joint through a thin tortuous pedicle (*arrow*) and expands towards the distal epiphysis of the radius. Color Doppler imaging gives a better depiction of the relationships between the ventral ganglion and the radial artery
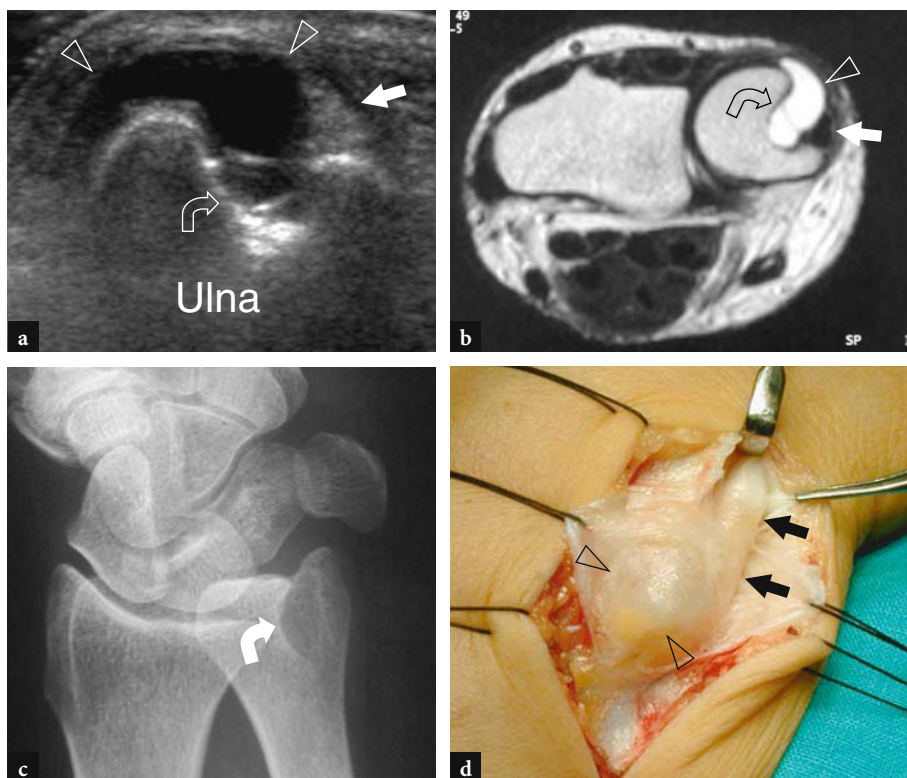
Fig. 10.88 a–d. Subperiosteal ganglion. **a** Transverse 12–5 MHz US image over the ulnar head in a patient showing mild local tenderness at clinical examination demonstrates a ganglion cyst (*arrowheads*) arising from the periosteum of the ulna and gradually sinking into the ulnar head (*curved arrow*) as a result of the pressure absorption of the bone below the enlarging cyst. Note the extensor carpi ulnaris tendon (*straight arrow*) displaced and compressed between the ganglion and the retinaculum. **b** Oblique radiographic view and **c** transverse T2w tSE MR imaging correlation confirm a deep bone erosion (*curved arrow*) in the ulnar head. **d** Gross operative view demonstrates the subperiosteal ganglion (*arrowheads*) adjacent to the extensor carpi ulnaris tendon (*arrows*)

of the palmar branch of the radial artery, which most often occur over the tubercle of the scaphoid and arise from chronic microtrauma secondary to repetitive squeezing of the artery against the tubercle of the scaphoid. US can detect them as anechoic lesions in continuity with the adjacent artery, characterized by internal flow signals at color Doppler imaging. Intraosseous and subperiosteal ganglia in the wrist and hand are exceptional (Fig. 10.88).

In clinical practice, high-resolution US is a useful tool for the diagnosis of wrist ganglia, especially in cases of small-sized occult lesions (CARDINAL et al. 1994; BLAM et al. 1998). This technique allows an accurate evaluation of the size of the cyst and is able to clarify its location and relationship with adjacent vessels, tendons and nerves. In selected cases, US can effectively guide the aspiration of the ganglion and the local injection of steroids within its cavity (BREIDAHL and ADLER 1996).

10.5.4.2
Carpal Boss

The differential diagnosis of dorsal ganglia includes the so-called carpal boss, a common abnormality which presents as a bony protuberance on the dorsal wrist intervening between the base of the second and third metacarpals, the capitate and the trapezoid. It either relates to an accessory ossification center, commonly referred to as the os styloideum, or may result from osteoarthritic changes at the carpometacarpal joint (TIMINS 1999) (Figs. 10.89, 10.90). Although generally asymptomatic, the carpal boss can occasionally lead to pain and limitation of hand motion owing to osteoarthritis or slippage of the extensor tendons. Although US cannot be considered the modality of choice to detect this abnormality, this technique may be performed to rule out a dorsal ganglion. In these cases, the os styloideum appears as a small accessory
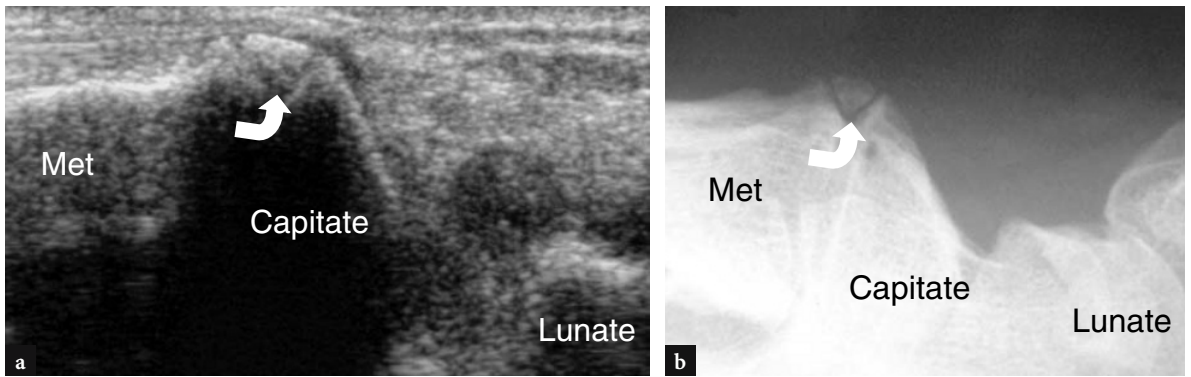
Fig. 10.89 a,b. Carpal boss due to os styloideum. **a** Longitudinal 12–5 MHz US image obtained at the dorsal aspect of the base of the third metacarpal with **b** corresponding lateral radiograph in a patient with a painless stiff dorsal mass demonstrates a small accessory bone (*curved arrow*) between the capitate and the third metacarpal *(Met)*, reflecting the os styloideum
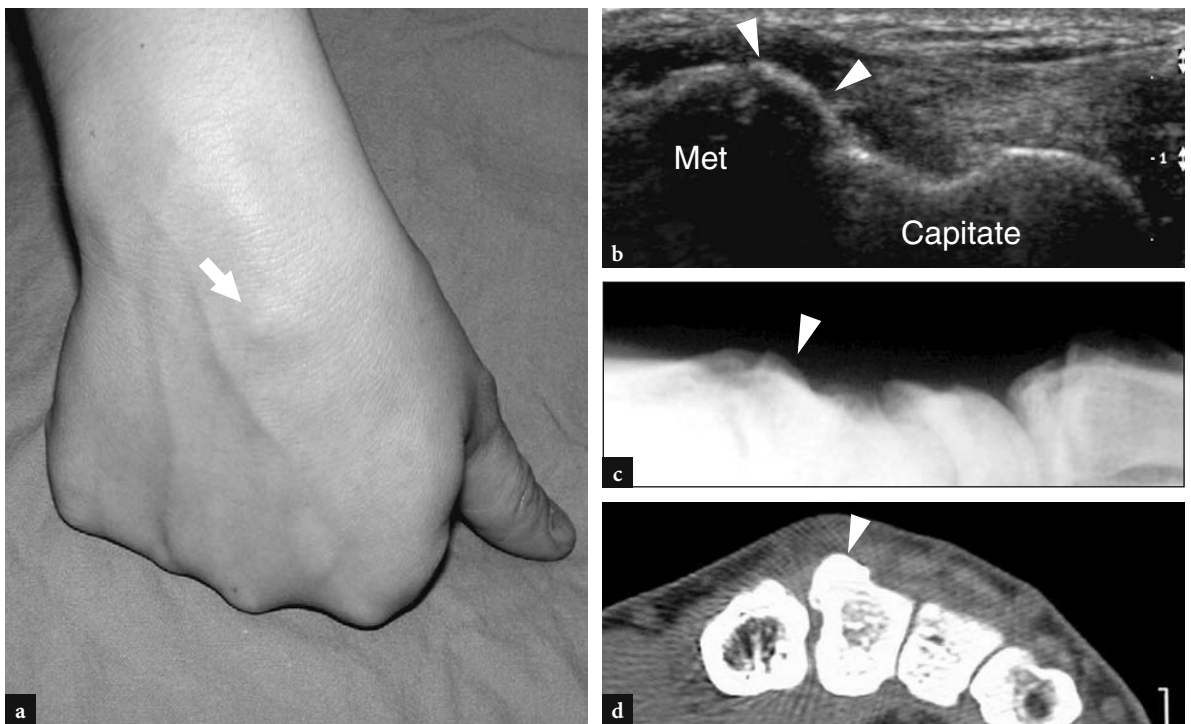
Fig. 10.90 a–d. Carpal boss due to carpometacarpal osteoarthritis. **a** Photograph of the dorsal wrist shows a stiff well-circum-scribed lump (*arrow*) which was interpreted as a ganglion cyst on clinical grounds. **b** Longitudinal 12–5 MHz US image over the lump with **c** radiographic and **d** axial CT imaging correlation reveals a bony prominence (*arrowheads*) related to osteophytes at the level of the articulation between capitate and the third metacarpal *(Met)*. In this case, standard radiograph and CT scan confirmed the absence of an os styloideum

bone located at the level of the carpometacarpal joint, whereas local osteophytes are shown as hyperechoic humps lying over the dorsal surfaces of wrist bones.

10.5.4.3
Neurogenic Tumors

Peripheral nerve tumors of the hand and wrist, including schwannomas, neurofibromas and neural fibrolipomas, are uncommon. Most involve the median nerve and typically present as soft, slowly enlarging masses occurring in the volar aspect of the hand and wrist. Nerve tumors have a nonspecific appearance on US as they appear as oval hypoechoic solid masses with well-defined margins (Fig. 10.91). The feature of value in differentiating these tumors from other soft-tissue masses is demonstration of the continuity between the mass and the nerve of origin (MARTINOLI et al. 1996). This requires careful scanning technique because the normal nerve portions connected at the opposite ends of the tumor may be displaced from their natural course by the enlarging mass. The nerve immediately adjacent to the tumor may be thickened and have loss of anisotropy, thus producing a tapering appearance to the oval mass. Tumors of the median nerve at the wrist may cause bowing of the transverse carpal ligament, and carpal tunnel syndrome may be a late symptom.

A rare neurogenic mass with marked predilection for the median nerve at wrist is the neural fibrolipoma, a developmental anomaly which is also referred to as fibrolipomatous hamartoma or intraneural lipoma. Syndactyly or macrodactyly of the index and middle fingers (macrodystrophia lipomatosa) are associated with it in up to two thirds of patients. Fibrolipomatous hamartoma affects young subjects, often in early childhood, and presents clinically as a mobile soft-tissue swelling in the volar aspect of the wrist (MURPHEY et al. 1999) due to the striking enlargement of the median nerve by mature fibrofatty tissue that infiltrates the interfascicular epineurium. US typically shows the fusiform enlargement of the nerve at the distal radius and within the carpal tunnel by large deposits of hyperechoic fat filling the epineurium and displacing normal or slightly enlarged hypoechoic fascicles (CHEN et al. 1996) (Fig. 10.92).

10.5.4.4
Anomalous Muscles

Accessory muscles can be encountered at the wrist as merely incidental findings in asymptomatic subjects. In some cases, however, these muscles may cause clinical concern when they present as space-occupying masses or when their hypertrophy or strenuous activity causes compressive neuropathy. The typical US appearance of anomalous wrist muscles does not differ from that of other muscles, including functional phases of contraction and relaxation. Familiarity with their location may help the examiner to make a correct diagnosis, thus avoiding confusion with other pathologic conditions. The most common anomalous muscles in the wrist are: the accessory abductor digiti minimi, the extensor digitorum brevis manus, the digastric flexor digitorum superficialis muscle of the index finger, and a proximal origin of the lumbrical muscles (TIMINS 1999).
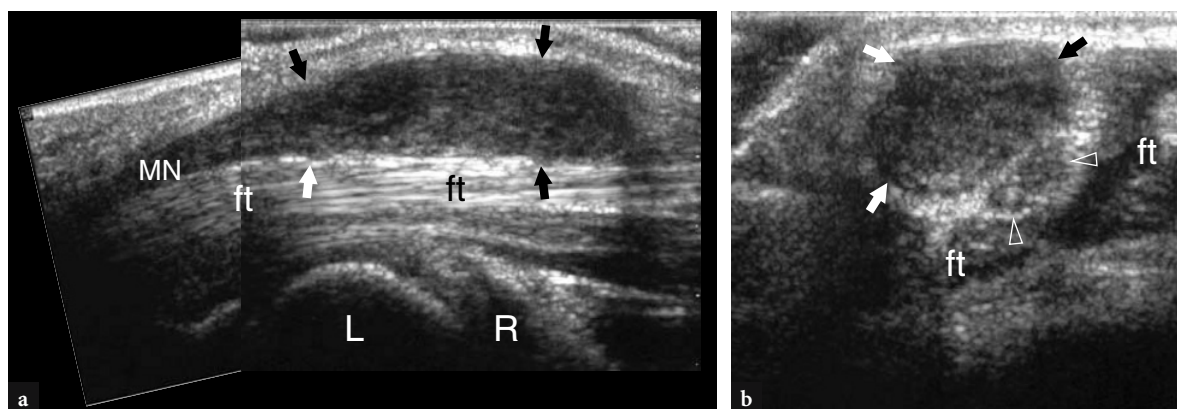
Fig. 10.91a,b. Schwannoma of the median nerve. **a** Longitudinal reconstructed and **b** transverse 10–5 MHz US images over the carpal tunnel demonstrate an elongated hypoechoic mass (*arrows*) in continuity with the median nerve *(MN)* in a patient presenting with soft-tissue swelling over the ventral wrist and mild symptoms related to carpal tunnel disease. The bulk of the tumor develops proximal to the transverse carpal ligament sparing some fascicles of the nerve (*arrowheads*). *ft*, flexor tendons; *L*, lunate; *R*, radius
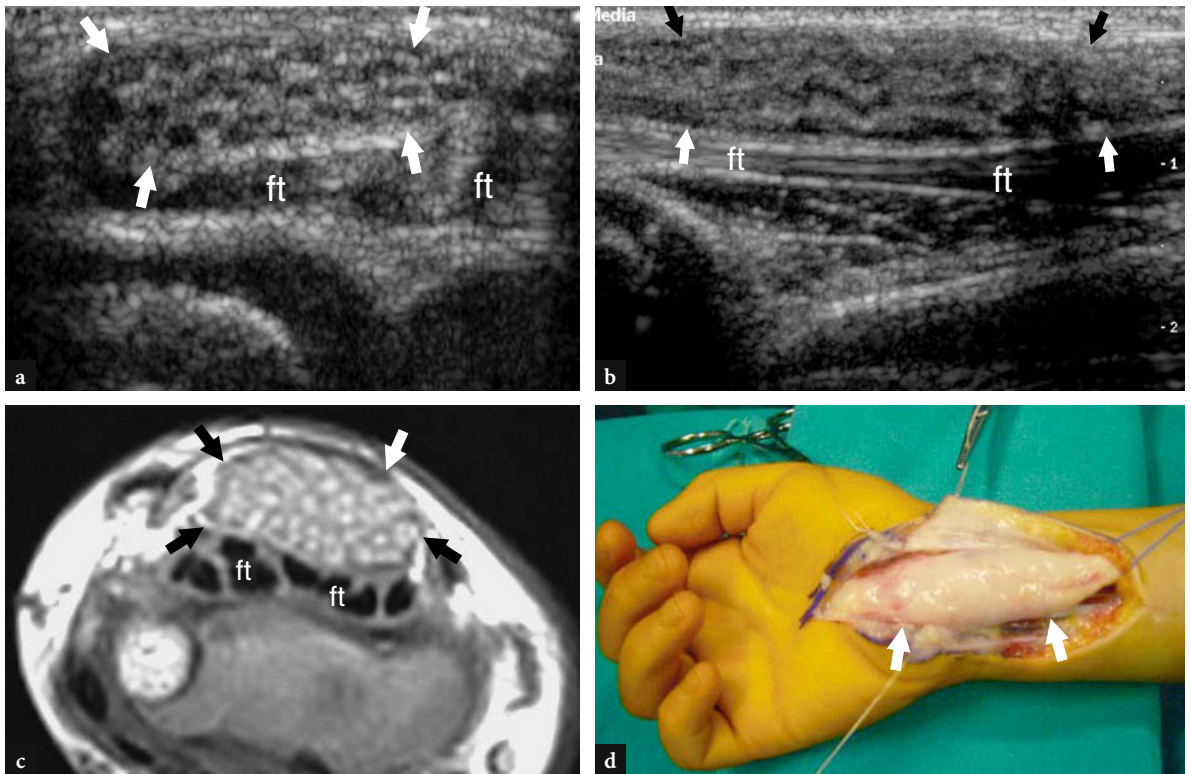
Fig. 10.92 a–d. Fibrolipomatous hamartoma of the median nerve. **a** Transverse 12–5 MHz US image in a child with diffuse swelling and tenderness over the ventral wrist with **b** T1w SE MR imaging correlation reveals an abnormal fusiform enlargement of the median nerve (*arrows*). The nerve thickened hypoechoic fascicles embedded in increased interfascicular fatty tissue. **c** Longitudinal 12–5 MHz US image over the nerve (*arrows*) shows the wavy course of the fascicles. ft, flexor tendons. **d** Gross operative view demonstrates the striking enlargement of the median nerve (*arrows*) at the wrist. The patient did not have macrodactyly and complained of only mild symptoms related to carpal tunnel disease
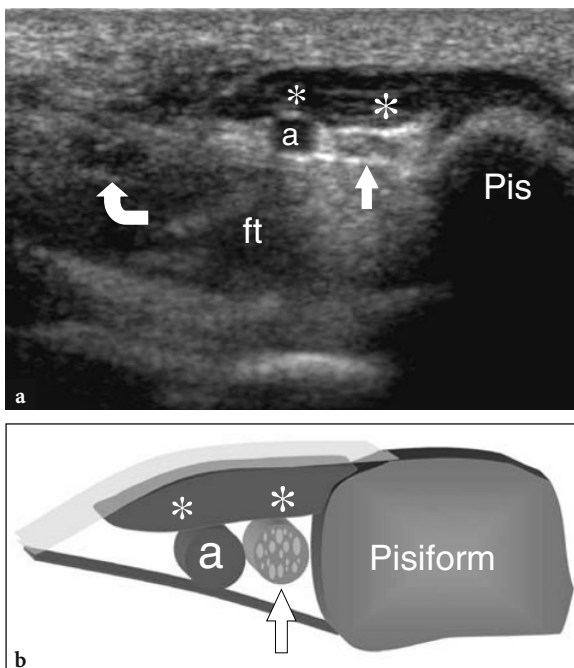
Fig. 10.93 a,b. Accessory abductor digiti minimi. **a** Transverse 12–5 MHz US image obtained over the Guyon tunnel in a patient with mild ulnar neuropathy and no palpable mass over the ventral wrist shows a fusiform hypoechoic belly (*asterisks*) overlying the ulnar nerve (*straight arrow*) and the ulnar artery *(a)* consistent with a hypertrophied accessory abductor digiti minimi. Note the flattened appearance of the ulnar nerve within the Guyon tunnel. *ft*, flexor tendons; *curved arrow*, median nerve. *Pis*, pisiform. **b** Diagram correlation

The accessory abductor digiti minimi is the most common accessory muscle of the wrist, accounting for approximately 24% of normal individuals (Zeiss and Guilliam-Hadet 1996). This muscle originates from the palmar carpal ligament and the palmaris longus and inserts on the abductor digiti minimi and the medial aspect of the base of the fifth proximal phalanx (Patel et al. 2002) (Fig. 10.93). Although usually asymptomatic, it may cause ulnar neuropathy by squeezing the ulnar nerve against the pisohamate ligament during its contraction. A difference in muscle thickness between normal subjects (mean 1.7 mm) and symptomatic patients (4 mm) has been observed, indicating that the muscle size may be a factor influencing the function of the underlying nerve.

The extensor digitorum brevis manus occurs less frequently, involving 1−3% of individuals (Gama 1983). It arises from the distal radius and the distal radiocarpal ligament and inserts onto the index or the middle finger. The extensor digitorum brevis manus appears as a muscle belly located alongside the extensor tendon of the index finger and can be easily mistaken for either a dorsal ganglion or tenosynovitis of the extensor tendon of the index

finger. US is able to identify the typical echotexture of a muscle and to depict muscle shape changes induced by voluntary contraction and relaxation (Fig. 10.94).

On the ventral wrist, an anomalous muscle belly of the flexor digitorum superficialis of the index finger may cause discomfort and symptoms related to carpal tunnel syndrome (Smith 1971). In these cases, the anomalous muscle can be seen entering the carpal tunnel during extension of the index finger. For a correct diagnosis, the examiner should best examine the wrist while keeping the fingers extended. Then, dynamic scanning during flexion and extension of the fingers can depict the muscle entering and exiting the tunnel (Fig. 10.95).

A proximal origin of the lumbrical muscles inside the carpal tunnel can be encountered in approximately 22% of subjects (Touborg-Jensen 1970). These muscles are pulled within the tunnel during flexion of the fingers and may be the cause of median neuropathy. Similar to the anomalous flexor digitorum superficialis of the index finger, dynamic scanning with flexion and extension of the fingers is essential for a proper diagnosis of anomalous lumbrical muscles.
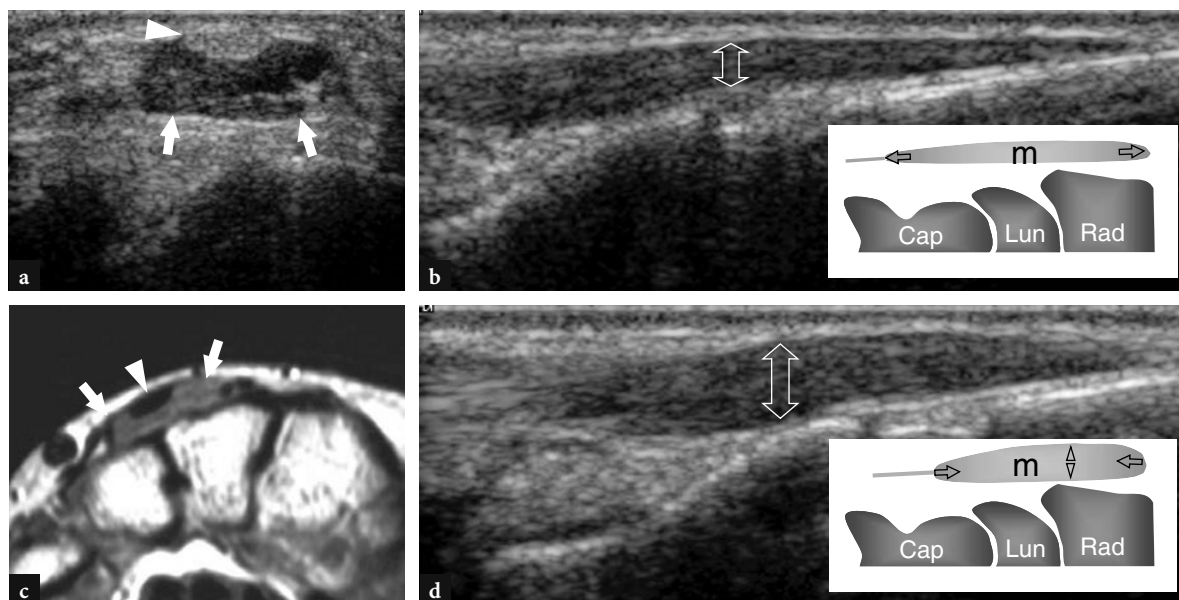
Fig. 10.94 a−d. Extensor digitorum brevis manus. **a** Transverse 12−5 MHz US image over the dorsal wrist in a patient with a local painless soft-tissue mass with **b** T1w SE MR imaging correlation reveals the anomalous muscle belly (*arrows*) located alongside the extensor tendons, reflecting the extensor digitorum brevis manus. Note the tendon (*arrowhead*) of the accessory muscle. **c,d** Long-axis 12−5 MHz US images over the anomalous muscle obtained **c** at rest and d during voluntary contraction of the muscle with correlative drawings (*see inserts*). Compared with the US image obtained at rest, active contraction leads to an increased thickness (*double arrow*) and shortening of the muscle belly *(m)*. This change can be easily palpated at physical examination. *Cap*, capitate; *Lun*, lunate; *Rad*, radius
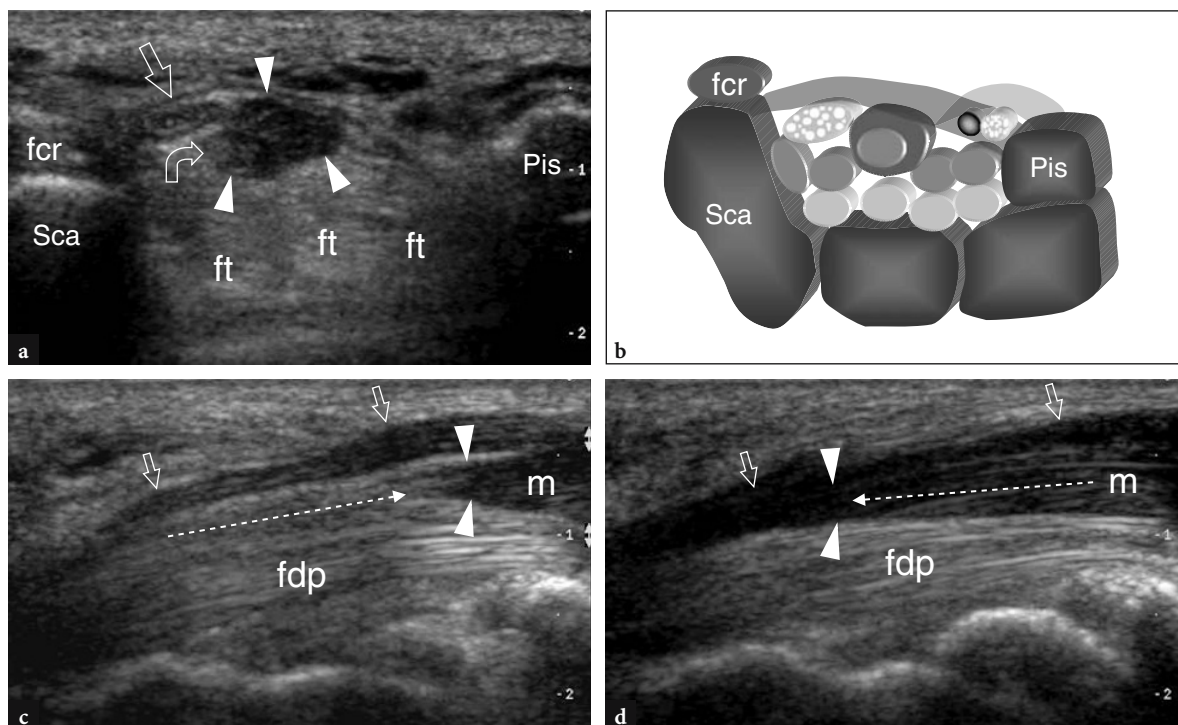
Fig. 10.95 a–d. Aberrant flexor muscle of the index finger. **a** Transverse 12–5 MHz US image of the proximal carpal tunnel in a young patient with carpal tunnel disease with **b** diagram correlation demonstrates an anomalous hypoechoic mass (*arrowheads*) reflecting an aberrant flexor muscle of the index finger among the median nerve (*straight arrow*), the flexor digitorum tendons (*ft*) and the transverse carpal ligament. Note the small hyperechoic tendon (*curved arrow*) inside the muscle belly. **c,d** Long-axis 12–5 MHz US images over the anomalous muscle obtained **c** during flexion and **d** extension of the index finger. With the finger flexed, the anomalous muscle belly *(m)* lies proximal to the entrance of the carpal tunnel. Progressive extension of the index finger pushes the muscle inside the tunnel, thus leading to dynamic compression of the median nerve (*arrows*). *Dashed arrows* indicate the vector of movement of the anomalous muscle belly. Flexion and extension movements of the other digits did not interfere with the muscle position. *fcr*, flexor carpi radialis; *fdp*, flexor digitorum profundus; *Pis*, pisiform; *Sca*, scaphoid; *arrowheads*, distal edge of the muscle

References

Anderson SE, Steinbach LS, De Monaco D et al (2004) „Baby wrist": MRI of an overuse syndrome in mothers. AJR Am J Roentgenol 182: 719-724 Bahm J, Szabo Z, Foucher G (1995) The anatomy of de Quervain's disease. Int Orthop 19:209–211

Berghoff RA Jr, Amadio PC (1993) Dorsal wrist ganglion. Cause of dorsal wrist pain. Orthopade 22:30–35

Bianchi S, Abdelwahab IF, Zwass A et al (1994) Ultrasonographic evaluation of wrist ganglia. Skeletal Radiol 23:201–203

Bianchi S, Martinoli C, Abdelwahab IF et al (1999) High-frequency ultrasound examination of the wrist and hand. Skeletal Radiol 28:121–129

Bianchi S, Martinoli C, Sureda D et al (2001) Ultrasound of the hand. Eur J Ultrasound 14:29–34

Blam O, Bindra R, Middleton W et al (1998) The occult dorsal carpal ganglion: usefulness of magnetic resonance imaging and ultrasound in diagnosis. Am J Orthop 27:107–110

Breidahl WH, Adler RS (1996) Ultrasound-guided injection of ganglia with corticosteroids. Skeletal Radiol 25:635–638

Buchberger W, Schon G, Strasser K et al (1991) High-resolu-tion ultrasonography of the carpal tunnel. J Ultrasound Med 10:531–537

Buchberger W, Judmaier W, Birbamer G et al (1992) Carpal tunnel syndrome: diagnosis with high-resolution sonography. AJR Am J Roentgenol 159:793–798

Cardinal E, Buckwalter KA, Braunstein EM et al (1994) Occult dorsal carpal ganglion: comparison of US and MR imaging. Radiology 193:259–262

Chen P, Massengill A, Maklad N et al (1996) Nerve territory-oriented macrodactyly: unusual cause of carpal tunnel syndrome. J Ultrasound Med 15:661–664

Chen P, Maklad N, Redwine M et al (1997) Dynamic high-resolution sonography of the carpal tunnel. AJR Am J Roentgenol 168:533–537

Chiou HJ, Chang CY, Chou YH et al (1998) Triangular fibrocartilage of wrist: presentation on high resolution ultrasonography. J Ultrasound Med 17:41–48

Chiou HJ, Chou YH, Chang CY (2001) Ultrasonography of the wrist. Can Assoc Radiol J 52:302–311

Creteur V, Peetrons P (2000) Ultrasonography of the wrist and the hand. J Radiol 81 [Suppl]:351–352

Daenen B, Houben G, Bauduin E et al (2004) Sonography in wrist tendon pathology. J Clin Ultrasound 32:462-469 De Faucal P, Planchon B, Dupas B et al (1991) Value of echography in the diagnosis of post-traumatic pathology of the ulnar artery, in manual workers. J Mal Vasc 16:9−12

De Flaviis L, Nessi R, del Bo P et al (1987) High-resolution ultrasonography of the wrist ganglia. J Clin Ultrasound 15:17−22

De Flaviis L, Scaglione P, Nessi R et al (1988) Ultrasonography of the hand in rheumatoid arthritis. Acta Radiol 29:457−460

Denman EE (1979) Rupture of extensor pollicis longus: a crush injury. Hand 11:295−298

Dias JJ, Hui AC, Lamont AC (1994) Real time ultrasonography in the assessment of movement at the site of a scaphoid fracture non-union. J Hand Surg [Br] 19:498−504

Duncan I, Sullivan P, Lomas F (1999) Sonography in the diagnosis of carpal tunnel syndrome. AJR Am J Roentgenol 173:681−683

Elias DA, Lax MJ, Anastakis DJ (2001) Musculoskeletal images. Ganglion cyst of Guyon's canal causing ulnar nerve compression. Can J Surg 44:331−332

Faithfull DK, Seeto BG (2000) The simple wrist ganglion-more than a minor surgical procedure? Hand Surg 5:139−143

Ferrara MA, Marcelis S (1997) Ultrasound examination of the wrist. J Belge Radiol 80:78−80

Fitton J, Shea FW, Goldie W (1968) Lesions of the flexor carpi radialis tendon and sheath causing pain at the wrist. J Bone Joint Surg Br 50:359−363

Fornage BD (1989) Soft-tissue changes in the hand in rheumatoid arthritis: evaluation with US. Radiology 173:735−737

Fornage BD, Rifkin MD (1988) Ultrasound examination of the hand and foot. Radiol Clin North Am 26:109−129

Fumiere E, Dugardeyn C, Roquet ME et al (2002) US demonstration of a thrombosed persistent median artery in carpal tunnel syndrome. JBR-BTR 85:1−3

Gama C (1983) Extensor digitorum brevis manus: a report on 38 cases and a review of the literature. J Hand Surg 8:578−582

Garcia J, Bianchi S (2001) Diagnostic imaging of tumors of the hand and wrist. Eur Radiol 11:1470−1482

Giovagnorio F, Andreoli C, De Cicco ML (1997) Ultrasonographic evaluation of de Quervain disease. J Ultrasound Med 16:685−689

Gooding GA (1988) Tenosynovitis of the wrist. A sonographic demonstration. J Ultrasound Med 7:225−226

Grechenig W, Clement H, Egner S et al (2000) Musculo-tendinous junction of the flexor carpi ulnaris muscle. An anatomical study. Surg Radiol Anat 22:255−260

Griffith JF, Chan DP, Ho PC et al (2001) Sonography of the normal scapholunate ligament and scapholunate joint space. J Clin Ultrasound 29:223−229

Gross MS, Gelberman RH (1984) The anatomy of distal ulnar tunnel. Clin Orthop 196:238−247

Hauger O, Bonnefoy O, Moinard M et al (2002) Occult fractures of the waist of the scaphoid: early diagnosis by high-spatial resolution sonography. AJR Am J Roentgenol 178:1239−1245

Herneth AM, Siegmeth A, Bader TR et al (2001) Scaphoid fractures: evaluation with high-spatial-resolution US initial results. Radiology 220:231−235

Ho PC, Griffiths J, Lo WN et al (2001) Current treatment of ganglion of the wrist. Hand Surg 6:49−58

Hodgkinson DW, Nicholson DA, Stewart G et al (1993) Scaphoid fracture: a new method of assessment. Clin Radiol 48:398−401

Hoglund M, Tordai P, Muren C (1994) Diagnosis of ganglions in the hand and wrist by sonography. Acta Radiol 35:35−39

Iannicelli E, Chianta GA, Salvini V et al (2000) Evaluation of bifid median nerve with sonography and MR imaging. J Ultrasound Med 19:481−485

Iannicelli E, Almberger M, Chianta GA et al (2001) Bifid median nerve in the carpal tunnel: integrated imaging. Radiol Med 101:456−458

Ikegaya N, Hishida A, Sawada K et al (1995) Ultrasonographic evaluation of the carpal tunnel syndrome in hemodialysis patients. Clin Nephrol 44:231−237

Jacobson JA, Oh E, Propeck T et al (2002) Sonography of the scapholunate ligament in four cadaveric wrists: correlation with MR arthrography and anatomy. AJR Am J Roentgenol 179:523-527 Jamadar DA, Jacobson JA, Hayes CW (2001) Sonographic evaluation of the median nerve at the wrist. J Ultrasound Med 20:1011−1014

Kamolz LP, Schrogendorfer KF, Rab M et al (2001) The precision of ultrasound imaging and its relevance for carpal tunnel syndrome. Surg Radiol Anat 23:117−121

Keogh CF, Wong NJ, Wells NJ et al (2004) High resolution sonography of the triangular fibrocartilage: initial experience and correlation with MRI and arthroscopic findings. AJR Am J Roentgenol 182:333-336 Kerboull L, Le Viet D (1995) Tendinitis of the long palmar muscle tendon. Physiopathology and results of surgical treatment. Apropos of 28 cases. Ann Chir Main Memb Super 14:135−141

Klein W, Rieger H, Grunert J et al (1991) Traumatically-induced thrombosis of the distal ulnar artery. Case report and review of the literature. Handchir Mikrochir Plast Chir 23:39−45

Koski JM (1992) Ultrasonography in the detection of effusion in the radiocarpal and midcarpal joints. Scand J Rheumatol 21:79−81

Koski JM, Hermunen H (2001) Intra-articular glucocorticoid treatment of the rheumatoid wrist. An ultrasonographic study. Scand J Rheumatol 30:268−270

Kuo MH, Leong CP, Cheng YF et al (2001) Static wrist position associated with least median nerve compression: sonographic evaluation. Am J Phys Med Rehabil 80:256−260

Lanteri M, Ptasznik R, Constable L et al (1997) Ultrasound changes in the wrist and hand in hemodialysis patients. Clin Nephrol 48:375−380

Le Viet D (1995) Les tendinites et apophysites du poignet. J Traumatol Sport 12:149−155

Lee D (1998) Sonography of the wrist and Hand. Semin Musculoskelet Radiol 2:237−244

Lee D, van Holsbeeck MT, Janevski PK et al (1999) Diagnosis of carpal tunnel syndrome. Ultrasound versus electromyography. Radiol Clin North Am 37:859−872

Lee JC, Healy JC (2005) Normal sonographic anatomy of the wrist and hand. RadioGraphics 25:1577-1590 Leslie BM, Ericson WB Jr, Morehead JR (1990) Incidence of a septum within the first dorsal compartment of the wrist. J Hand Surg [Am] 15:88−91

Lund PJ, Heikal A, Maricic MJ et al (1995) Ultrasonographic imaging of the hand and wrist in rheumatoid arthritis. Skeletal Radiol 24:591−596

Marini M, Boni S, Pingi A et al (1994) De Quervain's disease: diagnostic imaging. Chir Organi Mov 79:219−223

Martinoli C, Serafini G, Bianchi S et al (1996) Ultrasonography of peripheral nerves. J Periph Nerv Syst 1:169−178

Martinoli C, Bianchi S, Gandolfo N et al (2000) Ultrasound of nerve entrapments in osteofibrous tunnels. RadioGraphics 20:199−217

Massy-Westropp N, Grimmer K, Bain G (2001) The effect of a standard activity on the size of the median nerve as determined by ultrasound visualization. J Hand Surg [Am] 26:649−654

Milbradt H, Calleja Cancho E, Qaiyumi SA et al (1990) Sonography of the wrist and the hand. Radiologe 30:360−365

Murphey MD, Smith WS, Smith SE et al (1999) Imaging of musculoskeletal neurogenic tumors: radiologic-pathologic correlation. RadioGraphics 19:1253−1280

Nagaoka M, Matsuzaki H, Suzuki T (2000) Ultrasonographic examination of de Quervain's disease. J Orthop Sci 5:96−99

Nakamichi K, Tachibana S (1992) Transverse sliding of the median nerve beneath the flexor retinaculum. J Hand Surg [Br] 17:213−216

Nakamichi K, Tachibana S (1995) Restricted motion of the median nerve in carpal tunnel syndrome. J Hand Surg [Br] 20:460−464

Nakamichi KI, Tachibana S (2000) Enlarged median nerve in idiopathic carpal tunnel syndrome. Muscle Nerve 23:1713−1718

Osterwalder JJ, Widrig R, Stober R et al (1997) Diagnostic validity of ultrasound in patients with persistent wrist pain and suspected occult ganglion. J Hand Surg [Am] 22:1034−1040

Paivansalo M, Jalovaara P (1991) Ultrasound findings of ganglions of the wrist. Eur J Radiol 13:178−180

Parellada AJ, Morrison WB, Reiter SB et al (2006) Flexor carpi radialis tendinopathy: spectrum of imaging findings and association with triscaphe arthritis. Skeletal Radiol 35:572-578

Patel N, Harvie P, Ostlere SJ (2002) Ultrasound of accessory muscles at the Guyon canal. Session European Society of Musculoskeletal Radiology, IX Annual Meeting. Abstract book, p 156

Propeck T, Quinn TJ, Jacobson JA et al (2000) Sonography and MR imaging of bifid median nerve with anatomic and histologic correlation. AJR Am J Roentgenol 175:1721−1725

Read JW, Conolly WB, Lanzetta M et al (1996) Diagnostic ultrasound of the hand and wrist. J Hand Surg [Am] 21:1004−1010

Rodriguez-Niedenfuhr M, Sanudo JR, Vazquez T et al (1999) Median artery revisited. J Anat 195:57−63

Sarria L, Cabada T, Cozcolluela R et al (2000) Carpal tunnel syndrome: usefulness of sonography. Eur Radiol 10:1920−1925

Seboun P, Soussi M, Ebelin M et al (1989) II. Tumeurs et pseudo-tumeurs des parties molles. Resultats preliminaires à propos de 12 cas operes. J Radiol 70:346−351

Smith RJ (1971) Anomalous muscle belly of the flexor digitorum superficialis causing carpal-tunnel syndrome. Report of a case. J Bone Joint Surg Am 53:1215−1216

Steiner E, Steinbach LS, Schnarkowski P et al (1996) Ganglia and cysts around joints. Radiol Clin North Am 34:395−425

Sugimoto H, Takeda A, Hyodoh K (2000) Early-stage rheumatoid arthritis: prospective study of the effectiveness of MR imaging for diagnosis. Radiology 216:569−575

Takahashi T, Kato A, Ikegaya N et al (2002) Ultrasound changes of the carpal tunnel in patients receiving long-term hemodialysis: a cross-sectional and longitudinal study. Clin Nephrol 57:230−236

Taleisnik J (1973) The palmar cutaneous branch of the medial nerve and the approach to the carpal tunnel: an anatomical study. J Bone Joint Surg Am 55:1212−1217

Teefey SA, Middleton WD, Boyer MI (2000) Sonography of the hand and wrist. Semin Ultrasound CT MR 21:192−204

Timins ME (1999) Muscular anatomic variants of the wrist and hand: findings on MR imaging. AJR Am J Roentgenol 172:1397−1401

Timins ME (1999) Osseous anatomic variants of the wrist: findings on MR imaging. AJR Am J Roentgenol 173:339−344

Touborg-Jensen A (1970) Carpal-tunnel syndrome caused by an abnormal distribution of the lumbrical muscles. Case report. Scand J Plast Reconstr Surg 4:72−74

Trentanni C, Galli A, Melucci G et al (1997) Ultrasonic diagnosis of De Quervain's stenosing tenosynovitis. Radiol Med 93:194−198

Urayama H, Ohtake H, Kosugi I et al (1998) Distortion of the radial artery by a mucinous cyst. Case report. Scand J Plast Reconstr Surg 32:437−440

Van Vugt RM, van Dalen A, Bijlsma JW (1997) Ultrasound guided synovial biopsy of the wrist. Scand J Rheumatol 26:212−214

Van Vugt RM, van Dalen A, Bijlsma JW (1998) The current role of high-resolution ultrasonography of the hand and wrist in rheumatic diseases. Clin Exp Rheumatol 16:454−458

Waizenegger M, Wastie ML, Barton NJ et al (1994) Scintigraphy in the evaluation of the clinical scaphoid fractures. J Hand Surg [Br] 19:750−753

Wong SM, Griffith JF, Hui ACF et al (2004) Carpal tunnel syndrome: diagnostic usefulness of sonography. Radiology 232:93-99

Zeiss J, Guilluiam-Hadet L (1996) MR demonstration of anomalous muscles about the volar aspect of the wrist and forearm. Clin Imaging 20:219−221